Universidade do Minho
Escola de Engenharia

Subramani Pichandi

Development of composite auxetic structures for civil engineering applications

fevereiro 2016

Subramani Pichandi Development of composite auxetic structures for civil engineering applications
UMinho | 2016

Universidade do Minho
Escola de Engenharia

Subramani Pichandi

Development of composite auxetic structures for civil engineering applications

Tese de Doutoramento
Engenharia Têxtil

Trabalho efectuado sob a orientação do
Professor Doutor Raúl Fangueiro
Professor Doutor Daniel V. Oliveria

fevereiro 2016

STATEMENT OF INTEGRITY

I hereby declare having conducted my thesis with integrity. I confirm that I have not used plagrism or any form of falsification of results in the process of thesis elaboration.

I further declare that I have fully acknowledged the code of Ethical Conduct of the University of Minho.

University of Minho,_____

Full name: P. Subramani

Signature:_____

ACKNOWLEDGMENTS

This research was carried out at the Department of Textile Engineering of the University of Minho, Portugal, under the supervision of Prof. Daniel V. Oliveira and Prof. Raul Fangueiro. The project work was funded by University of Minho, under the scheme of "Strategic plan of school of engineering – Agenda 2020: Multidisciplinary projects", gratefully acknowledged.

I would like to express my sincere gratitude to Prof. Daniel Oliveira for his continuous support, advice, encouragement and enthusiasm. His guidance and motivation helped me in all the time of research and writing of this thesis.

I deeply grateful to Prof. Raul Fangueiro for his great support and motivation throughout of my study here. His support helped to complete my research and writing of thesis on time. Also, I express my gratitude both the Profs to allow me to do my research work without any pressure.

Also, I would like to express my gratitude to Dr. Sohel Rana for his wonderful support and guidance during my tenure here. He is my great mentor personally as well for my research work.

I would like to thank Dr. Bahman Ghiassi for his wonderful guidance and help to develop suitable analytical and numerical modelling for the developed auxetic structures.

I would like to thank Dr. Jose Xavier from University of Trás-os-Montes e Alto Douro, Portugal, for collaboration in performing tests with Digital Image Correlation technique and also the friendship established between us.

I would also like to thank the technicians of the laboratory of the Textile and Civil Engineering Department of University of Minho, engineers Joaquim George, Matos, Marco and Carlos for the extreme efforts and assistance during my experimental tests. I am also grateful to all my friends that supported and encouraged me and stayed near me in the tough times during the execution of this research work.

Finally, I would like to dedicate this work to my family who supported me all the way until here.

Abstract

Auxetic materials are a class of non-conventional materials having negative Poisson's ratio. They expand laterally when axially loaded or laterally shrink when compressed. Due to its counterintuitive behaviour, auxetic materials possess enhanced properties that could be beneficial for many specific applications. This thesis aimed to develop such a class of auxetic materials from braided composite rods which can be beneficial for civil engineering applications as a strengthening materials. The developed auxetic structures can be reinforced into either for existing structural elements or for newly built one.

Novel macro auxetic structures were developed from core fibre reinforced braided composite rods based on missing rib or lozenge grid and re-entrant hexagon or bow-tie auxetic structural design. The developed structures tested under tensile loading to study their tensile and auxetic behaviour. The auxetic behaviour was studied thorough images taken during tensile loading. Also, the auxetic and tensile behaviour of the developed structures were studied by varying their structural and material parameters. Developed auxetic structures exhibits negative Poisson's ratio and it is mainly depends up on structural parameters. The Poisson's ratio of the developed auxetic structures were studied by suitable analytical model either by existing model or by using newly developed model. These analytical models could be useful to predict the Poisson's ratio of the developed auxetic structures accurately. In addition to analytical model, the FE solver DIANA was used to develop a numerical modelling to predict the tensile and auxetic behaviour. The developed numerical model was accurate to predict the tensile and Poisson's ratio of the structures.

In addition, the auxetic structures were reinforced into the masonry wall specimens, which is built by cement hollow bricks. The reinforced masonry wall specimens were tested under three point flexural loading and the results were compared with plain grid (commercial design) reinforced masonry wall. The auxetic structures strengthened walls performed well under flexural load compared to plain grid reinforced wall, but the crack level was more for auxetic structures reinforced wall due to its lateral expansion. This research works opened novel opportunity to use auxetic materials in the civil engineering field and created huge scope to do more research work in this area.

Resumo

Materiais auxéticas são uma classe de materiais não convencionais que apresentam um Coeficiente de Poisson negativo. Assim, expandem lateralmente quando são carregados longitudialmente e encolhem quando comprimidos. Devido ao seu comportamento fora do comum, os materiais auxéticos possuem propriedades benéficas para muitas aplicações específicas. Este trabalho tem como objetivo o desenvolvimento de materiais compósitos auxéticas a partir de varões entrançados para utilização no reforço em engenharia civil. As estruturas auxéticas desenvolvidas podem ser usadas tanto na reabilitação e reforço de elementos existentes ou na construção de novos elementos estruturais.

Estruturas auxéticas inovadoras foram desenvolvidas a partir de varões compósitos entrançados com fibras de alto desempenho no núcleo em modelos teóricos de estruturas "missing rib" ou "lozenge grid" e "re-entrant hexagon" ou "bow-tie". As estruturas desenvolvidas foram ensaiadas em tração para estudar o seu comportamneto auxético e o seu comportamento e propriedades quando este tipo de cargas são aplicadas. O comportamento auxético foi estudado recorrendo a técnicas de análise imgagem (DIC-Digitally Correlation Image) retiradas durante o ensaio de tração. Para além disso, foi estudada a influência de diversos parãmetros da estrutura e do material correspondente no comportamento auxético, nomeadamente o tipo de fibra utilizada e o ângulo dos elemntos estruturais na estrutura auxética. Os resultados demonstram que as estruturas auxéticas desenvolvidas apresentam um Coeficiente de Poisson negativo devido ao comportamento estrutural da mesma. No âmbito deste trabalho, foi igualmente desenvolvido um modelo recorrendo a Elementos Finitos para previsão do comportamento auxético das estruturas estudadas tendo como base as alterações da sua geometria quando cargas de tração são aplicadas, prevendo igualmente a sua resistência à tração.

Além disso, as estruturas auxéticos em material compósito foram utilizadas no reforço de parede de alvenaria. Os provetes de parede de alvenaria reforçados foram testados à flexão em três pontos e os resultados foram comparados com uma parede de alvenaria reforçada convencionalmente recorrendo a uma grellha metálica. As paredes reforçadas por estruturas auxéticas apresentaram um bom desempenho sob carga de flexão quando comparadas com a parede convencional, no entanto, apresentaram maior nível de fissuração devido à expansão lateral do material de reforço. O presente trabalho de investigação abriu novas oportunidades para utilização de materiais auxéticas no campo da engenharia civil servindo como ponto de partida para os trabalhos, nesta área, que se seguirão.

TABLE OF CONTENTS

LIST OF FIGURES

LIST OF TABLES

LIST OF ACRONYM

FRP	-	Fibre reinforced polymer
BCRs	-	Braided composite rods
GFRP	-	Glass fibre reinforced polymer composites
CFRP	-	Carbon fibre reinforced polymer composites
AFRP	-	Aramid fibre reinforced polymer composites
BFRP	-	Basalt fibre reinforced polymer composites
NPR	-	Negative Poisson's ratio
GFRC	-	Glass fibre reinforced concrete
CFRC	-	Carbon fibre reinforced concrete
BFRC	-	Basalt fibre reinforced concrete
PP	-	Polypropylene fibre
RC	-	Reinforced concrete
NSM	-	Near surface mount
HAY	-	Helical auxetic yarn
FEA	-	Finite element analysis
DHY	-	Double helix yarn
CCD	-	Charge-coupled device
LED	-	Light emitting diode
WOR	-	Work of rupture

Chapter 1
Introduction

1.1. General framework and motivation

Composites refers as a combination of two or more materials that provide better properties than individual ones. The term Fibre Reinforced Composites refers to "*Composite materials are those solid materials composed of* ***binder*** *or* ***matrix*** *that surrounds and holds in place* ***reinforcements***" [1]. Fibres are the most widely using reinforcing material to produce composites namely fibre reinforced polymer (FRP) composites. Fibre reinforced polymers are a kind of composite materials, manufactured from high strength and modulus fibres embedded with or bonded to a matrix with distinct boundaries between them. Most commonly used fibres are glass, basalt, carbon, aramid and high strength steel; common polymer matrices are epoxies and esters [2 – 5].

FRPs have considerable advantages over conventional structural materials such as steel, including low weight due to less density of fibres, corrosion resistance and easy handling during applications. FRPs are very much suitable for structural applications mainly to repair concrete reinforced elements, pre-stressed concrete, masonry and wood structural elements [5]. FRPs started to be used in civil engineering application since 1980s, and since then a large numbers of projects have been started to demonstrate the application of FRPs in various structural elements. FRPs have been used successfully to retrofit all basic structural components, namely, columns, beams, slabs and walls. These

FRPs are applied to existing structures to enhance any or more of the following properties [5]:

- ✓ Tensile, shear or flexural load capacities;
- ✓ Ductility for enhanced seismic and blast application;
- ✓ Increased durability against worst environment conditions;
- ✓ Enhanced fatigue life;
- ✓ Stiffness increase.

Braided composite rods (BCRs) is a kind of composite material reinforced with high strength and modulus fibres in the core and low or high stiffness fibre in the sheath. BCRs were introduced in civil engineering applications for the replacement of steel mimicking its stress-strain characteristics. The load-deformation behaviour of the braided structures can be tailored by selecting the core and the sheath fibres. BCRs offer several advantages over the other type of FRP rods such as simple and economical manufacturing process, tailorable mechanical properties and good bonding behaviour with civil structural elements [6 – 8].

Auxetic materials are kind of innovative material which own unusual behaviour, i.e. possessing negative Poisson's ratio. It can be explained that usually when a material is stretched, for example an elastic band, it will become longer in the stretched direction and thinner in cross-section. Similarly, in compression expands transversely. Whereas, auxetic materials expands in transverse direction in tension and shrink laterally in compression [9-10]. Auxetic materials gained interest over the past three decades due to their superior physical properties due to their negative Poisson's ratio under strain. They are improved strength, enhanced fracture resistance, superior energy absorption, superior acoustic behaviour, good indentation resistance, and improved damping [11-18].

Auxetic materials are available in different forms, from micro to nano scales, for example, liquid crystalline polymers, microporous polymer, fibres, foams, honeycombs, bio-materials, structure, nano composites, FRP composites, etc. Auxetic composites can find potential applications in automotive, protection and aerospace industries, where non-auxetic composite with high specific strength and stiffness are currently used. The auxetic property can also be achieved with certain structural designs. In the last few decades, dissimilar geometric structures and models exhibiting auxetic behaviour have been proposed, studied and tested for their mechanical properties. The main auxetic structures

reported are two dimensional (2D) and three dimensional (3D) re-entrant structures, rotating rigid/semi-rigid units, chiral structures, and missing rib or lozenge grid [19 – 21]. Composite auxetic structures from BCRs offer novel solution combining the advantages of auxetic material and BCRs.

1.2. Objectives

The objective of this research is to development of novel auxetic structures based on fibre reinforced braided composites for civil engineering applications. In this way, it is intended to study various configurations of auxetic structural designs, selected from different literature already reported using braided composite rods as basic elements. These novel composite auxetic structures are optimized in terms of their mechanical behaviour and its masonry reinforcing capabilities analysed and discussed. The specific objectives of this thesis includes:

- Development of novel composite auxetic structures based on missing rib or lozenge grid and re-entrant hexagon design.
- Evaluation of the auxetic behaviour of the structures by feasible technique, e.g. image-based feature tracking method.
- Optimisation of developed auxetic structures by studying the effect of structural and material parameters on their mechanical behaviour (Poisson's ratio and tensile properties).
- Studying the auxetic behaviour of structures by suitable analytical model and development of numerical model for these novel structures.
- Studying the effect of auxetic structures reinforced civil structural elements (reinforced mortar and reinforced masonry) under tensile and flexural loads.

1.3. Outline of the thesis

The aforementioned objects are studied and elaborated in detailed manner in eight chapters, as follows:

Chapter 1 introduces the framework of the Thesis and motivation behind this novel works is provided along with specific objectives.

Chapter 2 provides the literature review about fibrous and composite materials used in civil structural applications and brief review about auxetic materials and structures. Also, this section describes the requirements of novel composite structure for structural applications.

Chapter 3 presents the materials used in this works and their mechanical properties. Also, the section contains the procedure of relevant testing carried out in this work. The calculation of Poisson's ratio and work of rupture is given in this section.

Chapter 4 presents development of composite auxetic structures from BCRs based on *missing rib or lozenge grid*. The auxetic behaviour of developed structures were evaluated by using image based tracking methods with suitable set-up. Also, the effect of structural and material parameters on auxetic and tensile behaviour was studied and summarized. The developed auxetic structures exhibits higher strain, which is drawback in the sense of civil engineering applications. The problem is resolved by modifying the basic auxetic structures and studied their auxetic and tensile behaviours.

Chapter 5 presents the development of composite auxetic structures from BCRs based on re-entrant hexagon design. The auxetic behaviour of structures were evaluated by using image analysis technique. The developed structure was optimized by studying their various parameters related to the structures. Also, the structure is modified to suit strengthening purpose of civil structural elements.

Chapter 6 presents the calculation of auxetic behaviour of developed structures using suitable analytical models which are reported in literature. The analytical model was modified to fit with developed auxetic structures. The new analytical models were developed to calculate the auxetic behaviour of structures developed based on modified designs. Also, the numerical modelling has been developed to study their tensile and auxetic behaviour of developed structures.

Chapter 7 presents the performance of the auxetic structures reinforced (both the design) structural elements (mortar and masonry) under tensile and flexural loads. The results are compared with plain grid (commercial design) reinforced structural elements. The overall effectiveness of the auxetic structures with structural elements also provided in this section.

Finally, Chapter 8 presents the main conclusions of the thesis and a proposal for future work.

Chapter 2

Literature Review

2.1. Introduction

Fibres have been used in the construction field since ancient time. Straw and hair fibres were used to reinforce brittle materials which was used to build house. In late 19th century, asbestos fibre was used in large quantity in the construction field. However, due to health hazards associated with asbestos fibres, alternate fibres started to be introduced in the field since 1950s. Glass and steel fibres were used as reinforcing elements into concrete and its behaviour extensively studied. The use of fibre reinforced construction materials offers many improvements in the properties, when compared to conventional materials, including tensile strength, elastic modulus, compressive strength, durability, crack resistance, crack control, fatigue life, etc.

Apart from glass and steel, other high performance fibres were started to be used to reinforce structural elements including carbon, basalt, aramid and polypropylene. In order to avoid the environmental problems of these manmade fibres, natural fibres (cotton, flax, jute, coconut, hemp, etc.) are also being extensively studied in civil engineering applications [22 – 26].

Other than fibres, fibre reinforced polymers (FRPs) or fibre reinforced polymer composites (FRPC) have been widely accepted and initiated to be used in structural

elements to enhance physical and mechanical properties. FRPs are applied externally to the structures with polymeric resins and improve ductility and energy absorption property, tensile strength along with shear strength. FRP materials also improve the stiffness of structural elements. FRPs have many superior properties such as high strength to weight ratios and are effectively corrosion free. FRPs can be used as a retrofit for existing structural elements very easily with minimal loss of existing space and disruption to the structure. The method is also cost-effective compared with other methods such as strengthening with bonded steel plates [27 – 34]. Composites widely used in the civil applications are glass fibre reinforced polymer composite (GFRP), carbon fibre reinforced polymer composite (CFRP), aramid fibre reinforced polymer composite (AFRP), basalt fibre reinforced polymer composite (BFRP), among others. [35, 36].

Auxetic materials are novel class of materials which possess negative Poisson's ratio (NPR). Due to the NPR, this materials exhibits improved properties compared to conventional materials including, fracture toughness, energy absorption, indentation resistance, etc. There are various auxetic materials such as polymer, fibre, fabric, composite, foam, etc. These auxetic materials can be used in wide range applications including, protective textiles, bulletproof materials, aeronautics materials, aerospace industry, etc. [17, 37 – 43].

This chapter further explains in detail about various fibres, resins, FRP composites used in civil engineering applications. Also, explained in detail about various auxetic fibrous materials, their properties and applications.

2.2. Fibrous and composite materials for civil applications

2.2.1. Fibres

The four main fibres used in the civil engineering applications are: glass, basalt, carbon, and aramid. Commonly, fibres can be used in various ways, with the performance changing of each [44]:

- The best performance in terms of strength and modulus in one direction comes from unidirectional reinforcement. When the fibres are arranged in parallel direction provides maximum performance under axial loading.
- Arranging the fibre in a weave or mat, strength can be achieved in more directions, although the maximum strength and modulus is reduced.

- Chopping the fibres into short lengths and arranged them randomly, uniform properties can be obtained in all directions. This is generally the cheapest technique, used for the least structurally demanding case.

Figure 2.1 shows fibrous materials configurations used to reinforce polymers with application in civil engineering.

Among the various fibres used in structural applications glass fibre is the least expensive and carbon fibre being the most expensive. The cost of basalt fibre slightly higher than glass fibre and the cost of aramid fibres is about the same as the lower grades of carbon fibre [45].

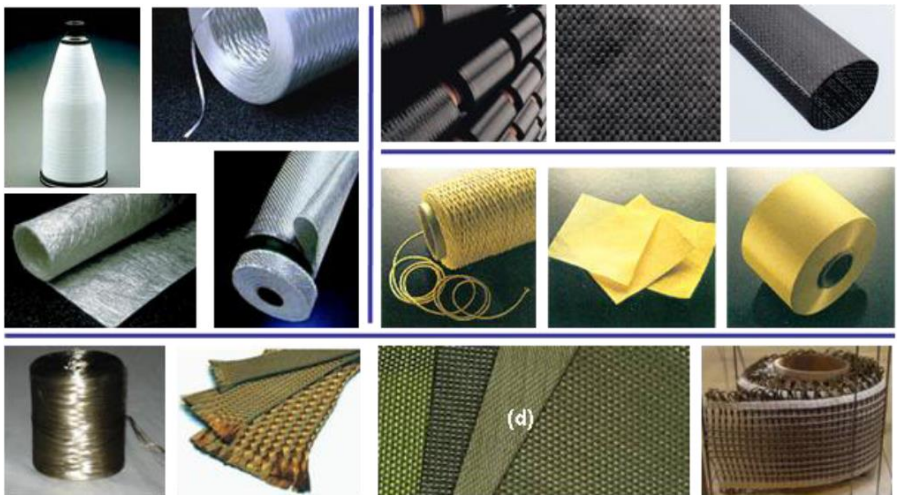

Figure 2.1. Fibre types in distinct configurations [45].

2.2.1.1. Glass fibre

Glass fibres exhibit the typical glass properties of corrosion resistance, hardness and inertness. Glass fibres are divided into three main classes – E-glass, S-glass and C-glass. The E-glass fibre is designed for electrical use and the S- glass for high strength. The C-glass is for corrosion resistance, and it is not uncommon for civil engineering applications. Among these three classes, E-glass fibre is the most common reinforcement material for civil engineering applications. It is produced from lime-alumina-borosilicate which can be easily extracted from abundance of raw materials like sand. The fibres are drawn into very fine filaments with diameters ranging from 2 to 13 μm. The glass fibre strength and modulus can deteriorate with aggregate temperature. Though the glass fibre creeps under a constant load, it can be designed to perform adequately. The fibre regarded

as an isotropic material and has a lower thermal expansion co-efficient than that of steel fibre. The properties of glass fibre is given in the Table 2.1 [46 – 50].

Table 2.1. Physical and mechanical properties of glass fibre [46-50]

Typical properties	**E- glass**	**S- glass**
Density (g/cm^3)	2.60	2.50
Young's modulus (GPa)	72	87
Tensile strength (GPa)	1.72	2.53
Tensile elongation (%)	2.4	2.9

***Properties of glass fibre reinforced concrete (GFRC)*:** GFRC doesn't fail instantly underload, but yields steadily nonetheless in cement and concrete. Tensile failure begins with micro cracks and propagate fast and cause damage. This is due to randomly distributed fibre in GFRC, uniformed dispersed fibres develops the loads in a wide range and let the matrix to behave cohesive. The presence of glass fibres in GFRC offer crack arresting behaviour. GFRC has higher tensile strength than steel. Generally, the higher the fibre content higher the strength.

GFRC perform excellently under the salt water and marine environment, as there is no steel reinforcement to corrode. GFRC also possess high damping capacity and low coefficient of thermal expansion. Resistance against acid attack is enhanced with addition of glass fibres into the concrete mixture. It is also noticed that there is no effect of sulphates on GFRC. Chloride permeability of GFRC shows less when compared with ordinary concrete [51 – 53].

2.2.1.2. Basalt fibre

Basalt fibres are produced by melting crushed volcanic rocks and known primarily for its resistance to high temperatures, strength, and durability, widely spread all around the world, in which SiO_2 accounts for the main part, followed by Al_2O_3, then Fe_2O_3, FeO, CaO and MgO. For this reason, basalt rocks are classified according to the SiO_2 content as alkaline (up to 42% SiO_2), mildly acidic (43 to 46% SiO_2) and acidic basalt (over 46% SiO_2). Only acidic types of basalt satisfy the conditions for fibre preparation. The properties of basalt fibre is given in the Table 2.2 [47, 54, 55].

Table 2.2. Physical and mechanical properties of basalt fibre [47, 54, 55]

Typical properties	Value
Density (g/cm^3)	2.65
Young's modulus (GPa)	79 – 93
Tensile strength (GPa)	3.0 – 4.8
Tensile elongation (%)	3.10

Properties of basalt fibre reinforced concrete (BFRC) includes [55 – 58]:

- Workability of concrete can be improved by addition of 0.5% by volume of basalt fibre into the mixture.
- Larger quantities of fibres compared to PP fibres can be added without any problems, i.e. balling or segregation.
- The performance of BFRC is almost similar compared to PPFRC.
- Compared to plain concrete, there is significant improvement in impact resistance and toughness.
- The addition of fibres into the concrete, leads to change on the failure mode from a brittle to ductile failure, when subjected to bending, impact and compression.
- Compressive strength of basalt fibre reinforced concrete increases up to 14% compared to plain concrete.
- Percentage increase of split tensile strength of basalt fibre reinforced concrete compared to plain concrete is about 62%.
- Flexural strength of basalt fibre reinforced concrete found increase about 50% than plain concrete.
- The level of strength increase of basalt fibre reinforced concrete depends on concrete age.

2.2.1.3. Carbon fibre

Carbon fibre can be produced from the three types of polymer precursors: polyacrylonitrile (PAN), rayon, and pitch. Pitch fibres are cheaper than PAN based fibres, but possess lower strength. The tensile stress-strain curve is linear to the point of breakage. There are many carbon fibres available in the market, but they can be arbitrarily categorized into three grades, as shown in the Table 2.3. Carbon fibres are lightweight and strong with excellent chemical resistance. Carbon fibres have lower thermal

expansion co-efficient than both aramid and glass fibres. The fibre is an anisotropic material, and its transverse modulus are greater than longitudinal modulus in an order of magnitude. The fibre has a very high fatigue and creep resistance [47,49,50,54,59 – 61].

Table 2.3 Physical and mechanical properties of carbon fibres [59-61]

Typical properties	**High strength**	**High modulus**	**Ultra-high modulus**
Density (g/cm^3)	1.8	1.9	2.0 – 2.1
Young's modulus (GPa)	230	370	520 – 620
Tensile strength (GPa)	2.48	1.79	1.03 – 1.31
Tensile elongation (%)	1.1	0.5	0.2

The characteristics of carbon fibre reinforced concrete (CFRC) includes [61]:

- High tensile strength – smaller cross section, earth quake resistance;
- Higher durability – corrosion free and less running cost;
- Eco-friendly – less materials needed for maintenance and construction;
- Low weight – easy to handle;
- High flexibility;
- High abrasion resistance – suitable for highway construction;
- Low co-efficient of thermal expansion – high fire resistance;
- Increase of flexural strength and toughness;
- High compressive strength;
- Decrease of electrical resistance;
- Decrease of dry shrinkage;
- High split tensile strength.

2.2.1.4. Aramid fibres

Aramid fibres are polymeric fibres, where polymeric chains are aligned and made rigid aromatic rings linked by hydrogen bridges. Fibres main properties are high strength, impact resistance due to their energy absorption, low-density and moderate modulus. Aramid fibres are susceptible to degradation under moisture and UV light, but exhibit resistance to acids and alkalis. They have excellent fatigue and creep resistance. As an anisotropic fibre, its transverse shear modulus is less than those of longitudinal direction. The fibres can have difficulty achieving a chemical or mechanical bond with the resin.

The properties of commercially available aramid fibres are given in Table 2.4 [47, 49, 50, 62 – 64].

Table 2.4 Physical and mechanical properties of aramid fibres [49, 50, 63]

Fibre type	**Density, (g/cm^3)**	**Elongation, %**	**Modulus, GPa**	**Tenacity, GPa**
Kevlar 29	1.43	3.6	70	20-23
Kevlar 49	1.45	2.8	135	20-26
Kevlar 119	1.44	4.4	55	--
Kevlar 129	1.45	3.3	99	--
Kevlar 149	1.47	1.5	143	18
Nomex	1.38	22	17	5.8

2.2.1.5. Polypropylene fibres

Polypropylene (PP) is a thermoplastic polymer used in wide variety applications including textiles, packaging, civil, marine ropes, etc. Mostly, isotactic PP is used for industrial applications due to their high crystallinity. PP is normally tough, flexible and resistance to fatigue. The suitable properties of PP with respect to civil engineering application includes:

- The fibre has good resistance to almost all chemicals. Any chemicals that will not attack the concrete mixture will have no effect on the fibre either.
- The fibre is hydrophobic and it will not wet by cement paste helps prevent chopped fibres from balling effect during mixing like other fibres.
- The orientation leaves the film feeble in the horizontal direction which helps fibrillation. The cement matrix can therefore infiltrate in the mesh structure between the individual fibrils and develop mechanical bond between fibre and matrix. The properties of PP fibre are given in Table 2.5 [47, 65, 66].

Table 2.5 Physical and mechanical properties of PP fibre [47, 65, 66]

Typical properties	**Values**
Density (g/cm^3)	0.91
Tenacity (g / denier)	3.5 – 9.0
Elongation (%)	10 – 45
Moisture regain (%)	0.0

Properties of PP reinforced concrete

Fibres before mixing into the concrete, the amount and length and design mix variables need to be adjusted to prevent the fibres from balling. Good fibre reinforced concrete mixture normally comprise a high mortar volume as compared to conventional concrete mixtures. The aspect ratio for the fibres are usually chosen between 100 to 200 since fibres which are too long tend to "ball" in the mix and create work-ability problems.

PP fibres are used in two different ways to reinforce cementitious matrices. One is in thin sheet constituents in which PP offers the principal reinforcement. Its volume content is relatively high over 5%, in order to get both toughening and strengthening. Other is in fibre form and volume content is less than 0.3%, and it is anticipated to act as mainly as secondary reinforcement to control crack.

Effects on Fresh concrete: the work-ability of concrete mainly decides on slump test. The addition of PP fibres decreases slump value significantly. The concrete mixture with PP fibres leads to fewer rate of bleeding and segregation as compared to plain concrete. PP fibres in concrete mixtures also help reduce early plastic shrinkage cracking, improve the tensile capacity, decrease the number of cracks, and bridging of cracks.

Effects on hardened concrete: the addition of fibres in the concrete increases the splitting tensile strength approximately 20 – 50%.

Compressive strength: the inclusion of fibre in concrete has null effect on compressive property of concrete.

Flexural tensile strength: flexural tensile strength increases with increase of volume fraction of fibre. It is also noticed there was improvement in strength for with the increase of fibre aspect ratio.

Fracture properties: the failure behaviour of high strength concrete is successfully improved by the use of fibres. The typical shear bond failure due to strain localization could be avoided.

Creep and shrinkage properties: addition of fibres decreases creep strain. Shrinkage of concrete, which is the result of removal of water from concrete during drying, is also decreased by fibres.

Flexural impact properties: the properties improved significantly with relatively low fibre volume ratio [67 – 73].

2.2.1.6. Other fibres

Apart from above said synthetic fibres some natural fibres are also used in civil engineering applications. Vegetable fibres are extracted from various part of plants and categorized as seed fibres, leaf fibres, bast fibres, stalk fibres, and fruit fibres. Seed fibres are fibres extracted from seeds of the plants, e.g. cotton and Kapok. Leaf fibres are fibre collected from leaves of the plants, e.g. sansevieria, fique, sisal, banana and agave. Bast fibres are fibres collected from the skin or bast surrounding the stem of the plants. These fibres has higher tensile strength than other vegetable fibres, e.g. Jute, Flax, kenaf, hemp, ramie, rattan and vine fibres. Fruit fibres are collected from the fruit of the plants or tree, e.g. coconut (coir) fibre. Stalk fibres are actually stalk of the plants, e.g., straws of wheat, rice, barley, and other crops include bamboo and grass.

The most used vegetable fibres in the civil engineering applications for the reinforcement of mortars and concrete are cotton, flax, hemp, sisal, jute, bamboo and coconut (coir) fibres. The use of vegetable fibres in concrete provides an exciting challenge to the housing construction industry, particularly in non-industrialized countries since they are a cheap and readily available form of reinforcement, require only a low degree of industrialization for their processing and, in comparison with an equivalent weight of the most common synthetic reinforcing fibres, the energy required for their production is small and hence the cost of fabricating these composites is also low. In addition, the use of a random mixture of vegetable fibres in cement matrices leads to a technique that requires only a small number of trained personnel in the construction industry. Vegetable fibre cement composites this pose the challenge and the solution for combining unconventional building materials with conventional construction methods [74 – 76]. The properties of fibres used in civil engineering applications are given in the Table 2.6.

Table 2.6 Physical and mechanical properties of various natural used in civil engineering applications [77]

Properties	**Sisal fibre**	**Coir fibre**	**Jute fibre**	**Hemp fibre**	**Flax fibre**
Density (g/cm^3)	1.3 – 1.5	0.67 – 1.2	1.3 – 1.5	1.5	1.4 – 1.5
Elongation (%)	2.0 – 2.5	15 – 30	1.5 – 1.8	1.6	1.2 – 3.2
Young's modulus (GPa)	9.4 – 28	4 – 6	10 – 55	70	50 – 70
Tensile strength (MPa)	511 – 635	131 – 230	390 – 800	550 – 900	340 – 1500

2.2.1.7. Resins

Resins are the polymer binders that hold the fibres together and transfer the loads between the fibres in addition to guarding them from environmental factors and carrying shear loads. There are various polymer matrices which can be used to produce FRP composites, but in construction industry only a relatively small number is actually used. According to their nature, there are two major types of polymers, which determine the methods of manufacturing and the properties of the composite: (i) thermoplastic and (ii) thermosetting. FRPs were all based on thermosetting polymers and, besides the fact that thermoplastic have seen rapid growth in recent years, thermosetting is still the most used in civil engineering applications [78].

Thermoplastic polymers are long chain molecules held together by relatively weak *Van der Waals* forces. These polymers can be amorphous, which implies a random structure with a high concentration of entanglement, or crystalline, with a high degree of molecular order [79]. The semi-crystalline polypropylene and nylon are especially popular as matrices. Thermosetting polymers are usually made from liquid or semi-solid precursors which harden irreversibly; this chemical reaction is known as cure and on completion, the liquid resin is converted to a hard solid by chemical cross-linking which produces a three dimensional network of polymer chains. This family of polymers has an imperative quality when used as matrices in FRP, which is the low viscosity of the precursor liquids, prior to cross linking that facilitates wetting of reinforcement fibres. The main polymers used in construction under this heading are:

- ❖ Unsaturated polyesters. Currently, these are the most widely used polymers in construction, as matrix of FRP. They are relatively low cost materials and are easy to process at an ambient temperature of cure. They can be formulated in hundreds of diverse ways to craft their properties to numerous manufacturing process and can easily be filled and pigmented.
- ❖ Epoxies. In general, epoxies have high dimensional stability and specific strength. They are particularly known by their adhesion ability with many substrates, and low shrinkage during the cure. A wide variety of formulations are available giving a broad spectrum of properties. They can be processed at both room and elevated temperatures. Epoxies have excellent environmental and chemical resistance, when compared with unsaturated polyester.
- ❖ Vinyl esters. These polymers have similar mechanical and in-service properties to those of the epoxy resins and equivalent processing techniques to those of the unsaturated polyesters. Generally they have good wetting characteristics and have resistance to strong acids and strong alkali conditions. They can, also, be processed at both room and elevated temperatures.
- ❖ Phenolic. The most important characteristic of this family of polymers is there good flame retardant properties, low smoke generation and high heat resistance. For this reason, they are used when required fire resistance.

According to Hollaway and Head [80], the requirements for a good FRP matrix are the following:

- ✓ wet out the fibre and cure satisfactory in the required conditions;
- ✓ bind together the fibres and protect their surfaces from abrasion and environmental ageing;
- ✓ disperse the fibres an separate them in order to avoid any catastrophic propagation of cracks;
- ✓ transfer stresses to the fibres efficiently;
- ✓ chemically and thermally compatible with fibres;
- ✓ have appropriate fire resistance and limit smoke propagation;
- ✓ provide well aesthetic finish (colour and surface).

The properties of thermoset polymer matrices given in Table 2.7 [80].

Table 2.7 Physical and mechanical properties of thermoset resins [80]

Property	Polyester	Vinylester	Epoxy
Strength (MPa)	20 – 70	68 – 82	60 – 80
Elastic modulus (GPa)	2 – 3	3.5	2 – 4
Strain at failure (%)	1 – 5	3 – 4	1 – 8
Density (g/cm^3)	1.2 – 1.3	1.12 – 1.16	1.2 – 1.3
Glass transition temperature (Tg) (°C)	70 – 120	102 – 150	100 – 270

2.2.2. Fibre reinforced polymer composites

Fibre reinforced polymer composites (FRPC) are advanced composite materials made of a polymer matrix reinforced with fibres. The fibres are usually glass, carbon and aramid, while the polymer matrix are usually polyester, vinyl ester and epoxy thermosetting polymers.

2.2.2.1. Glass fibre reinforce polymer composites (GFRP)

Glass fibre reinforced polymer composite is one of the major FRPs used in the construction field to improve the properties of structural elements, e.g. shear strength, flexural strength, tensile strength, etc. There are many varieties of glass fibres such as S-glass, E-glass, A-glass, C-glass, AR-glass, etc. Out of this, both *S* and *E* glass are found suitable for making reinforcement fabrics; but E-glass fibre is more economical and does not lose its stiffness with time or at high temperatures compared to S- glass fibre [49, 81-83]. E-glass fibre is an alumino-borosilicate glass, and it has less percentage of alkali. This low alkali content will be beneficial while interacting with cement material. Epoxy and Vinyl ester are the most widely used resins for retrofitting of structures with GFRPs as well as for making composite laminates. GFRPs can be made into many shape including strips, continuous sheets, rods, rebars and sandwich structures with other fibrous materials and used in existing civil structures to increase their mechanical behaviour [83].

Researchers have used composite laminates prepared from various commercially available glass fabrics to improve properties of civil structures. The range of properties of GFRP laminates is given in Table 2.8 [84-88].

Table 2.8 Physical and mechanical properties of GFRP composite [84-88]

Properties	Values in Range
Tensile Strength (MPa)	300 – 2300
Tensile Modulus (GPa)	17 – 72
Elongation at break (%)	2.08 – 3.2
Thickness (mm)	0.33 – 1.3
Weight (g/m^2)	325 – 915

Characteristics of glass fibre reinforced composites includes:

- ✓ Linear elastic behaviour up to failure (no ductility);
- ✓ Orthotropic behaviour;
- ✓ High longitudinal strength (similar to steel);
- ✓ Low elasticity (10 – 20% of steel) and shear modulus;
- ✓ Low density (20 – 25% of steel).

2.2.2.2. Carbon fibre reinforced polymer composites (CFRP)

CFRP is an extremely strong and light FRP material. The polymer most often used in CFRP is epoxy, but other polymers, such as vinyl ester, polyester or nylon are sometimes used [89, 90].

The following are the general properties of CFRP:

- The strength and modulus of elasticity are very high when compared to GFRP and aramid-FRP, even for the same fibre weight.
- The design strength is significantly higher compared to other FRPs. The strain is low for CFRP and this gives a higher design capacity (see Figure 2.2).
- The durability with the time of carbon fibre wraps is far better than that of other FRPs.
- CFRP shows good fatigue resistance [91].

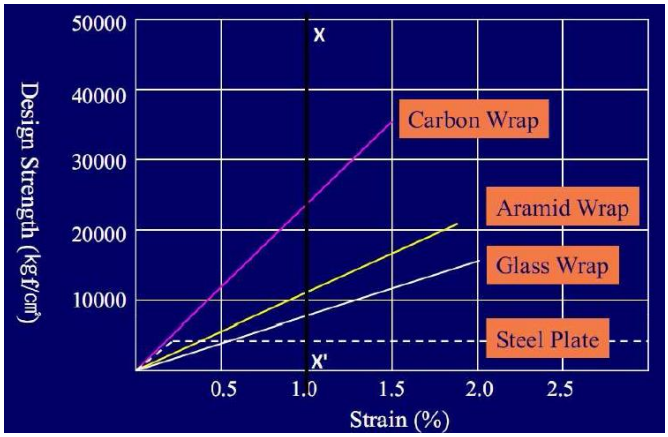

Figure 2.2 - Design strength vs. strain for major FRPs used in civil engineering applications [91].

Over the past two decades, CFRPs has become an increasingly notable material for structural engineering applications. Applied to reinforced concrete (RC) to improve flexural properties, CFRPs typically have large impact on strength (doubling or more increase in strength is not uncommon), but provide only moderate increase in stiffness. CFRPs can also be applied to enhance the shear strength of RC by wrapping fabrics or fibres around the section to be strengthened. Wrapping around sections (such as bridge or building columns) can also enhance the ductility of the section, greatly increasing the resistance to collapse under blast loading. CFRPs has very good durability than other FRPs and it's relatively high stiffness can afford efficient confinement with minimum wraps [49, 92]. Properties of carbon fibre reinforced polymer composites are given in Table 2.9.

Table 2.9 Physical and mechanical properties of CFRP composite [49, 92]

Properties	**Values in Range**
Tensile strength (GPa)	3 - 7
Tensile modulus (GPa)	150 - 450
Elongation at break (%)	1.8 – 2.0
Density (g/cm^3)	1.5 – 1.6

2.2.2.3 Aramid fibre reinforced polymer composite (AFRP)

AFRP have high fracture toughness, high strength, high elastic modulus, and 40% lower density than GFRP. The AFRP is much costlier than GFRP and basalt fibre

reinforced polymer composite (BFRP) making them little consideration in civil engineering applications. AFRP absorbs moisture, so careful storage and planning of project using AFRP is critical when applied to structures. The composite has less compressive strength than other FRPs. The properties of AFRP are given in Table 2.10 [93, 94].

Table 2.10 Physical and mechanical properties of AFRP composite [93, 94]

Properties	Values in Range
Tensile strength (MPa)	3000
Tensile modulus (GPa)	70 - 120
Elongation at break (%)	1.6 – 1.8
Density (g/cm^3)	1.4

2.2.2.4. Braided composite rods (BCRs)

Braiding technique is one of the most ancient production process (since 1800s) to produce textile structures. This technique is commonly used for the production of ropes and cables. A braiding machine has fibre carriers (more than three) moving in circular pattern. Half of the carriers move clockwise, and others move anticlockwise, in an intertwining serpentine motion producing a desired braided pattern (see the Figure 2.3). Braided structures are also very interesting for composite reinforcements due to their characteristics: conform-ability, in-plane multi-axial orientation, excellent damage tolerance and low cost [95, 96].

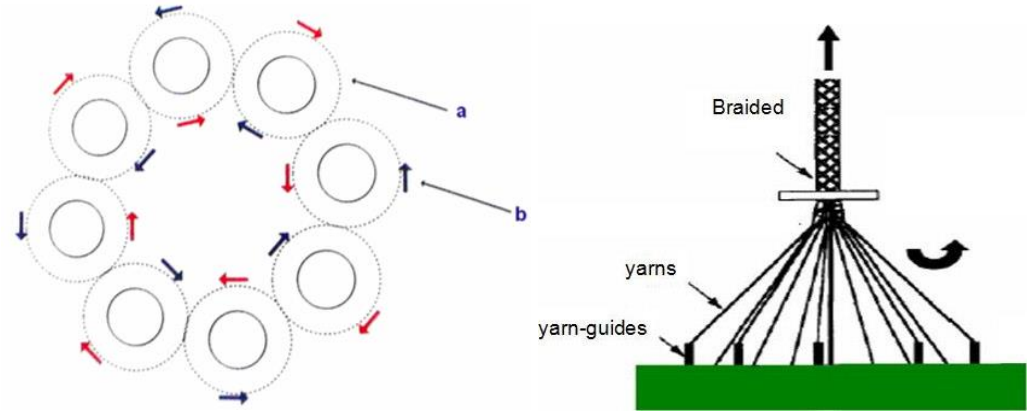

Figure 2.3. Carriers moving direction and braiding machine [95, 96].

Axial (core) reinforced braided structures are braided tubular structures presenting, besides one system of yarns moving helically and a core reinforcement yarns introduced axially (Figure 2.4). The two systems of yarns or fibres can be varied according to the requirements of specific applications [97].

The core reinforcement fibres are responsible for the mechanical performance of core reinforced braided structures. Braided composite rods (BCRs) are produced by using conventional braiding machine with minor adjustment in the machine. The braiding machine is equipped with a resin bath where the core reinforcement fibres pass through in a polymer matrix, at the point before braiding action (Figure 2.5). Therefore, it is ensured that the impregnation of the axial reinforced braided structure occurs from inside to the outside of the structure [97].

In addition, a braiding ribbed structure can be produced by varying linear density of the sheath yarns. Also, the braided composite rods can be produced by varying axial reinforcement fibres and type of resin. With help of braiding technique composite rods can be produced with specific mechanical, physical and chemical properties for specific applications [97].

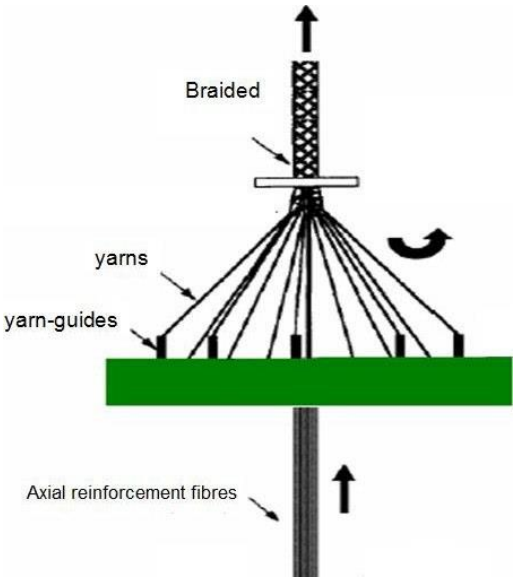

Figure 2.4. Braiding with axial reinforcement fibres [97].

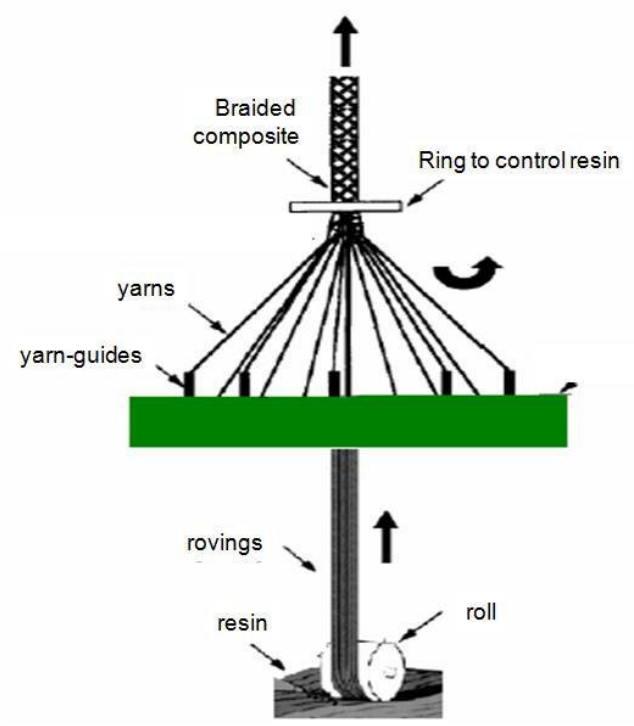

Figure 2.5. Braiding with axial reinforcement and resin bath set-up [97].

2.2.2.5. FRPs for structural applications

Recently, composites found potential application in construction industry as strengthening material for many problems associated with the deterioration of civil structures. Over the period, composites are considered replacement of steel in construction industry due to their superior properties and reduction of cost of FRPC materials [98]. Composites are used to improve the various properties of structural elements and they are explained in detail as follows,

Flexural strength: Flexural strengthening of reinforced concrete (RC) beams using composites can be offered by epoxy bonding of FRPC plate to the portion of elements in tension, with fibres parallel to the principal stress direction. If fibres are placed perpendicular to cracks, a huge increase in stiffness and strength is achieved compared to situation where fibres are placed diagonal to the cracks. Flexural performance of strengthened RC beams with FRPC is depends on several factors including, type of fibres, length of laminate, width of laminate, amount of main and shear reinforcement, FRPC configuration, number of layers in FRPC, damage and loading condition, concrete strength and cover, etc.[98].

Ductility: A variety of indices including deformability ratios, energy ratios have been suggested measuring ductility. Experiments have indicated catastrophic failure of strengthened beams due to low ductility. Researchers have suggested anchorage system to enhance ductility, which is not affected by the change in the loading rate. Researchers performed experiments by using innovative triaxially braided ductile fabric which was reported to increase ductility. It was reported that torsional capacity of RC beams can be increased up to 70% with the help of FRPC strengthening. It is also observed from the results fatigue life of reinforced concrete beams could be significantly enhanced through the use of externally bonded CFRPC laminate and it is largely depended on the stress range applied to steel reinforcements [98].

Shear strength: Shear strengthening of RC elements can be offered by epoxy bonding of FRPC materials with the fibres parallel to the direction of the shear stresses. It was perceived that the shear strength of newly constructed RC beam can be improved by 60 – 120% using FRPC sheets. Fibre orientation may be perpendicular to the shear cracks. Shear contribution by the FRPC strengthening to the total shear capacity depends on many parameters including surface preparation, amount of main and shear reinforcement, composite fabric shear reinforcement ratio, strength of FRPC, shear span to effective depth ratio, number of FRPC layers, etc. U-wrap of sheet offered the most effective strengthening of beams with about 119% increase in shear strength [98].

Energy absorption: Wrapping of FRPC sheets around concrete columns is a promising method for structural rehabilitation and strengthening. One of the deficiency in concrete columns is the lack of lateral confinement and low energy absorption capacity. Externally confinement of concrete considerably increases strength, energy absorption and ductility of concrete specimens by building RC cage around existing columns [98].

Seismic retrofit: Retrofitting of column components to withstand earthquakes is a recent and widespread task and one of the more complex engineering challenges. Seismic resistance of FRPC retrofitted column increases considerably because of confining action of FRPC wraps. The technique has been noticed to enhance displacement ductility as well as strength [98].

Blast resistance: The numerous blast resistance studies have been conducted on civil structural elements retrofitted with various form fibrous and composite materials. The types of fibrous and composite materials are GFRP, CFRP, steel fibre, aramid, PU; Nano-

particle reinforced Polyurea and hybrid textile (aramid/glass). Fibrous and composite materials are used in blast protection of structural elements in various form includes; fibres, composite strips, laces, rebars, spray-on materials and NSM rods. The composite materials produced from glass and carbon fibres are used to protect the structural elements from high mass of explosives at different stand-off distances (close or far from the blast source). Researchers measured or observed blast resistance property of retrofitted structural elements in terms of delamination of composite materials from elements, wall failure pattern, debris speed and debris level, increase of ductility, cracks of the wall, wall displacement, increase of flexural strength, energy absorption, toughness, etc., These studies showed that the utilization of fibrous and composite materials as retrofits of existing structures can significantly increase the blast protection by reducing the fragmentation and debris which will help further to avoid loss of occupant lives and to protect property and structures [2].

2.3. Auxetic materials

2.3.1. Introduction of auxetic materials

The Poisson's ratio of any material is defined as the negative ratio of transverse strain to axial strain in the direction of loading (longitudinal strain). In general, materials have positive Poisson's ratio, i.e. stretching in one direction (axial) results in reduced dimension in the other direction (transverse); but in auxetic materials the phenomenon is just the opposite, i.e. stretching in one direction results in widening in another direction (Figure 2.6). Therefore, auxetic materials possess negative Poisson's ratio. Wide range of auxetic materials and structures has been discovered and manufactured both at micro and macro scales. For anisotropic materials, the values of Poisson's ratio can vary in a wider range as compared to those of isotropic materials. The variation in the Poisson's ratio clearly depicts that the negative Poisson's ratios or auxetic effects are theoretically permissible.

Auxetic materials are of particular interest due to their counterintuitive behaviour under strain as well as improved properties such as enhanced strength, better acoustic behaviour, improved fracture toughness, superior energy absorption, damping improvement, and indentation resistance [99].

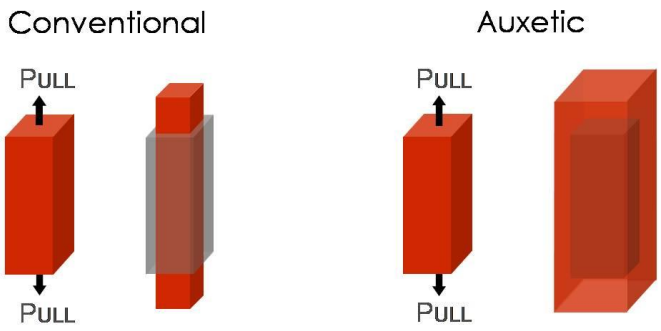

Figure 2.6. Auxetic material and conventional material [99].

2.3.2. Auxetic fibre, yarn and fabric

2.3.2.1 Auxetic textile fibre

Researchers produced various auxetic textile fibres including polyester, polyamide and PP. These fibres found potential applications such as fibrous filters, protective clothing, biomedical materials, and reinforcement in composites. The details of various auxetic textile fibres are given below.

Auxetic polyester fibre was produced from using polytrimethyleneterephthalate, which is procured from DuPont in the granule form. The granules are converted into powder form using cryogenic grinding before the extrusion. For the extrusion purpose the polyester particles of less than 150 µm were sorted out. 3GT granules and powder were pre-dried under partial vacuum oven at 108ºC for two days before extrusion. The 3GT powders are underwent melt spinning process to produce fibres. The fibres produced at 225°C with take-up speed 5 mpm (0.075 m/sec) and screw speed 5 rpm (0.525 rad/sec) exhibits negative Poisson's ratio, $\nu = -0.72 \pm 0.05$ [100, 101].

To produce auxetic nylon fibres, nylon® powder was used, which is commercially available Nylon-R grade, purchased from Nylon Colours. To know about thermal processing window the powder was subjected to DSC analysis. The SEM micrographs used to know about average powder particles size and it was found 43 µm. To avoid hydrolysis during extrusion, the nylon® powder was over dried for two days in vacuum at 80ºC. Melt spinning method was used to produce fibre and fibres produced at 195°C with screw speed 10 rpm (1.05 rad s^{-1}) and take-up speed of 2 mpm (0.03 ms^{-1}) exhibits negative Poisson's ratio, ranging between -0.15 to -0.25 [102].

Auxetic PP fibres produced from Coathylene PB 0580 powder supplied by Univar plc, UK. Fibre exhibit better mechanical properties and auxetic behaviour produced at processing temperature of 159°C with take-off speed of 2 mpm, screw speed of 1.047 rad s-1 and die diameter of 0.55 mm. The negative Poisson's ratio obtained through this process is about -2.5 [102].

2.3.2.2 Auxetic yarns

One of the most gifted auxetic material for practical application is helical auxetic yarn (HAY), first reported by Hook in 2003. HAY is a fibre structure consists of two fibres (flexible and stiff fibre), one fibre being the *core* around which is helically wound the second fibre, *wrap* (see Figure 2.7).

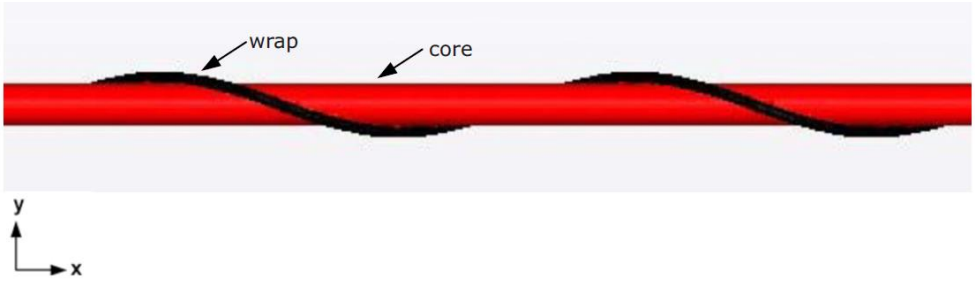

Figure 2.7. Components of HAY [103, 104].

Underload, the wrap fibre become straight which causes core displacement laterally in the helical manner (see Figure 2.8). If the wrap fibre have less diameter and stiff than core will results in nett increase in the effective diameter of the HAY under tension – a negative Poisson's ration. This novel behaviour leads to interesting textile application based on developing the ability to cause pores to open (see Figure 2.9).

Figure 2.8. Auxetic behaviour under tension [103, 104].

Figure 2.9. Textile application - pores open under tension in a complementary pair of HAYs [103, 104].

The static behaviour of this HAY has been examined under tension using Finite Element Analysis (FEA). The results show that the stiffness of the component fibres and the initial helical wrap angle are key design parameters, also the strain-dependent changes in cross-section should be taken in to consideration. It is observed that the structures shown non-linear behaviour due to non-zero individual components Poisson's ratio. The Poisson's ratio of the helical structures was observed as -5.0.

The key geometric parameters used to tailor the auxetic behaviour of HAY are:

- The starting angle of the wrap fibre dominates the magnitude of auxetic behaviour.
- The auxetic performance is also affected by the diameter ratio of wrap to core fibres and the inherent Poisson's ratio of the fibres [16, 103 – 105].

2.3.2.3 Auxetic fabrics

Knitting technology is one of the most attractive textile technology that can be used to produce fabrics with auxetic (negative Poisson's ratio) behaviour due to its high structure variety. There are various techniques to produce knitted fabrics such as weft and warp knitting.

Weft Knitted Auxetic Fabric: A suitable geometric design is chosen to produce NPR effect weft knitted fabric using computerized flat knitting machine. The knit pattern which will produce NPR effect is shown in Figure 2.10. The knitted fabric at the relaxed state is shown in Figure 2.11. The Poisson's ratio value obtained for these kinds of fabric is in the range of -0.02 to -0.5. The Poisson's ratio values are decreases with increase of strain. Also, the NPR value depends up on the structural parameters. Among the various parameters, the initial opening angle θ_0 is a key factor that affects the NPR effect. The fabric which are closely folded can lead to less θ_0 and consequently have higher NPR value [106].

There are few more auxetic weft-knitted fabrics based on three kinds of geometrical structures, i.e. re-entrant hexagon, rotating rectangle and foldable structure using computerized flat knitting machine. The fabrics are shown in Figure 2.12.

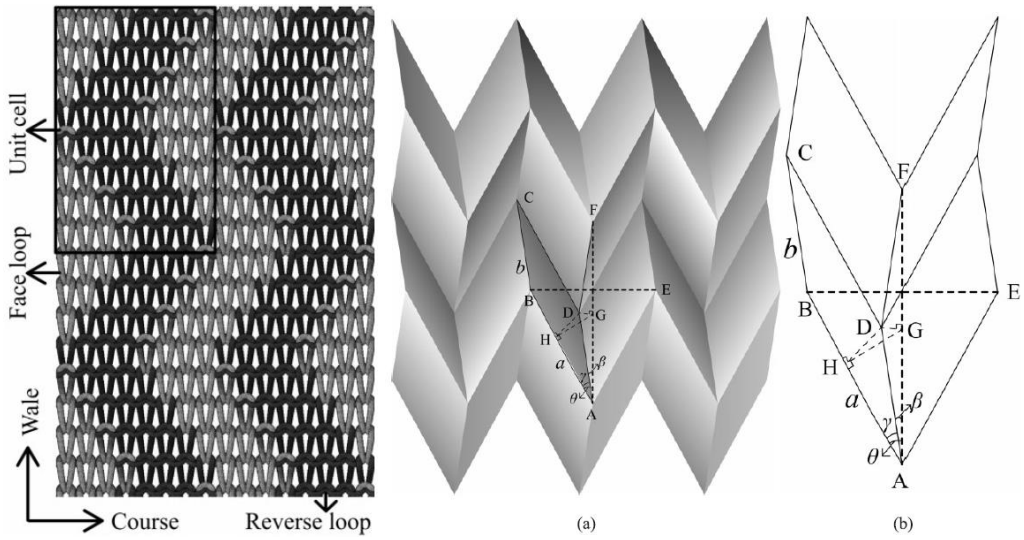

Figure 2.10. i) knit pattern and ii) (a) three dimensional structure and (b) unit cell [106].

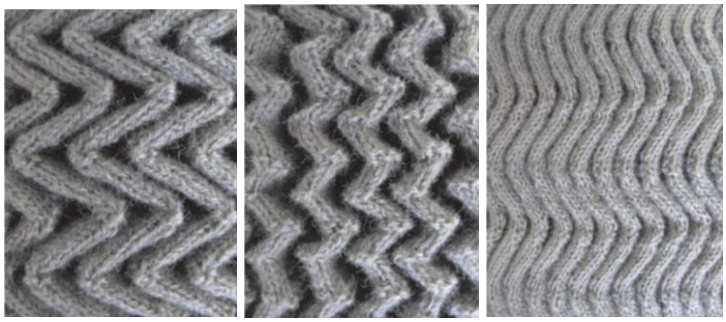

Figure 2.11. Auxetic weft knitted fabric at related state [106].

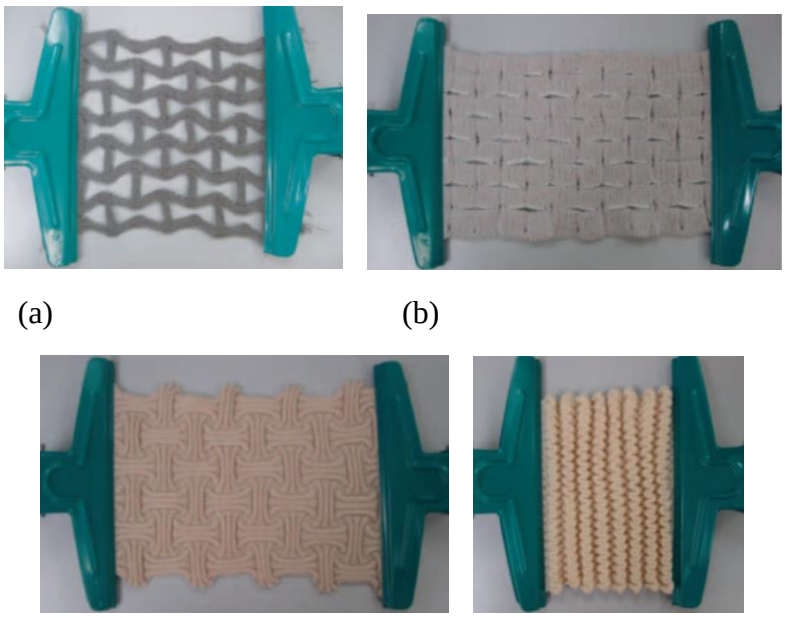

(a) (b)

(c) (d)

Figure 2.12. Auxetic weft knitted fabric. (a) Re-entrant hexagon, (b) rotating rectangle and (c and d) foldable structure [107].

The maximum negative Poisson's ratio value of the developed auxetic knitted fabrics are around -0.13, and -0.18 to -0.42 for foldable structure, -0.5 for rotating rectangle, and -0.6 for re-entrant hexagon. The Poisson's ratio value of these fabrics decreased with the increase of axial strain, except for one foldable structure (Figure 2.12d'). For this foldable structure, auxetic effect firstly increases and then decreases with the axial strain. The auxetic behaviour of the auxetic knitted fabrics against axial strain are shown in Figure 2.13[107].

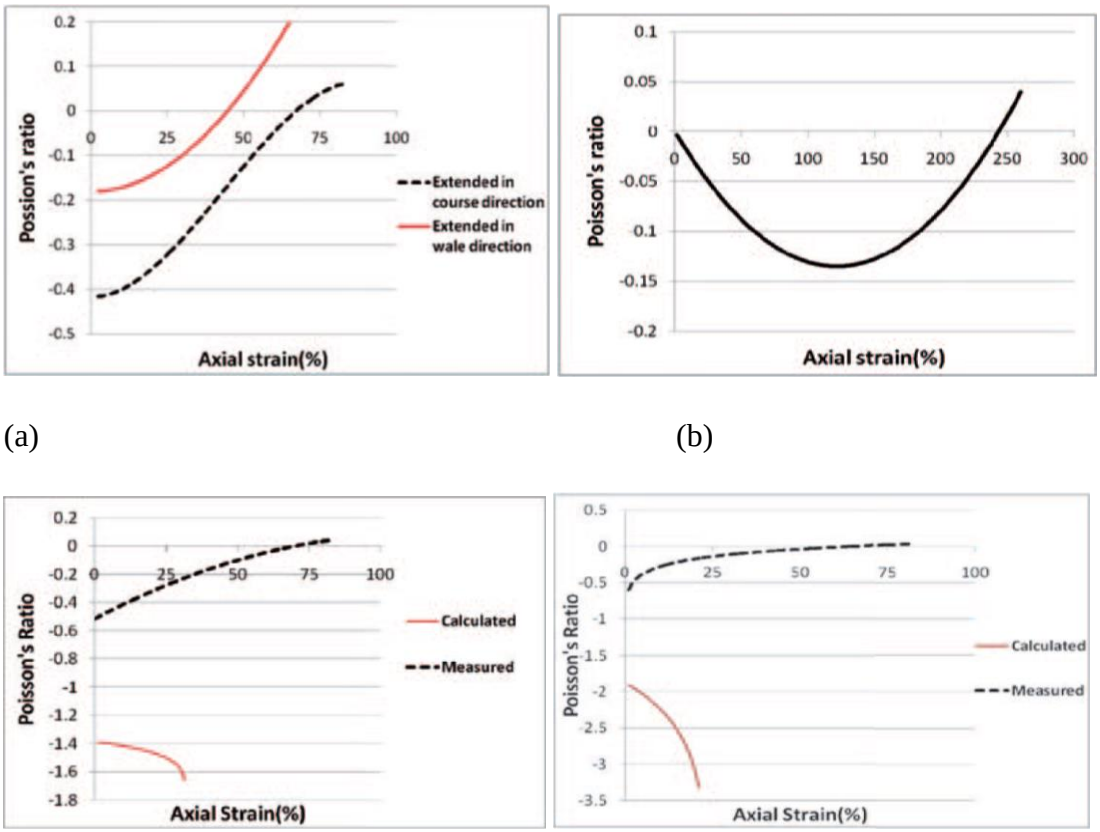

Figure 2.13. Poisson's ratio vs. axial strain for the auxetic knitted fabric. (a) & (b) foldable structures, (c) rotatable rectangle, and (d) re-entrant hexagon [107].

Warp knitted auxetic fabric: The auxetic knitted fabrics can be produced by warp knit technique. To produce warp knitted fabrics the triangular or double arrowhead topology was selected, as shown in the Figure 2.14. This produces the auxetic effect by hinging, leading to opening of arrowheads. To get this design in to the fabric an 18-gauge machine was employed. The fabrics were developed with help of two components – one is the auxetic component and the other is the stabilizing component.

Figure 2.15 shows the stitch pattern used to produce auxetic warp knit fabric and real fabric. The guide bar settings and fibres used to produce fabric is given in the Table 2.11.

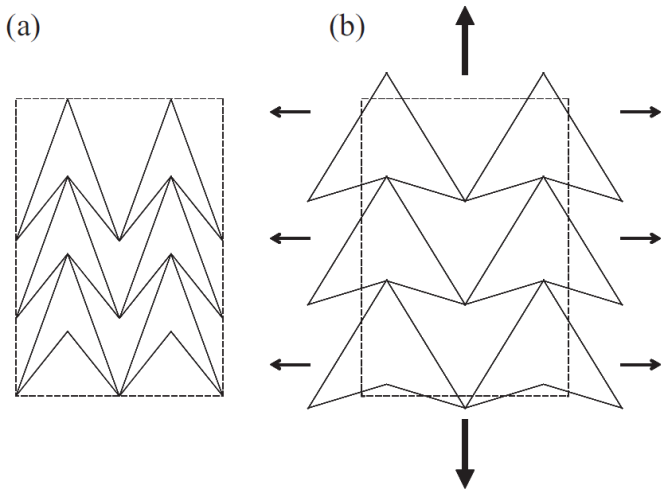

Figure 2.14. Triangular or double arrowhead auxetic topology. (a) Relaxed state and (b) with load [108].

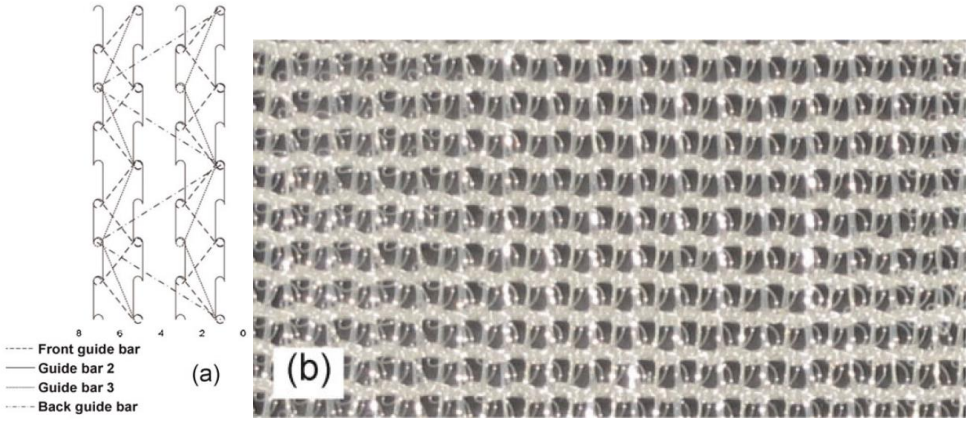

Figure 2.15. (a) Stitch pattern (b) real fabric based on the given stitch pattern [108].

Table 2.11. Guide bar setting and fibre details of auxetic fabric [108]

Bar	**Setting**	**Fibre**
Front	2-0/2-4 (1 in-1 miss)	480 dtex Dorlastan V500
2	0-2/2-0 (Full set)	480 dtex Dorlastan V500
3	0-0/4-4/8-8/4-4 (1 in-1 miss)	Mono-filament PES 0.25 mm
Rear	2-0/2-2/2-4/2-2 (1 in-1 miss)	Mono-filament PES 0.15 mm

The fabric exhibit negative Poisson's ratio tested at +45° (ν_{21} = -0.13 ± 0.04) (45°), near conventional behaviour tested at -45° (ν_{12} = -0.02 ± 0.02), and conventional behaviour test at *x* and *y* co-ordinates (see Figure 2.16).

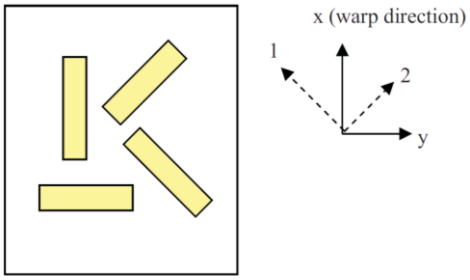

Figure 2.16. Schematic of test sample orientations [108].

Another warp knitted fabric was produced by modifying guide bar setting and fabric exhibited auxetic behaviour tested at ± 45° and conventional behaviour at *x* and *y* directions. The obtained Poisson's ratio values are ν_{21} = -0.13 ± 0.02, ν_{12} = -0.22 ± 0.03, ν_{xy} = 0.1 ± 0.06, and ν_{yx} = 0.23 ± 0.05. The guide bar setting are given in the Table 2.12 and stitch pattern & real knitted fabric are shown in the Figure 2.17[108].

Table 2.12. Guide bar setting and fibre details of auxetic fabric [108]

Bar	**Setting**	**Fibre**
Front	2-0/2-4 (1 in-1 out)	480 dtex Dorlastan V500
2	2-4/0-2 (1 in-1 out)	480 dtex Dorlastan V500
3	0-0/4-4/8-8/4-4	Mono-filament PES 0.25 mm
4	2-0/2-2/2-4/2-2 (1 in-1 out)	Mono-filament PES 0.15 mm

Warp knitted auxetic spacer fabric: Auxetic warp knitted spacer fabric (3D) was produced based on the special geometrical configuration which is formed with parallelograms (refer Figure 2.18).

In this spacer fabric, two face fabric layers are connected together by a group of spacer yarn as the middle layer. In this kind of structure, usually monofilaments are used as spacer yarn to better keep the space made between two face fabric layers. To produce auxetic spacer fabric, the design of geometrical structure which can produce auxetic effect is important. The chosen geometrical structures should meet following requirements,

- To be able to exhibit the auxetic behaviour in various fabric directions.

- To be able knit in warp knitting machine
- The resultant fabric structure should be stable.

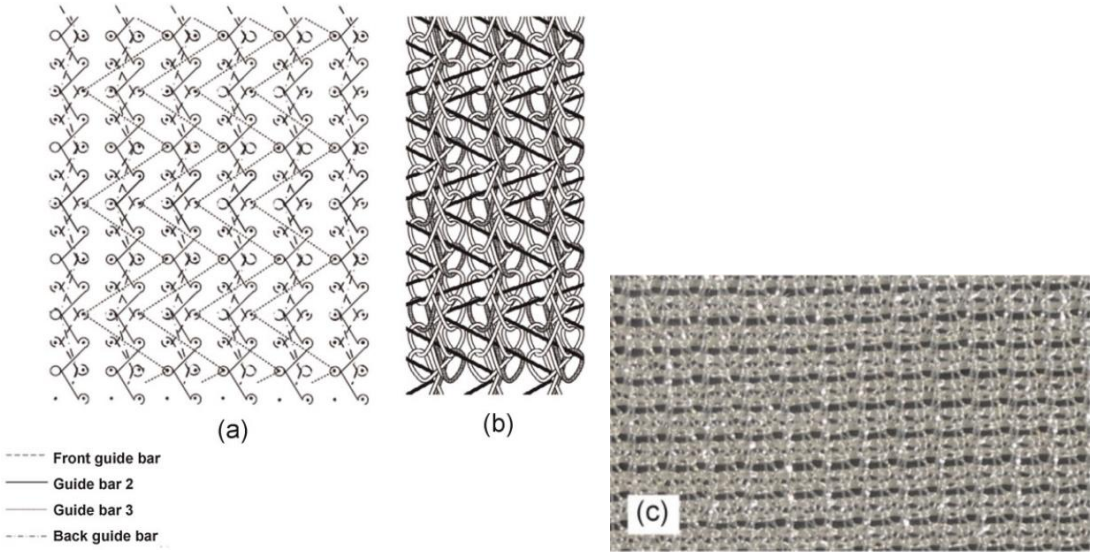

Figure 2.17. (a) Stitch pattern, (b) loop diagram, and (c) knitted fabric [109].

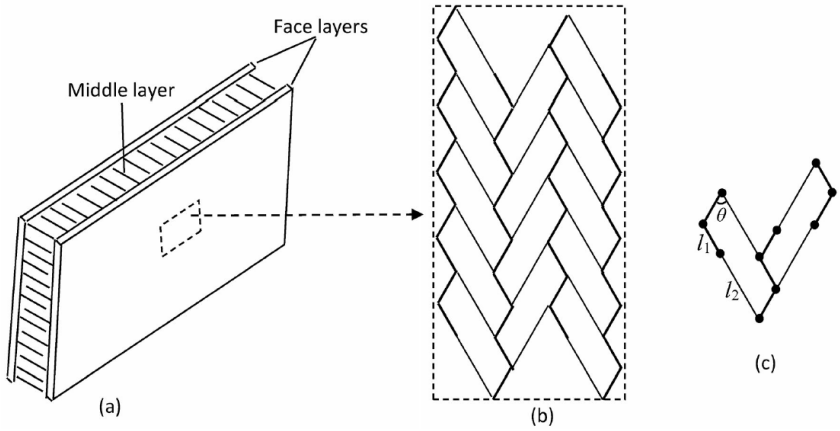

Figure 2.18. Sketch drawing of (a) auxetic spacer fabric, (b) geometrical structural for face fabric layers and (c) reprinting unit [109].

The design shown in Figure 2.18 (above) meet the requirements. Three geometrical parameters, i.e. length of short rib l_1, length of long rib l_2, and angle θ are enough to know the geometric feature of the structure. The auxetic effect of the structure mainly comes from the rotation of ribs around their connecting points when a tensile load applied to the fabric structure. The fabrics were fabricated using multifilament polyester in the

face layers and polyester monofilament in the middle layers. After knitting, the fabric undergone heat treatment to stabilize the geometric configuration in the fabric. The fabrics were produced with varying angle θ and rib length (l_1 and l_2) and studied their auxetic behaviour. The warp knitted spacer fabric is shown in Figure 2.19.

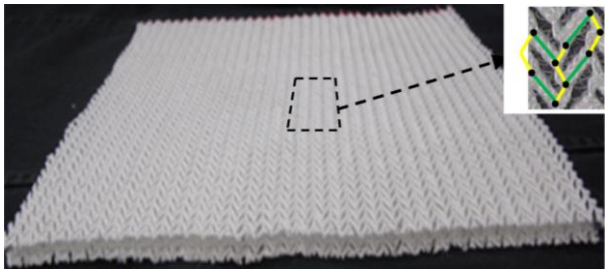

Figure 2.19. Warp knitted spacer fabric [109].

The auxetic behaviour of this structure tested at different directions is shown in the Figure 2.20.

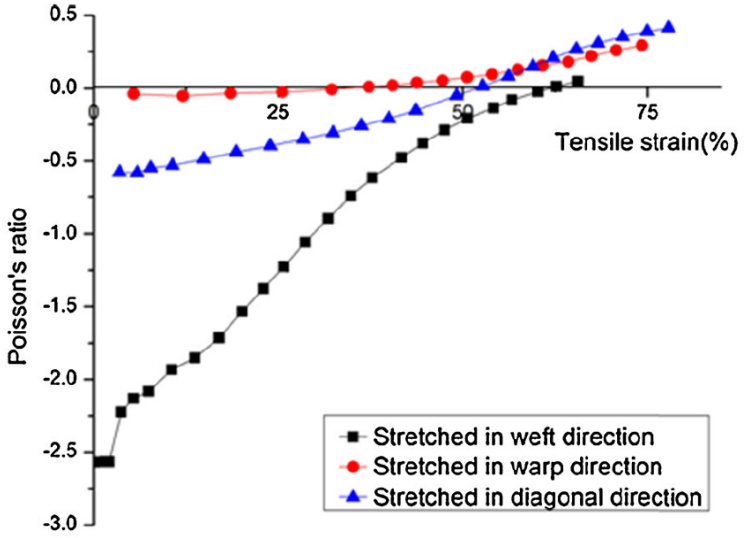

Figure 2.20. Poisson's ratio vs. tensile strain tested at different direction of fabric [109].

The fabric exhibits negative Poisson's ratio tested in all direction. The fabric exhibited higher Poisson's ratio value in weft direction and less in warp direction. The Poisson's ratio value of the fabric structure decreases with increase of tensile strain. The geometrical parameters have an obvious effect on Poisson's ratio value of the structure. The closer the fabric structure (less θ value) will have the higher auxetic effect (high negative Poisson's ratio value). The developed auxetic fabric exhibited better shape fitting ability than conventional fabric (refer Figure 2.21). This behaviour will helpful where shape fitting is highly required [109].

Figure 2.21. Shape fitting ability of spacer fabric. (a) Conventional fabric and (b) auxetic fabric [109].

2.3.3. Auxetic composites

Presently, there exist two main approaches for producing auxetic composites: (1) angle ply method, i.e. through stacking of composite laminates at specific angles and (2) fabrication of composites in which one or more phases are auxetic. In the angle ply approach, unidirectional carbon fibre/epoxy laminates are stacked in a certain sequence resulting in negative Poisson's ratio either in in-plane or through-thickness direction. Poisson's ratio achieved using this method lies in the range of -0.21 to -0.37. The angle of laminates in these composites is kept between ±15° to 30° [21]. In the other approach, auxetic composites are manufactured using double helix yarns (DHY) [41, 103, 105]. Helical yarns are used to produce auxetic composites in two different ways. In one method, carbon double helix yarns are used to reinforce polyester matrix unidirectionally to produce composites with stiffness of 4 GPa and negative Poisson's ratio of -6.8 at 30% fibre volume fraction [41]. In the second method, helical yarns are woven into a fabric and silicone rubber is used as the matrix to produce flexible composites with Poisson's ratio of -0.1 and low elastic modulus (5.8 MPa) [105].

2.3.4. Auxetic structures

In the last few decades, dissimilar geometric structures and models exhibiting auxetic behaviour have been proposed, studied and tested their mechanical properties. The main auxetic structures reported are two dimensional (2D) and three dimensional (3D) re-entrant structures, rotating rigid/semi-rigid units, chiral structures, hard molecules, liquid crystalline polymers and microporous polymers. Some of these auxetic structures are presented in Figure 2.22 [38, 13, 19 – 21].

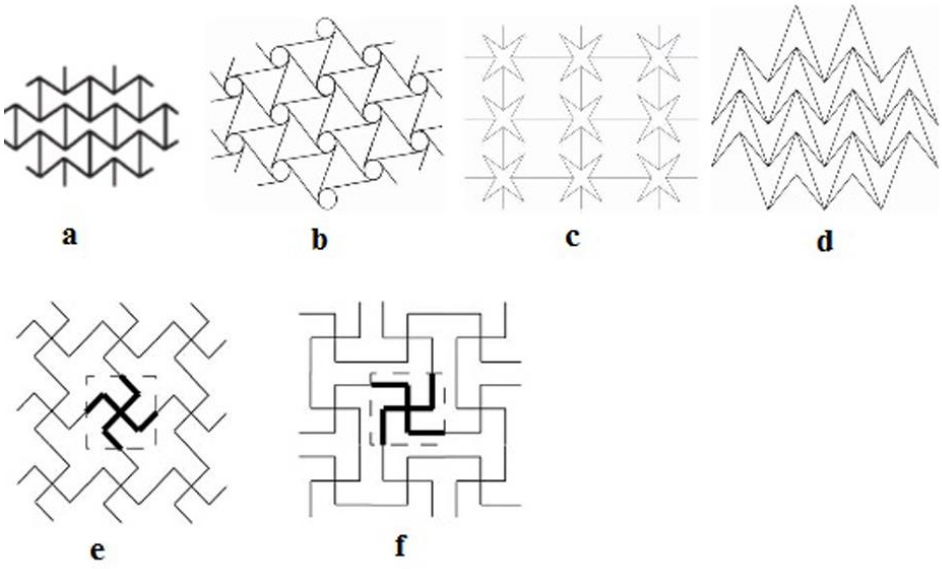

Figure 2.22. Auxetic structures: (a) re-entrant hexagon, (b) chiral honeycomb, (c) star-shaped honeycomb topology, (d) double arrow head honeycomb topology, and (e & f) missing rib or lozenge grid [38, 13, 19 – 21].

2.3.5. Properties of auxetic materials

Auxetic materials have special properties compared to non-auxetic materials including:

- Good fracture toughness,
- High in-plane indentation resistance,
- High dynamic properties,
- High transverse shear modulus,
- Superior energy absorption,
- Improved damping,
- Improved strength,
- Porosity and permeability variation with strain.

2.3.6. Applications of auxetic fibrous materials

Auxetic materials can be used in wide range of applications in apparel textiles (auxetic fibres, threads, functional fabrics, etc.), technical textiles (air filter, gasket, fishnet, fastener, shock absorber, sound absorber, etc.), aerospace industry (curved body parts, wing panel, and aircraft nose-cones), materials for protection (crash helmet,

projectile-resistant materials, shin pad, glove, protective clothing, car bumpers, etc.), bio-medical industry (bandage, wound pressure pad, dental floss, artificial blood vessel, drug release devices, etc.), furniture and also in sensors and actuators (hydrophone, piezoelectric devices, miniaturized sensors) [37, 38, 43].

2.4. Conclusion

The key purpose of this research works is to develop a novel material for the civil engineering applications which has the combining features of fibre reinforced composites and auxetic materials. The development of the novel materials mainly for the existing structural elements to enhance their resistance against earth quake, blast or impact load caused by explosions. The key requirements for these applications are higher energy absorption, ductility, catching the debris caused by explosion, etc. Existing FRP materials available for this type of application is not up to the level, i.e. less ductility and energy absorption.

Until now, there is no auxetic materials, which is meant for civil engineering applications. In this research works, the suitable auxetic structural designs are adopted and auxetic composite structures developed from fibre reinforced braided composite rods. These novel auxetic materials expected to show higher ductility, enough strength, and higher energy absorption than other FRP materials.

Chapter 3

Materials and Methods

3.1. Introduction

This chapter explained about fibres used in the experimental work and its tensile properties. Also, it is explained the production of the core reinforced braided structures and the developed auxetic structures in this research work consists of both undulation and straight form of BCRs, it is necessary to understand their tensile behaviour. So the tensile testing was carried out for both undulation and straight form BCRs. In addition, preparation of auxetic structures for tensile and Poisson's ratio testing explained and also, an evaluation method of mechanical behaviour (Poisson's ratio and work of rupture) of the auxetic structures provided briefly.

3.2. Fibres and resin

For the production of braided composite rods, glass fibre roving with linear density of 1200 tex and 4800 tex was purchased from Owens Corning, France. Also, basalt fibre roving with 4800 tex and carbon fibre roving with linear density of 1600 tex were purchased from Basaltex, Belgium and Toho Tenax, Germany, respectively. These core fibres are used to produce braided structures with required linear density by varying number of rovings during braiding. The epoxy resin used to in this work was supplied by

Sika, Germany, in two parts: Biresin CR83 Resin and Biresin CH-83-2 Hardner. The resin and hardener components were mixed in a weight ratio of 100:30 prior to use. The important properties of fibre and resin are given in Table 3.1.

Table 3.1. Physical and mechanical properties of core fibres and resin

S. No.	Properties	Basalt	Glass	Carbon	Epoxy
1	Density (g/cm^3)	2.63	2.62	1.77	1.15
2	Filament diameter (µm)	17	--	13	--
3	Tensile strength (MPa)	> 4000	3100 – 3800	4400	122
4	Tensile modulus (GPa)	87	80 – 81	240	3.3
5	Elongation (%)	--	--	1.8	6.7

3.3. Production of braided structures

The core fibre reinforced braided structures were produced by using vertical braiding machine (Figure 3.1). The core fibres used to produce braided structures are glass, basalt and carbon fibres. The sheath was multifilament polyester fibre with linear density of 110 tex and total 16 bobbins were used. The following are the braided structures produced for this research work.

- ✓ Glass fibre braided structure – 2400, 4800, and 6000 tex
- ✓ Basalt fibre braided structure – 4800 tex
- ✓ Carbon fibre braided structure – 4800 tex

Figure 3.1. Vertical braiding machine.

These braided structures were produced to develop auxetic structures based on missing rib or lozenge grid and re-entrant hexagon or bow-tie design. Also, the braided structures were tested under tensile loading to study their tensile behaviour which can be useful to understand the tensile behaviour of auxetic structures. As the braided structures are used both undulation and straight forms to develop auxetic structures, the tensile testing of braided structures carried out with both forms.

3.3.1. Tensile properties of BCRs in straight form

The epoxy resin was applied to the braided structures. The braided structures after resin application and curing became circular composites termed as braided composite rods (BCR). The weight percentage of core fibre in each of these rods was around 51 ± 2%. Resin application was necessary to give sufficient mechanical stability to the braided materials in order to handle them easily and turn them in to auxetic structures. Also, the braided structures display suitable mechanical properties necessary for the targeted use only after resin application and formation of BCR, since the epoxy matrix holds the various components (core and sheath) of braided structures together, enabling them to act as a single structure. In absence of resin, there may be slippage between the core and sheath as well as between the core fibres causing in poor mechanical properties. In these BCRs, the cover or sheath influences the adhesion property and provides environmental protection, whereas the axial reinforcement (core fibre) is responsible for their mechanical performance.

The tensile test of BCRs (straight form, see Figure 3.2) was carried out using Universal Tensile Testing machine. The cross-head speed of tensile testing was 2 mm/min. The gauge length of BCRs in straight form is 40 cm and tensile properties of the BCRs produced with different type of core fibres are provided in Table 3.2.

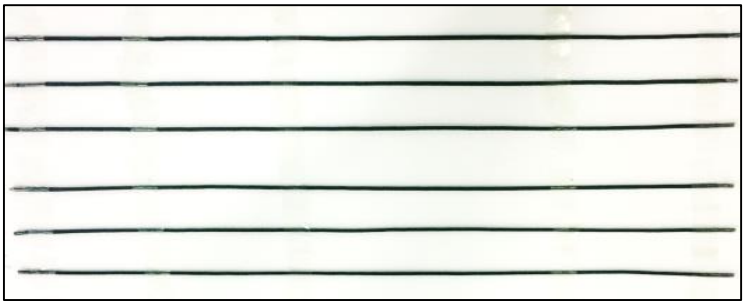

Figure 3.2. Braided composite rods in straight form.

Table 3.2. Tensile properties of BCRs (straight form) with resin

Fibre type	BCRs core linear density (tex)	BCR diameter (mm)	Tensile strength (MPa)	Tensile Modulus (GPa)	Elongation (%)
Glass	4800	2.39	600	14.8	4.10
Basalt	4800	2.41	680	14.5	4.70
Carbon	4800	2.90	885	29.0	3.05

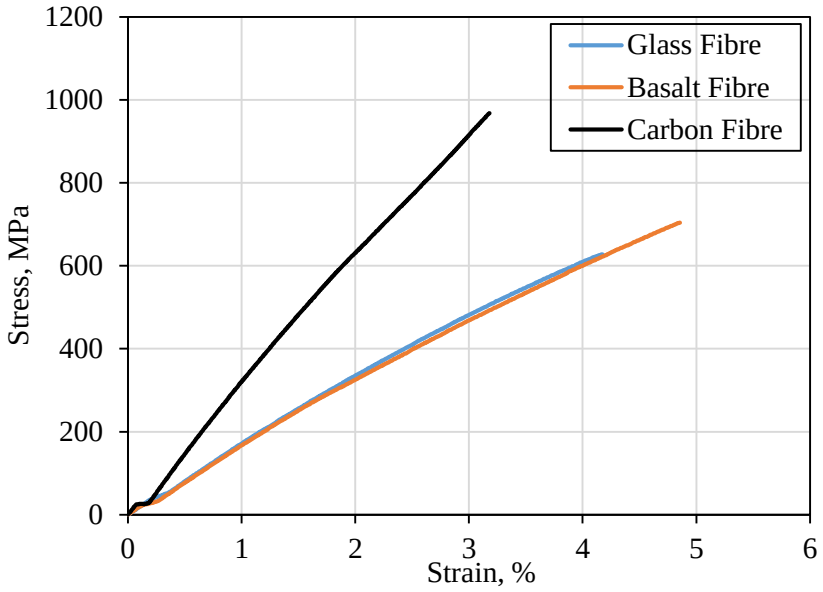

Figure 3.3. Stress vs. strain curves of BCRs produced with different core fibres (4800 tex).

The stress - strain curves for the BCRs produced with different types of core fibres are shown in Figure 3.3. The results show that carbon fibre exhibits highest tensile strength and modulus than basalt and glass fibre. Basalt fibre shows higher tensile load compared to glass fibre, however, the tensile modulus of basalt is almost similar to glass fibre.

3.3.2. Tensile properties of BCRs in undulation form

Tensile testing of BCRs produced with different core fibres (glass, basalt and carbon) having undulation (see Figure 3.4) was carried out using Universal Tensile Testing machine. The cross-head speed of testing was 25 mm/min. The gauge length of

the samples were 40 cm. The tensile properties of undulation BCRs is provided in the Table 3.3 and the tensile behaviour is shown in the Figure 3.5.

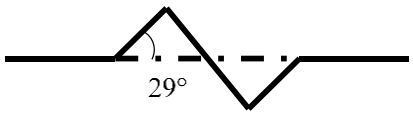

(a)

(b)

Figure 3.4. (a) Schematic diagram of undulation rod with angle and (b) braided composite rods in undulation form.

Table 3.3. Tensile properties of undulation BCRs

Fibre type	BCRs core linear density (tex)	BCR diameter (mm)	Tensile strength (kN)	Elongation (%)
Glass	4800	2.39	1.57	8.11
Basalt	4800	2.41	2.13	9.20
Carbon	4800	2.90	2.70	7.82

The results show that carbon fibre undulation BCR exhibits higher tensile load, followed by basalt and glass fibre undulation BCR. Also, compared with straight BCR, the tensile load is less and elongation is more. This is due to the presence of inclination in the BCR and it takes more time to become straight. In addition, the bending of core fibres in the undulation BCRs results less tensile load.

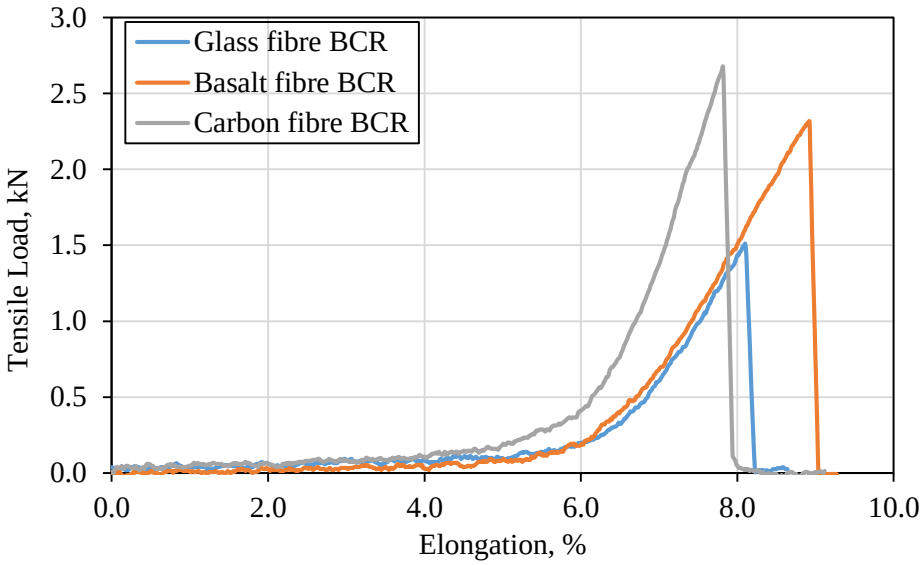

Figure 3.5. Tensile behaviour of undulation BCRs.

3.4. Testing of auxetic structures

Auxetic structures were prepared from using braided structures and tested in tensile testing machine to study their auxetic and tensile behaviour. The preparation of the samples for the tensile testing is explained here.

3.4.1. Sample preparation

While producing auxetic structures extra length (10 cm) have been given in the structures at top and bottom for the clamping purpose (see Figure 3.6). To produce the clamp for the tensile testing, first, few layers of glass fabric with resin were applied both sides at top and bottom of the structures. After resin curing, the Zincor (electrogalvanized steel plate with zinc coating) metal plates (14 cm x 10 cm x 0.15 cm) were applied top and bottom of the samples on both sides. This type of clamping helps avoid slippage during testing.

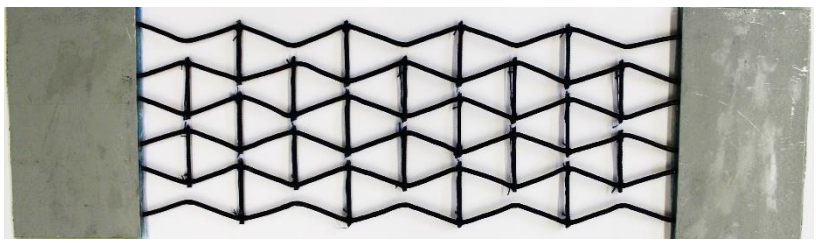

Figure 3.6. Auxetic structure with clamping plate at the top and bottom.

3.4.2. Tensile testing

The auxetic structures were tested in Universal Tensile Testing machine. Testing was carried out with the cross-head speed of 25 mm/min. Videos were captured during testing to study the deformation of the structures to evaluate the Poisson's ratio of the structures, using image based tracking methods.

3.5. Evaluation of the mechanical properties of the structures

3.5.1. Calculation of Poisson's ratio of the structures

The white marking was provided on the structures at top, middle and bottom of the structure. The distance between the points marked in the structures both in lateral and longitudinal directions were measured in pixels using ImageJ software manually. The vertical and transverse strains calculated by using following formulae:

$$\varepsilon_x = \frac{x_n - x_0}{x_0} \tag{3.1}$$

$$\varepsilon_y = \frac{y_n - y_0}{y_0} \tag{3.2}$$

Where x_n and y_n are the distance between the points marked on the structure at n^{th} of loading, x_0 and y_0 are the original distance between the marks at zero loading. The average lateral strain was calculated by averaging the lateral strains calculated at top, middle and bottom points. The average longitudinal strain was calculated from longitudinal strains measured from left and right points of the structures. Later, the Poisson's ratio was calculated from the average strains using Eq. 3.3,

$$\nu_{xy} = - \frac{\langle \varepsilon_x \rangle}{\langle \varepsilon_y \rangle} \tag{3.3}$$

3.5.2. Calculation of work of rupture of the structures

Work of rupture or energy required to break the structure has been calculated using load-elongation curve. To calculate the area under the curve there are numerous formulae with different approaches. Numerical integration using the rectangle rule based on the midpoint was used in this work. Figure 3.7 shows a representation of this method where the blue area is the exact area and the grey value estimated by the integral method.

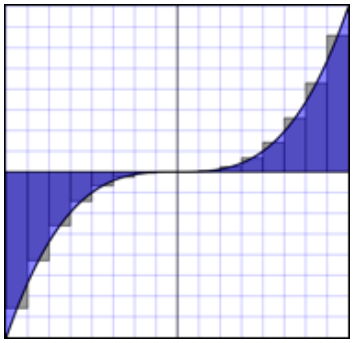

Figure 3.7. Area under the curve by rectangle method.

This is an approximation of an integral of a function by dividing an interval (a - b) and in (m) sub-intervals, the area of each subinterval is calculated.

The function can be defined by:

$$\int_a^b f(x) \approx \sum_{k=0}^{m-1} f\left(\frac{x_k + x_{k+1}}{2}\right) h \quad (3.4)$$

3.6. Conclusion

This chapter detailed about physical properties of fibres used in this research works. Also, the tensile testing of BCRs with straight and undulation forms were carried out. As the developed auxetic structures composed of BCRs with undulation and straight form. So tensile testing of single rods will be helpful to understand the tensile behaviour of the structures. BCRs in straight form shows linear tensile behaviour, whereas BCRs in an undulation form shows linear behaviour after the undulation becomes straight and at initial stage the load carried by the rods is less and it will be varied based on the level of the undulations of the axial rods. The chapter also explained methods of tensile testing and calculation of strains, Poisson's ratio, and work of rupture of the auxetic structures.

Chapter 4

Development and Optimization of Auxetic Structures Based on Lozenge Grid

4.1. Introduction

This chapter discusses the development and optimization of auxetic structures from braided composite rods in detail. There are many auxetic structural design reported in the literature (see also Figure 2.22) and out of that one simple design has been chosen to develop auxetic structures from fibre reinforced braided composites. The auxetic design chosen was “lozenge grid or missing rib”. Primarily, the auxetic structures were produced by varying their structural parameters (rib length and angle) and studied auxetic and tensile behaviour in detailed manner. The developed auxetic structure had some drawbacks like the opening between the longitudinal and transverse elements was much compared with commercial grid and tensile behaviour of the structures also is less when compared to commercial grids.

Later the basic lozenge grid design was modified and optimized to suit for the strengthening purpose of civil structural elements by studying structural and material parameters. The structural parameters studied are the angle, rib length and design. The

material parameters studied were types of core fibres and linear density of core fibre. The auxetic behaviour of the developed auxetic structures were carried out by two different image-based approaches. The first method is an image-based tracking method, in which the image captured at particular intervals using a high resolution camera automatically and later the images were analysed using Mat Lab software. Another method is manual process, in which videos were captured and later they were converted in to images at required interval to analyse manually.

4.2. Development of auxetic structure: Preliminary study

The auxetic structural design considered in this research is "missing rib" (Figure 2.22e) due to its simple design and ease of manufacturing using braided structures. This type of auxetic structures has been developed for the first time in macro-scale using composite materials, based on the auxetic structural design previously reported. These structures were subjected to tensile loading in a Universal Testing Machine and auxetic behaviour (Poisson's ratio) was characterized by means of an image-based tracking method. The influence of the structural angle on Poisson´s ratio and tensile properties was thoroughly investigated. An analysis of the auxetic behaviour was performed using a previously reported analytical model and the experimental values were compared with the predicted values obtained from the analytical model.

4.2.1 Materials and methods

Fibre reinforced braided structures were used to develop the auxetic structure in the following steps: (1) the auxetic structural design (Figure 4.1) was drawn on a white chart paper; (2) the chart paper was placed on a board and the braided structures were placed over the drawn design firmly with help of adhesive tape; (3) the cross-over points were tied by polyester filaments and epoxy resin was applied over the structures using a brush; (4) after curing, the structures were removed from the board. The braided structures after resin application and curing became circular composites termed as BCRs.

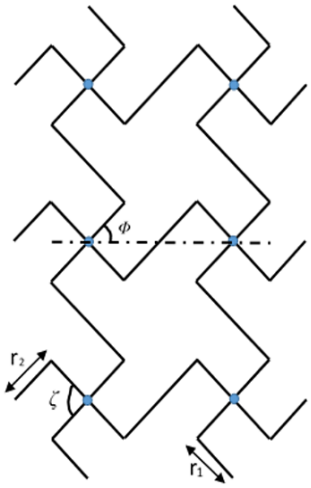

Figure 4.1. Missing rib or lozenge grid auxetic structural design.

Resin application was necessary to give sufficient mechanical stability to the braided materials in order to handle them easily and turn them in to auxetic structures. Also, the braided structures show suitable mechanical properties necessary for the targeted use only after resin application and formation of BCR, since the epoxy matrix holds the various components (core and sheath) of braided structures together, enabling them to act as a single structure. In absence of resin, there may be slippage between the core and sheath as well as between the core fibres resulting in poor mechanical properties. Therefore, although without epoxy resin the developed structures may permit higher flexibility and structural movement (similar to flexible knitted auxetic structures) leading to better auxetic property, application of epoxy resin was necessary to achieve suitable mechanical properties for the targeted applications. Five different auxetic structures were prepared by changing their structural angles, φ and ζ (Figure 4.2). The dimension of these structures was kept constant for all specimens, i.e. 20 cm in width and 40 cm in length, with additional length for clamping during testing. In this study, only the effect of angle (φ,ζ) on the auxetic and tensile behaviour was addressed. Five different types of auxetic structures produced within this study are shown in Figure 4.2 and their structural angles are provided in Table 4.1. Four specimens were produced and tested for each type of auxetic structure.

Table 4.1. Values of the structural angles and rib length

Structure	Angle	Value, °	Rib	Value, cm
1	φ	45	r_1	7.0
	ζ	91	r_2	3.5
2	φ	52	r_1	6.3
	ζ	102	r_2	4.0
3	φ	64	r_1	5.6
	ζ	122	r_2	4.6
4	φ	68	r_1	5.4
	ζ	127	r_2	4.6
5	φ	79	r_1	5.1
	ζ	138	r_2	4.6

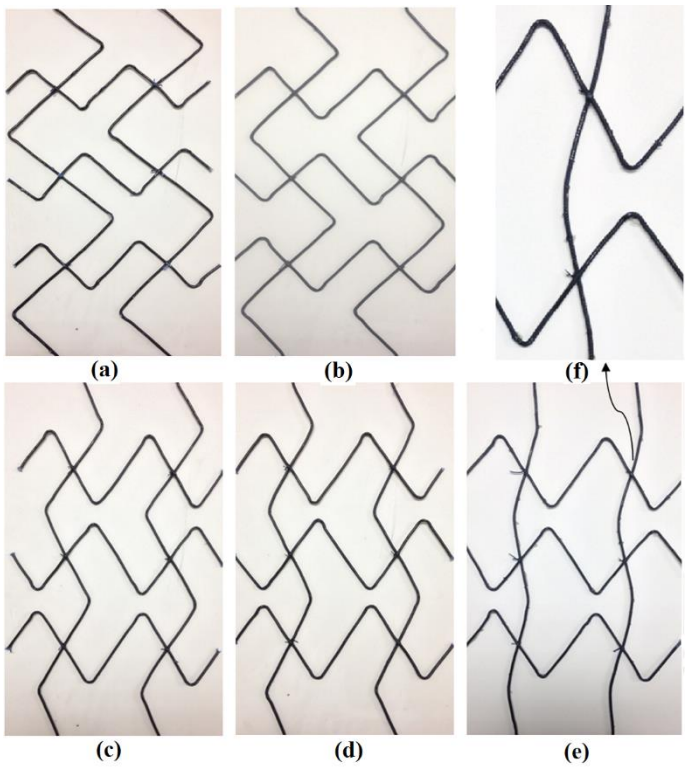

Figure 4.2. Developed auxetic structures: a) structure-1, b) structure-2, c) structure-3, d) structure-4, e) structure-5, and f) magnified image of structure-5.

4.2.2. Evaluation of auxetic and tensile behaviours of the structures

The tensile and auxetic behaviours of the five structures were evaluated simultaneously using tensile testing machine. The cross-head speed of tensile testing machine was kept at 25 mm/min. To observe the dimensional changes in the structures

under tensile load using feature tracking method, white marks were painted on the structures at discrete nodes, as shown in Figure 4.3 [110, 111]. This optical technique has the advantage of being contact-free, providing relative displacements between target points over the region of interest. The photo-mechanical set-up was adjusted in order to provide suitable resolution for the purpose of the study. A camera-lens optical system was used for image grabbing. A charge-coupled device (CCD) 8-bit Baumer Optronic FWX20 camera (resolution of 1624 × 1236 pixels^2, pixel size of 4.4 μm and sensor format of 1/1.8'') was coupled with a Nikon AF Micro-Nikkon105 mm *f*/4D IF-ED lens. The working distance was set to 2755 mm and the focal length to about 50 mm, in order to be less sensitive to out-of-plane parasite movements. The lens aperture was set to *f*/16 in order to enhance the depth of focus during testing. LED lighting system was used and a matte black environment around the specimen was created to enhance sharp white-black contrast of the target marks.

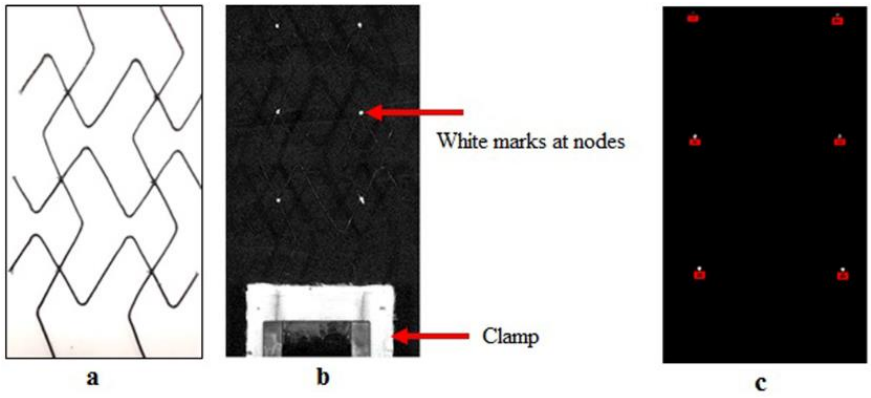

Figure 4.3. Auxetic structure during testing. (a) Structure before testing; (b) structures with white marks painted at nodes; (c) binary image resulting from the post-processing using an image-based tracking algorithm.

The size of the marks with regard to the field of view was chosen to compromise between spatial resolution (smaller marks) and accuracy (large marks). These marks represent a carrier for measuring the relative displacement in the structure under analysis. During tests, images were recorded with an acquisition frequency of 0.4 Hz using a shutter time of 14 ms. The recorded images of the structures were analysed by image processing. The centroid of target objects in the images were tracked during image sequence based on a combination of threshold segmentation and mathematical morphological operators [110, 111]. The relative distance variation among the selected marks allowed to evaluate the strain on the structures. Before testing, static and translation

rigid-body tests were carried out in order to evaluate the resolution of the technique. The advantage of such tests is that the measured field is theoretically known, allowing a statistical evaluation of noise [112, 113]. Therefore, the standard deviation over the noise field (understood as a white Gaussian noise) is the estimation of the accuracy of the technique. Regarding the size of the marks and photo-mechanical set-up, in this case, a resolution of 10^{-1} pixels (26 μm) in displacement was obtained. Taking a reference base length between adjacent marks of 100 mm, a resolution in strain of 0.026 % was then achieved. Specimens were tested until failure.

4.2.3. Results and discussion

4.2.3.1. Auxetic behaviour of the structures

Poisson's ratio of the structures was calculated by strain components obtained from the image-based tracking method and presented in Figure 4.4 to Figure 4.8. The comparison of auxetic behaviour of five different structures is shown in Figure 4.9, which presents the behaviour of only one representative sample from each category.

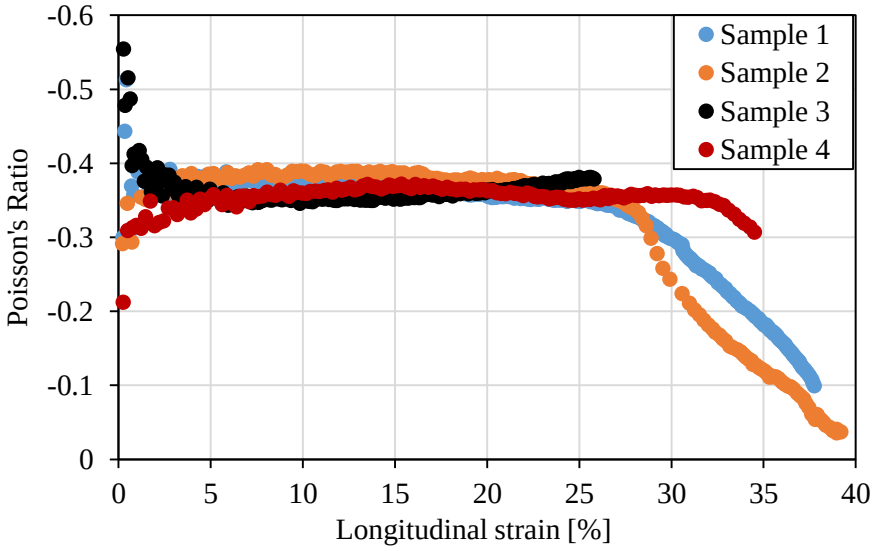

Figure 4.4. Auxetic behaviour of structure-1.

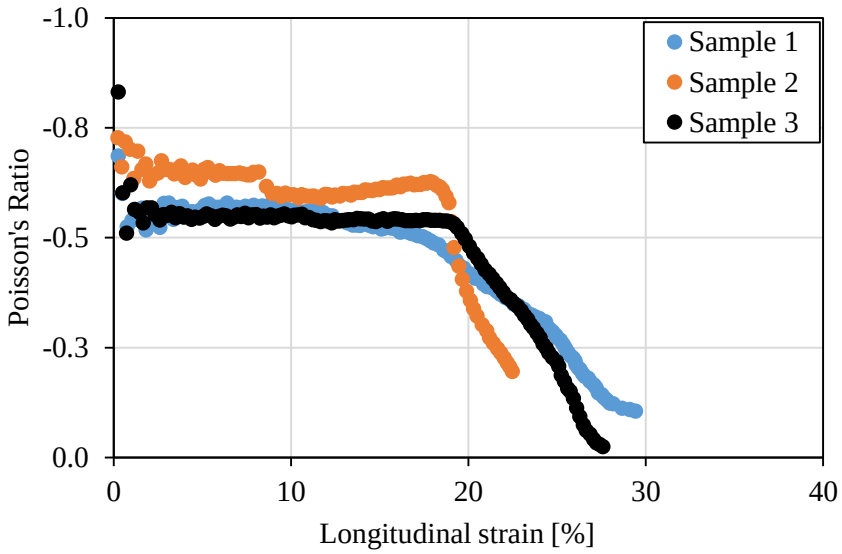

Figure 4.5. Auxetic behaviour of structure-2.

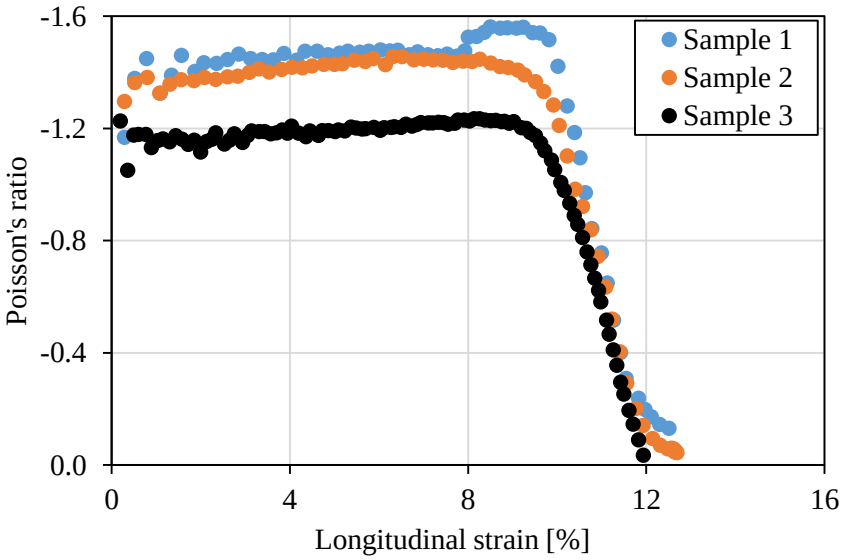

Figure 4.6. Auxetic behaviour of structure-3.

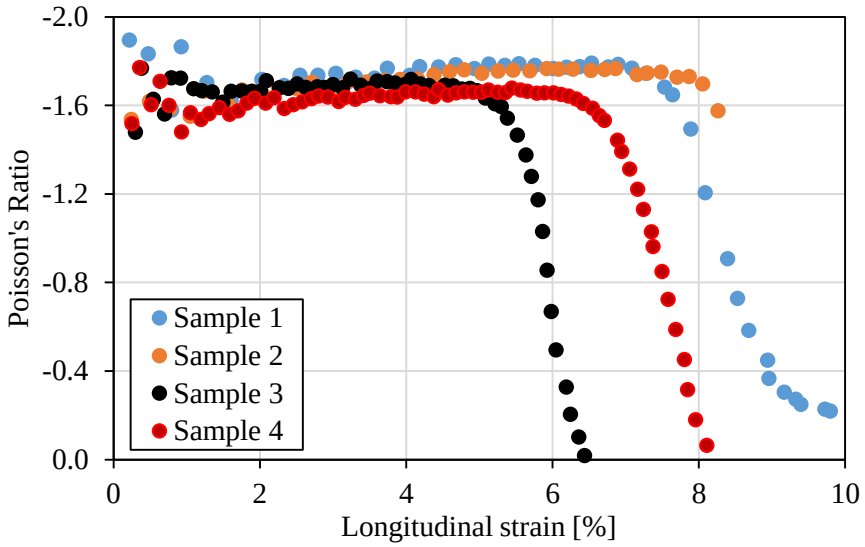

Figure 4.7. Auxetic behaviour of structure-4.

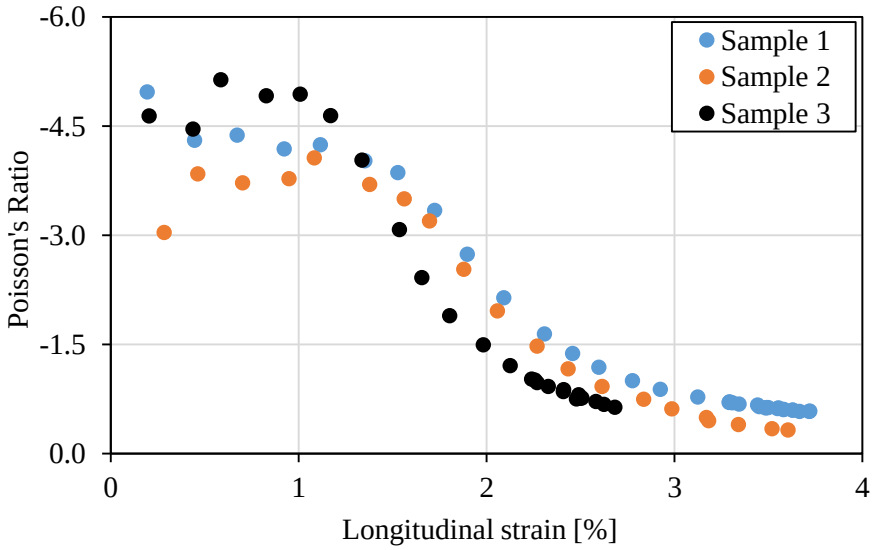

Figure 4.8. Auxetic behaviour of structure-5.

The results show that the auxetic structures have Poisson's ratio in the range -5.00 to -0.30. Poisson's ratio of developed auxetic structures increase with the increase in angle φ. The auxetic behaviour of samples from each structure is similar with less sample to sample variation. Also, the absolute value of Poisson's ratio decreases with the increase in longitudinal strain level. In these structures, the longitudinal and transverse rods contain undulation and are arranged in a special configuration. As the cross-over points or nodes are tied by filaments, when tensile load is applied in the longitudinal direction, the load is transmitted to the transverse direction through these nodes. The undulation in

the longitudinal rods continues to straighten under loads, leading to the increase in specimen´s width due to straightening of the transverse rods.

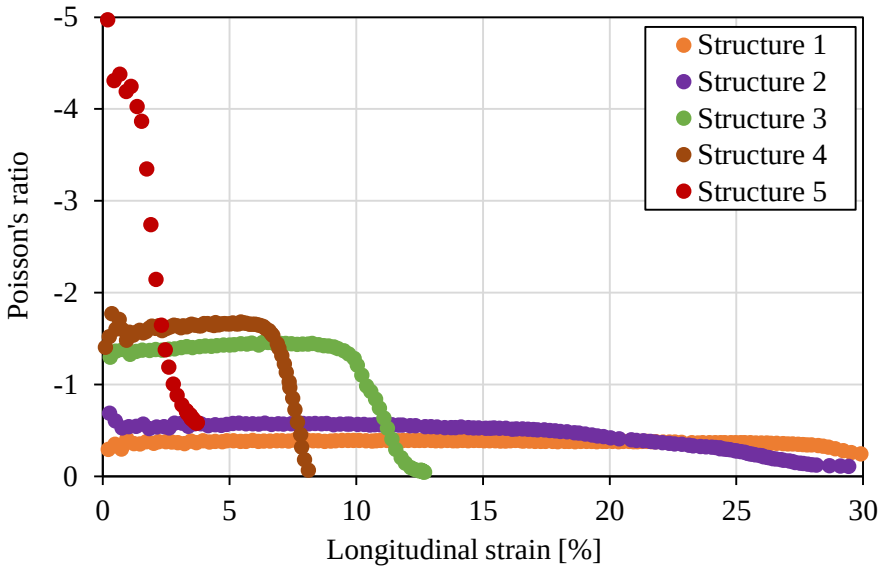

Figure 4.9. Change of Poisson's ratio with longitudinal strain for the auxetic structures.

4.2.3.2. Relationship between angle φ and Poisson's ratio

The change in angle φ was measured from images taken at regular intervals at different strains for all structures. The variation of Poisson's ratio with respect to variation of angle φ is given in Figure 4.10.

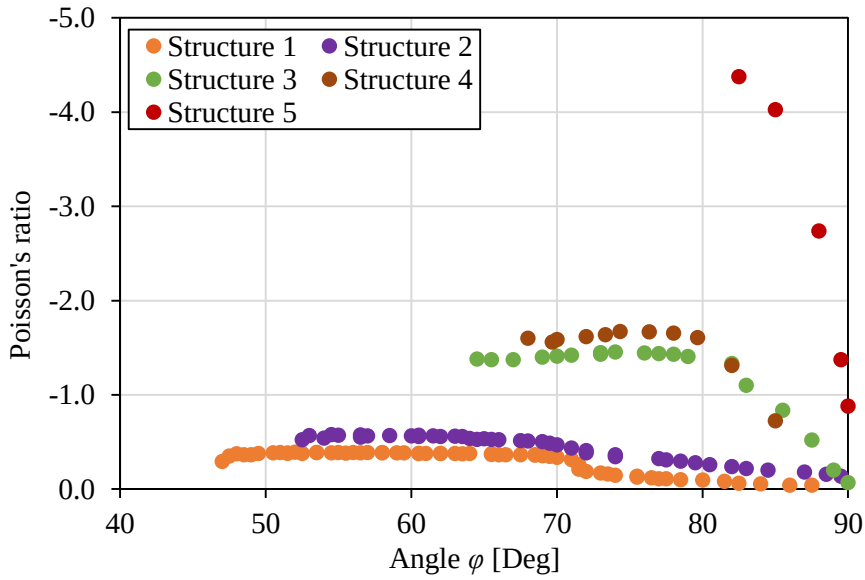

Figure 4.10. Change of Poisson's ratio as a function of angle φ of the structures.

As the tensile load is applied to the structures, angle φ continuously increases until the longitudinal rods become straight, i.e. angle φ reaches 90°. The results showed that Poisson's ratio of the structures decreases with the increase in angle φ, but the trend is different for different structure. For structure-1 to 4, Poisson's ratio initially exhibits a relatively constant value and then starts to decrease continuously with increasing φ. On the other hand, for structure-5, Poisson's ratio decreases continuously with increasing φ. The different behaviour of structure-5 may be due to the higher initial value of angle φ (i.e. at zero load condition). Although the auxetic structures produced at micro-scale using the same auxetic design showed similar influence of angle φ on Poisson's ratio in the lower φ range (lower than 56º), this effect was not studied for the higher range of φ (45-90º), as investigated in the present research (Figure 4.2).

4.2.3.3. Relationship between angle φ and longitudinal strain

The relationship between angle φ and longitudinal strain measured using image-based tracking method is shown in Figure 4.11. The results show that the longitudinal strain increases with increase in angle φ for all structures.

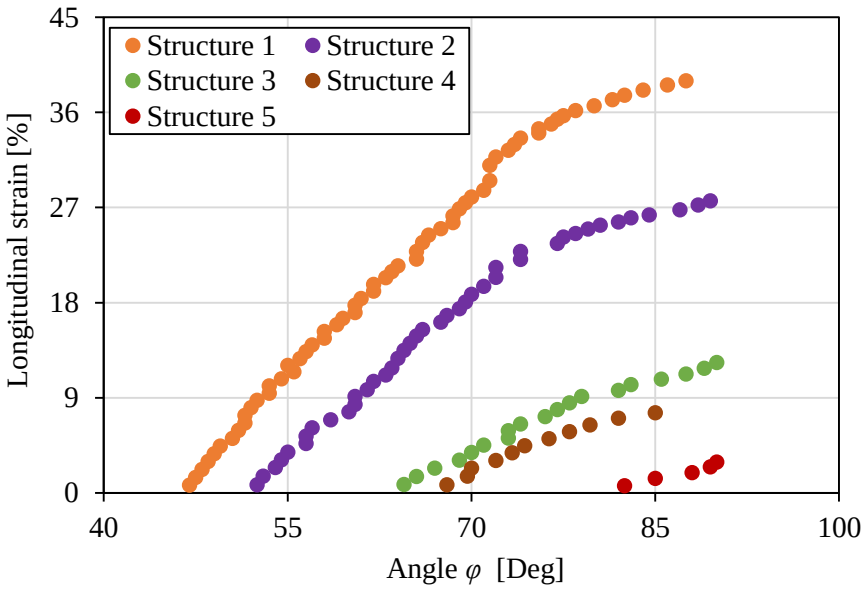

Figure 4.11. Measured longitudinal strain as a function of angle φ of the structures.

4.2.3.4. Tensile behaviour of developed structures

Tensile test results of the developed auxetic structures are provided in Table 4.2 Figure 4.12 shows the tensile behaviour of the developed structures. Tensile behaviour of

these structures varies according to their initial angle φ. The lower is the value of initial angle φ, lower is the maximum tensile load, which increases with the increase in initial angle φ of the structures. Structure-5 shows the maximum tensile load (initial φ – 79^{o}) among all structures, and unlike other structures, exhibits good tensile load bearing capacity even at lower strain level.

Table 4.2. Tensile test results of the structures

Structure	**Avg. max. tensile load, kN**	**Avg. elongation at max. tensile load, %**	**Avg. work of rupture, J**
1	1.15 (0.2)	38.8 (5.5)	13.8 (20.9)
2	1.48 (0.7)	25.8 (2.7)	12.1 (18.3)
3	2.34 (0.6)	11.4 (4.1)	14.4 (8.0)
4	3.00 (0.6)	8.6 (5.5)	19.7 (22.5)
5	4.55 (0.7)	5.6 (6.1)	43.7 (18.5)

Note – Values of CV% are given in the bracket.

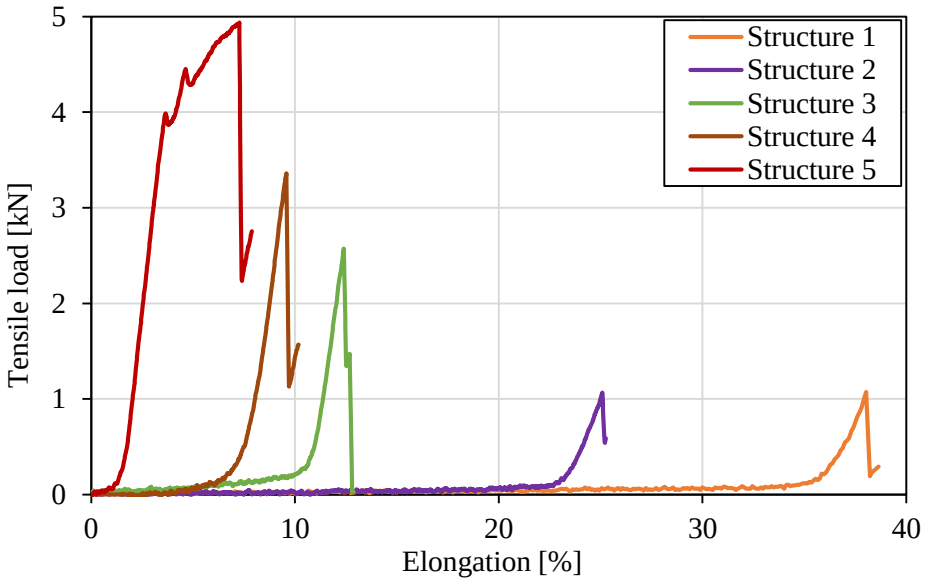

Figure 4.12. Tensile behaviour of developed auxetic structures.

Tensile behaviour of structure-3 and structure-5 can be analysed by dividing the load-elongation curve in to three different phases (for the detailed analysis of tensile property, structure-3 and structure-5 are considered because structure-1 to structure-4 behaved in a similar manner), as shown in Figure 4.13 and Figure 4.14. These three phases are explained as follows:

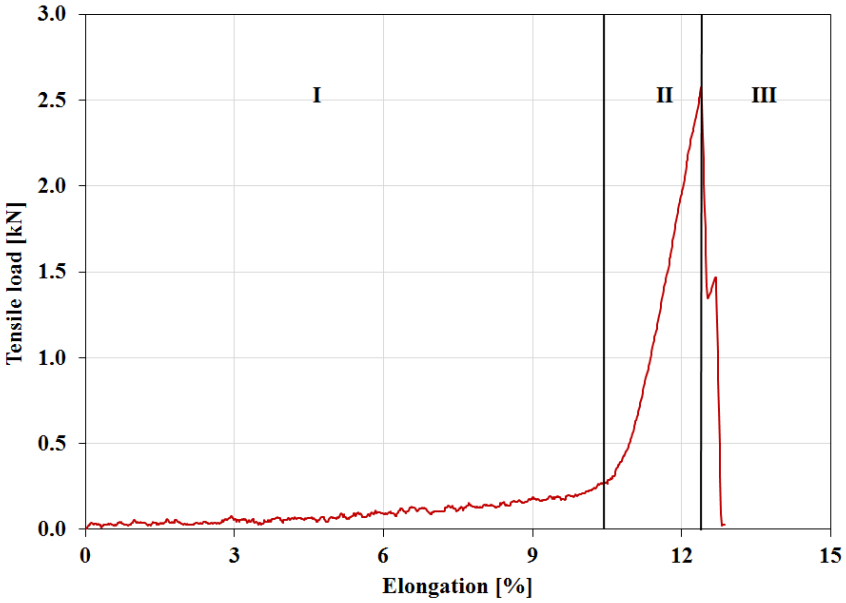

Figure 4.13. Tensile behaviour of auxetic structure-3.

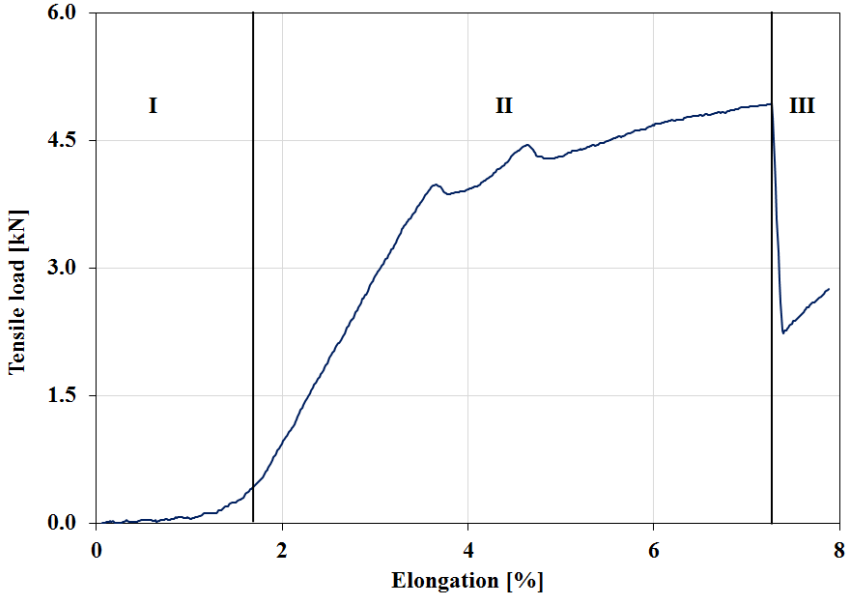

Figure 4.14. Tensile behaviour of auxetic structure-5.

Phase I

Structure-3: Upon loading, the structure starts to bear load due to straightening of the longitudinal rods and shows less load bearing capacity and high elongation in this phase due to lower initial angle φ (64°).

Structure-5: Upon loading, the structure starts to bear load due to straightening of the longitudinal rods and shows higher load bearing capacity and lower elongation in this phase than structure-3 due to higher initial angle φ (79°). The structures in phase I are shown in Figure 4.15.

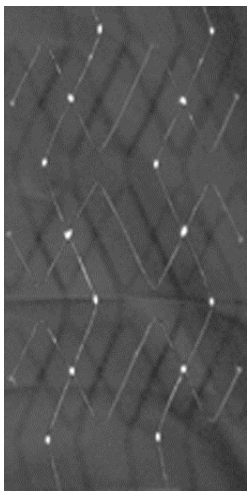

Figure 4.15. Structure at phase 1.

Phase II

Structure-3: The curves are steeper in this region since the longitudinal rods became already straight in phase I, and start to bear load due to tensile deformation until fracture. The elongation of this phase is less.

Structure-5: Initially, the curves are steeper and linear in this region due to elastic deformation of the longitudinal rods and then shows yielding before fracture. Therefore, structure-5 shows higher elongation and some pseudo-ductile behaviour when compared to structure-3. The structures in Phase II are shown in Figure 4.16.

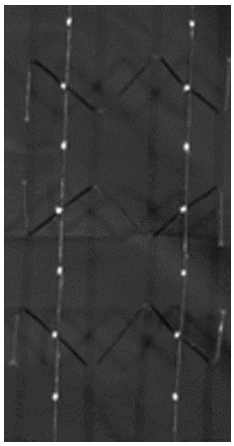

Figure 4.16. Structure at phase II.

Phase III

Structure-3 & 5: The failure of longitudinal rods occurs in phase III. (The arrow marks shown in Figure 4.17)

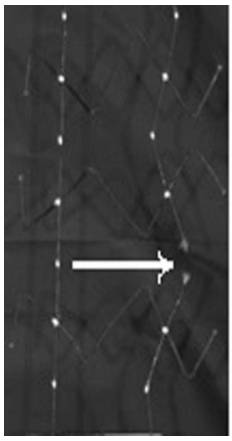

Figure 4.17. Structure at phase III.

Due to less undulation of the longitudinal rods in structure-5, the rods become straight quickly and therefore, exhibits lower strain in phase I. However, in other structures, the undulation of longitudinal rods is high and therefore, these structures take more time to become straight, resulting in higher strain in phase I. Higher undulation of longitudinal rods in structure-1 to structure-4 cause development weakest points and stress concentration at the bending locations, and therefore, failure occurs suddenly at these weakest points. On the other hand, less undulation of longitudinal rods in structure-5 does not create weakest points at the bending locations and therefore, failure does not preferably occur at these locations. As a result, the structure-5 can show its complete tensile behaviour, i.e., a linear elastic behaviour due to elongation of core fibres and subsequent plastic behaviour probably due to matrix deformation and load transfer to the sheath polyester fibres.

4.2.3.5. Work of rupture

Work of rupture (WOR), i.e. work done or energy required to break the structures has been calculated using load-elongation curve of the structures and given in Table 4.2. Work of rupture for the auxetic structure-5 is two to three times higher than the other structures.

4.3. Development of auxetic structure based on lozenge grid: optimized structure

The auxetic structure explained in previous section was optimized based on design aspects to improve the structural integrity and strengthening behaviour. The auxetic structures explained in previous section have the drawback of low strength at initial stage and too much space between longitudinal and transverse rods in the structures. The parameters studied to optimize the structure is explained in following sections of this chapter.

4.3.1. Parameters of developed structures

In order to study the influence of different parameters, auxetic structures were produced using different types of core fibre having different linear densities (2400 tex, 4800 tex, and 6000 tex glass fibre; 4800 tex basalt fibre and 4800 tex carbon fibre). Also, structures angle φ (66°, 72°, and 78°) varied and studied effect on auxetic and tensile behaviour. Moreover, modification of basic structures through addition of straight longitudinal rod and change in structural angle resulted in different structural parameters, which are listed in Table 4.3 along with material parameters. Also, the developed structures are given in the Figure 4.18.

The dimension of the structures was kept constant for all specimens, i.e. 15 cm in width and 40 cm in length, with additional length for clamping. Four specimens were produced for each type of auxetic structure.

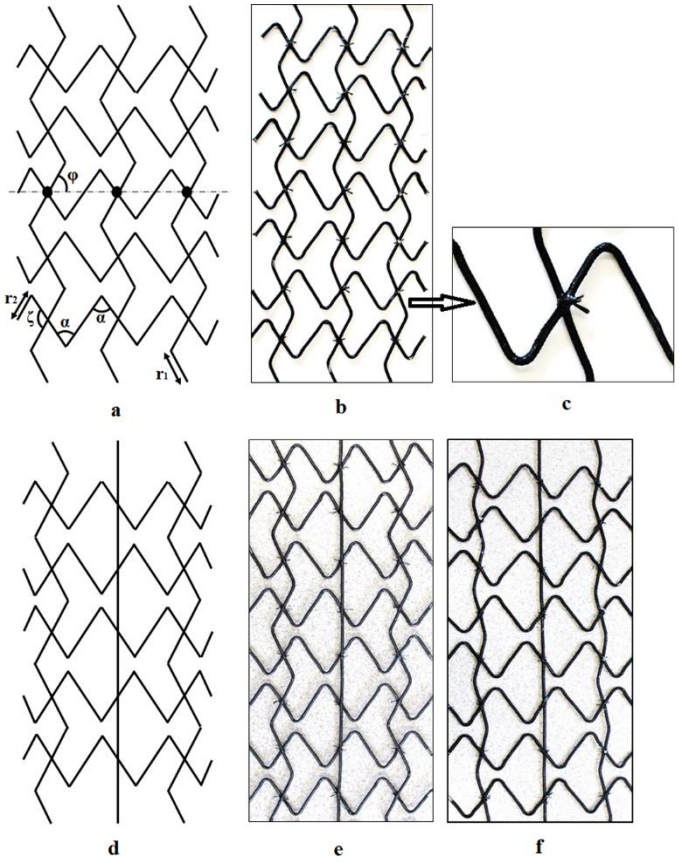

Figure 4.18. Auxetic structural design used in the present study showing the structural angles (r_1 – longitudinal rod rib length and r_2 – transversional rod rib length). (a) Schematic of structure-1, (b) real structure-1, (c) portion of structure in close-up, (d) schematic of structure-2 and (e and f) structure-2 and structure-3.

Table 4.3. Parameters of developed auxetic structures

Structure	**Core fibre type**	**Core fibre, tex**	**Angle *φ*, °**	**Rib length, cm**
S – 1	Glass	2400	66	r_1 – 2.7 & r_2 – 2.35
S – 1	Glass	4800	66	r_1 – 2.7 & r_2 – 2.35
S – 1	Glass	6000	66	r_1 – 2.7 & r_2 – 2.35
S – 1	Glass	4800	72	r_1 – 2.6 & r_2 – 2.35
S – 1	Glass	4800	78	r_1 – 2.5 & r_2 – 2.35
S – 1	Basalt	4800	66	r_1 – 2.7 & r_2 – 2.35
S – 1	Carbon	4800	66	r_1 – 2.7 & r_2 – 2.35
S – 2*	Glass	4800	66	r_1 – 2.7 & r_2 – 2.35
S – 3*	Glass	4800	78	r_1 – 2.5 & r_2 – 2.35

Note: *S – 2 and S – 3 consists both undulation and straight vertical rods

4.3.2. Measurement of Poisson's ratio and tensile properties

The measurement of Poisson's ratio and tensile properties of the auxetic structures developed were carried out in a Universal Tensile Testing Machine. The cross-head speed of tensile testing machine was kept at 25 mm/min. White marks were painted on the structures at top, middle and bottom as shown in Figure 4.19. During tensile testing, the video of sample deformation was captured using Canon EOS 650D and later, the video was converted in to images at specific interval. The distance between the marks in the structures, both in longitudinal and transverse directions, was measured in pixels using ImageJ software. The longitudinal and transverse strains were then calculated by using equations 3.1 and 3.2.

Figure 4.19. Auxetic structure with marks.

Where x_n and y_n are the distance between the points marked on the structure at n^{th} of loading, x_0 and y_0 are the original distance between the marks at zero loading. The average transverse strain was calculated by averaging the transverse strain calculated at top, middle and bottom points. Similarly, the average longitudinal strain was calculated from longitudinal strains measured from left and right points of the structures. The measurement principle has been illustrated in Figure 4.20. Later, the Poisson's ratio was calculated from the average strains by using equation 3.3.

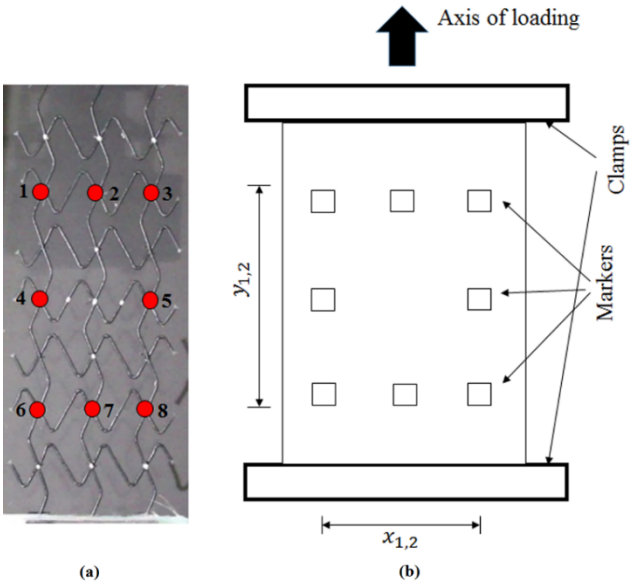

Figure 4.20. (a) Auxetic structure with painted marks, and (b) points for strain calculation.

4.3.3. Results and discussion

4.3.3.1. Auxetic behaviour of the basic structures

Axial strain on the longitudinal undulation rods induced by the tensile load results straightening of the rods, thus leads to expansion in the transverse direction through an opening of transverse undulation rods. The deformation of the structures unit cell elements at various stages during tensile loading are presented in Figure 4.21.

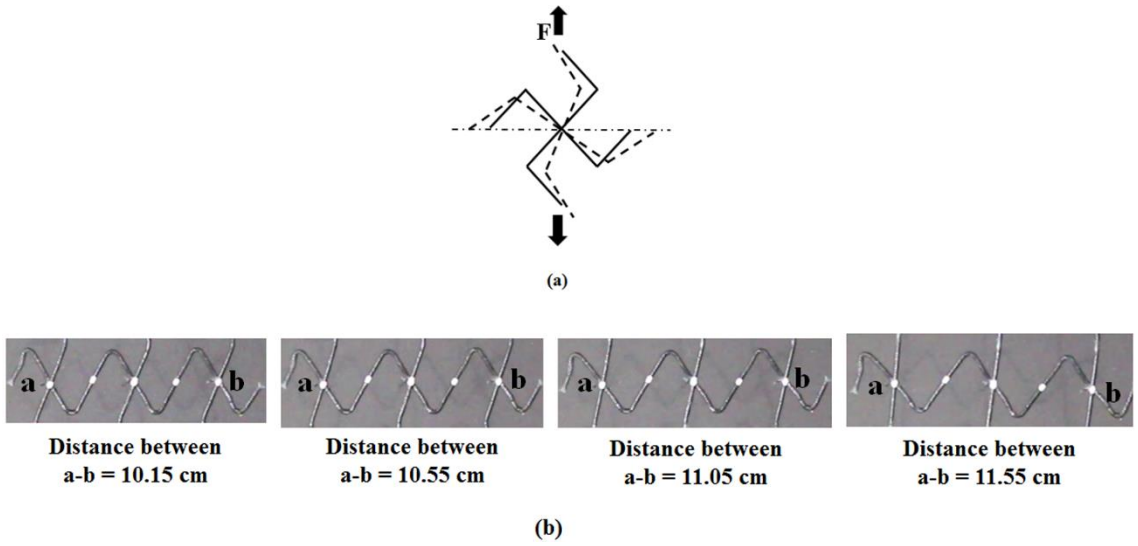

Figure 4.21. (a) Schematic of unit cell movement during loading and (b) Structures unit cell at various stages of loading.

4.3.3.2. Effect of core fibre type on auxetic behaviour of structures

To study the effect of core fibre types, auxetic structures were produced with braided rods consisting of glass, basalt, and carbon core fibres with same linear density, 4800 tex. As presented in Figure 4.22 and listed in Table 4.4, the core fibre type shows no influence on the auxetic behaviour and the trend of Poisson's ratio change with longitudinal strain is the same for all fibres.

The Poisson's ratio values remain constant until around ~5.5% longitudinal strain and then start to decrease with additional increase of strain until failure of the structures. The straightening of longitudinal rods stop at this strain level (~5.5%), i.e. they become fully straight and no further transverse expansion is possible. Further axial strain after this point, therefore, results in reduction of Poisson's ratio.

Table 4.4. Poisson's ratio of the auxetic structures developed from the glass, basalt and carbon fibres

Core fibre (tex)	**Type of fibre**	**Avg. diameter of BCR (mm)**	**Avg. Poisson's ratio at around 1% strain**
4800	Glass	2.4 (2.1)	-1.59 (11.6)
4800	Basalt	2.4 (3.4)	-1.59 (13.1)
4800	Carbon	2.1 (4.0)	-1.57 (14.3)

Note: Values of CV% are given inside brackets.

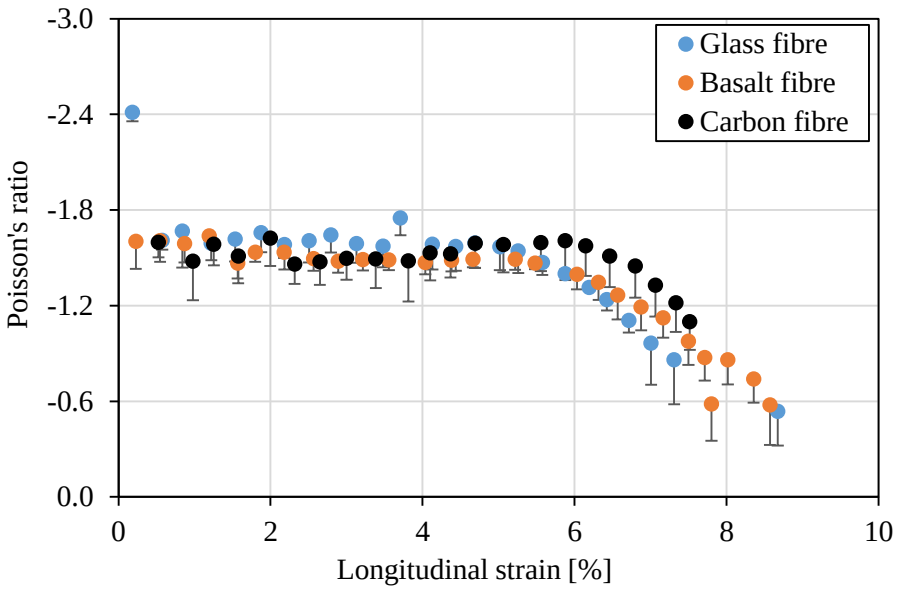

Figure 4.22. Auxetic behaviour of structure-1 having different types of fibres as core.

4.3.3.3. Effect of linear density of braided composite rods on auxetic behaviour

The effect of linear density of core fibres on auxetic behaviour of developed structures can be seen from Table 4.5 and Figure 4.23. It is obvious from the Table 4.5 that the diameter of BCRs increases with the increase in linear density of core fibre. The change in the BCR diameter causes change in the auxetic behaviour of the structures. An increase in the BCR diameter reduces the auxetic behaviour (2400 tex > 4800 > 6000 tex). This is due to the fact that higher diameter (i.e. high linear density core) longitudinal and transverse elements present more resistance towards deformation, resulting in lower transverse expansion and Poisson's ratio.

Table 4.5. The diameter values of BCRs produced from various linear density of glass fibre

Glass fibre (Tex)	**Avg. diameter (mm)**	**Avg. Poisson's ratio at around 1% strain**	**Percentage of change in Poisson's ratio w.r.t 2400 tex**
2400	2.1 (3.9)	-1.78 (13.7)	--
4800	2.4 (2.1)	-1.71 (5.1)	↓ 3.9
6000	2.7 (2.4)	-1.57 (6.7)	↓ 11.8

Note: Values of CV% are given inside brackets.

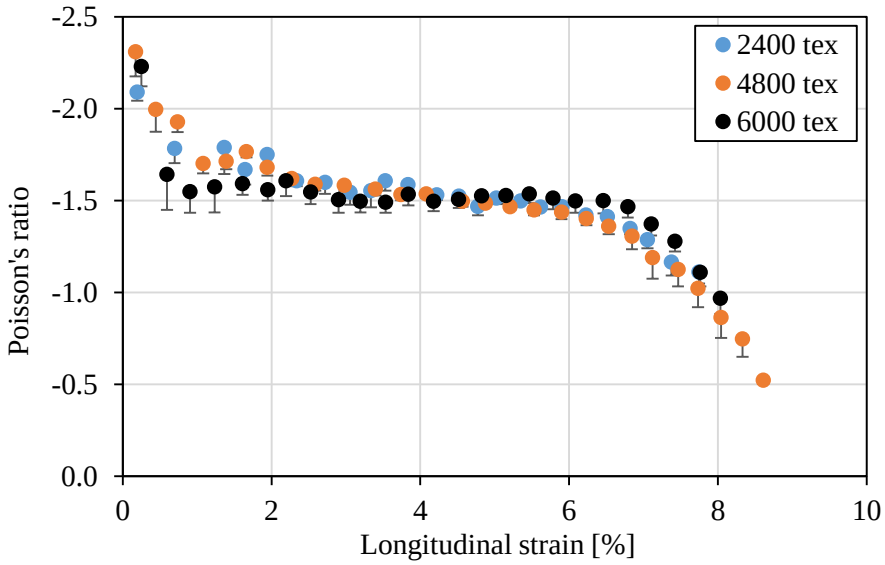

Figure 4.23. Auxetic behaviour of structure-1 having glass fibre as core with different linear density.

4.3.3.4. Effect of angle φ on auxetic behaviour of the structures

Table 4.6 and Figure 4.24 shows that effect of increasing of initial angle φ. It can be observed that an increase in φ increases the Poisson's ratio value. Higher angle of the longitudinal inclined rods results in improved tensile load bearing capability and this, in turn, leads to higher deformation in transverse direction and higher Poisson's ratio. Maximum Poisson's ratio obtained with initial structural angle 66° was ~15% and ~96% lower as compared to 72° and 78°, respectively.

Table 4.6. Auxetic behaviour of structures having different initial angle φ

Initial angle φ (°)	**Avg. Poisson's ratio at around 1% strain**	**CV%**	**Percentage of change in Poisson's ratio w.r.t 66°**
66	-1.70	8.5	--
72	-1.96	7.3	↑ 15.3
78	-3.34	7.4	↑ 96.5

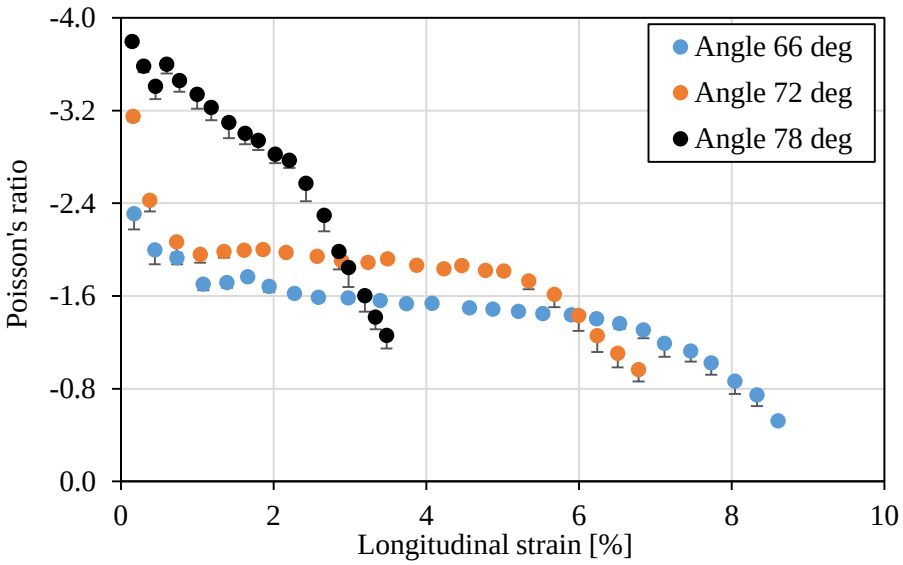

Figure 4.24. Auxetic behaviour of structure-1 having different initial angle φ.

4.3.3.5. Influence of structural modification on auxetic behaviour

The basic auxetic structure, i.e. missing rib or lozenge grid design has been modified with longitudinal straight rods to improve their strengthening behaviour, so that auxetic structures will be suitable for strengthening of structural elements. The auxetic behaviour of the modified auxetic structure is shown in Figure 4.25. Even though the modified structure consists of straight vertical rod, it exhibits negative Poisson's ratio. But the Poisson's ratio value significantly decreased compared with basic structure (structure-1) as expected. This is due to the presence of straight vertical rod that partially restricts the transverse expansion of the structure, as the core fibre of the BCRs straining due to the application of axial load has transverse expansion. The Poisson's ratio value trend of the structure starts with higher value and then drops. Again, it increases until 3% of strain value and decreases continuously until the failure of structure. This is attributed with breakage of longitudinal straight rod breaks at around 3% longitudinal strain value. The initial angle φ of the longitudinal undulation rod of the structure-2 is 66°. This angle is increased to 78° to enhance further its strengthening behaviours. This structure referred as structure-3 and its auxetic behaviour is shown in Figure 4.26. The Poisson's ratio value for the structure-3 is increased considerably and the value decreases with increase of longitudinal strain. This higher Poisson's ratio value compared to structure-2 is due to the higher initial angle φ of longitudinal undulation rods.

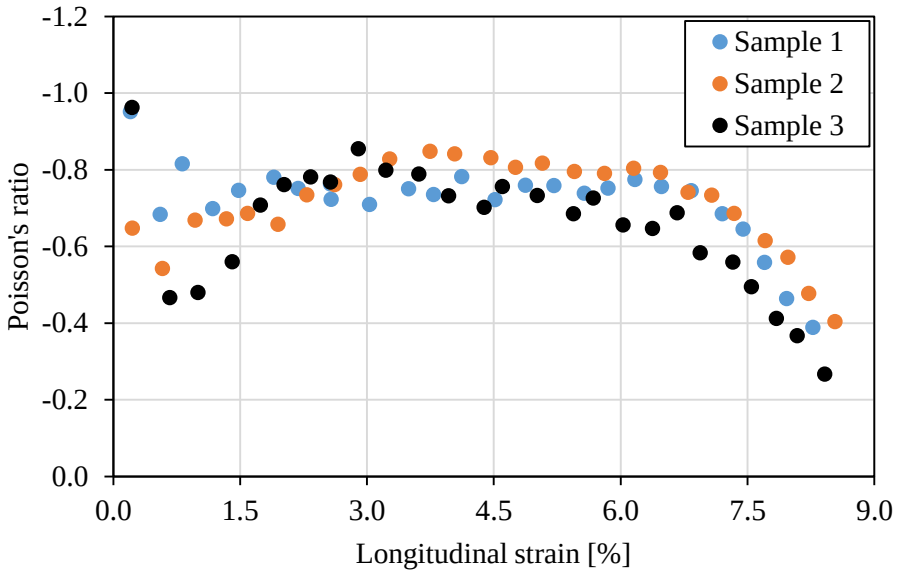

Figure 4.25. Auxetic behaviour of the structure-2 (with straight rod).

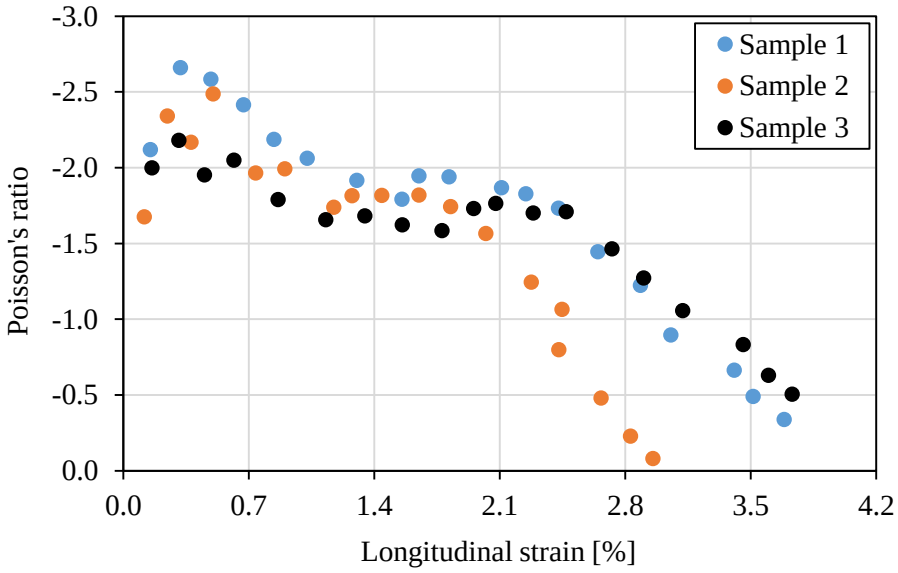

Figure 4.26. Auxetic behaviour of the structure-3 (with straight rod).

4.3.3.6. Tensile properties of auxetic structures

The tensile properties of auxetic structures are provided in Table 4.7. The tensile load was higher for carbon, which was followed by basalt and glass, in decreasing order. It is obvious that carbon fibre is stronger than glass and basalt, so it has provided highest tensile load. The typical tensile behaviour of the developed auxetic structures are shown in Figure 4.27.

It is clear from Table 4.7 that increase of linear density of core fibre increases tensile load and decreases elongation (%) value. This is due to increase of linear density (6000 tex) increases the number of filaments in the BCRs cross-section which bears more load compared lower linear density BCRs (2400 tex). It is also noted from Table 4.7, increase of initial angle φ increases the tensile load of the structures. This is due to with higher initial angle φ (78°), the vertical undulation rods becomes straight sooner and started to bear more loads compared lower initial angle φ (66°).

Table 4.7. Tensile properties of various developed auxetic structures.

Structure	**Fibre type**	**Tex**	**Angle φ, Deg**	**Avg. max. tensile load, kN**	**Avg. elongation at max. tensile load, %**	**Avg. work of rupture, J**
S – 1	Glass	2400	66	4.2 (10.6)	10.0 (4.1)	35.2 (12.0)
S – 1	Glass	4800	66	4.9 (15.2)	9.3 (6.3)	38.2 (2.7)
S – 1	Glass	6000	66	5.9 (10.5)	9.1 (2.2)	49.2 (5.0)
S – 1	Glass	4800	72	5.1 (12.7)	7.2 (6.5)	42.9 (6.0)
S – 1	Glass	4800	78	6.9 (10.1)	4.3 (9.7)	47.8 (8.7)
S – 1	Basalt	4800	66	6.1 (14.7)	9.5 (1.9)	45.7 (14.5)
S – 1	Carbon	4800	66	7.3 (15.5)	8.7 (5.6)	71.3 (12.4)
S – 2	Glass	4800	66	3.4 (11.2)	8.9 (5.0)	43.7 (10.5)
S – 3	Glass	4800	78	5.5 (8.3)	3.0 (7.9)	48.8 (6.1)

Note: Values of CV% are given inside brackets.

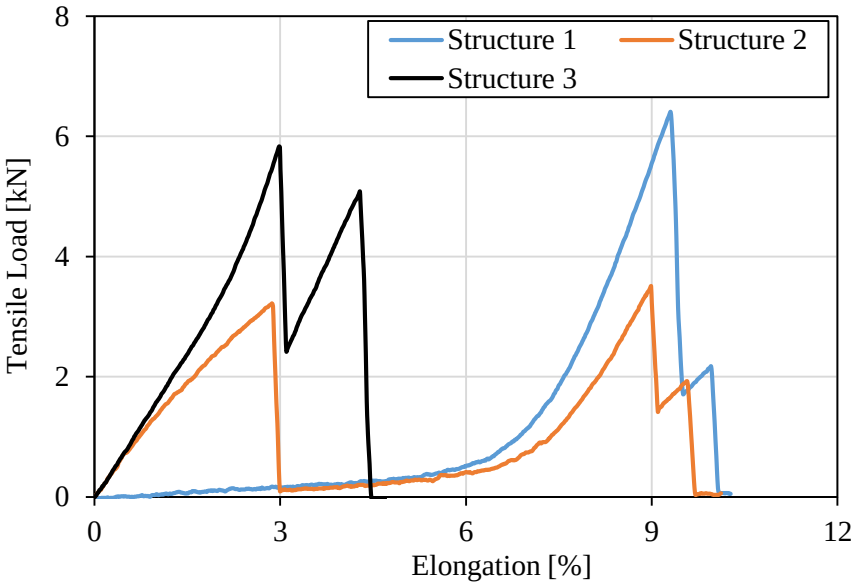

Figure 4.27. Tensile behaviour of developed auxetic structures.

The tensile results and curve of structure-2 and structure-3 shows that the maximum tensile load value is decreased compared with structure-1 and the curves are totally different in behaviour. Tensile behaviour of structure-1 to structure-3 explained in detailed manner by dividing the tensile vs. elongation curve in three phase and it is shown in Figure 4.28, Figure 4.29, and Figure 4.30.

Phase I

Structure-1: the tensile load applying on vertical undulation rods results straightening of undulation and becomes straight at the end of phase. The load bearing of structure is less due to undulation of vertical rods.

Structure-2: as the structure has straight vertical rods, the structure takes more load so the curve is steep. End of this phase the straight vertical rod was broken. Also, the structure's vertical undulation rods getting straight in this phase.

Structure-3: structure consists of straight and less undulation vertical rods results more bearing of tensile load compared to structure-2. This is due to undulation becomes straight quickly and start to bear more loads. At 2% of longitudinal strain structure-2 bears 2.5 kN load, but structure-3 bears 3.4 kN tensile load. End of this straight vertical rod was broken and undulation vertical rods are become straight. The Figure 4.31 shows the all structures in Phase I.

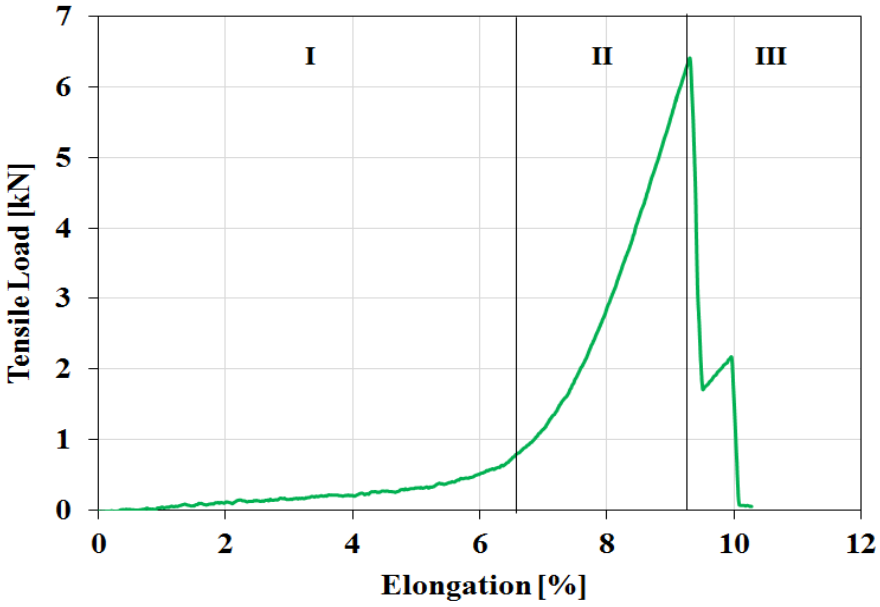

Figure 4.28. Tensile behaviour of structure-1.

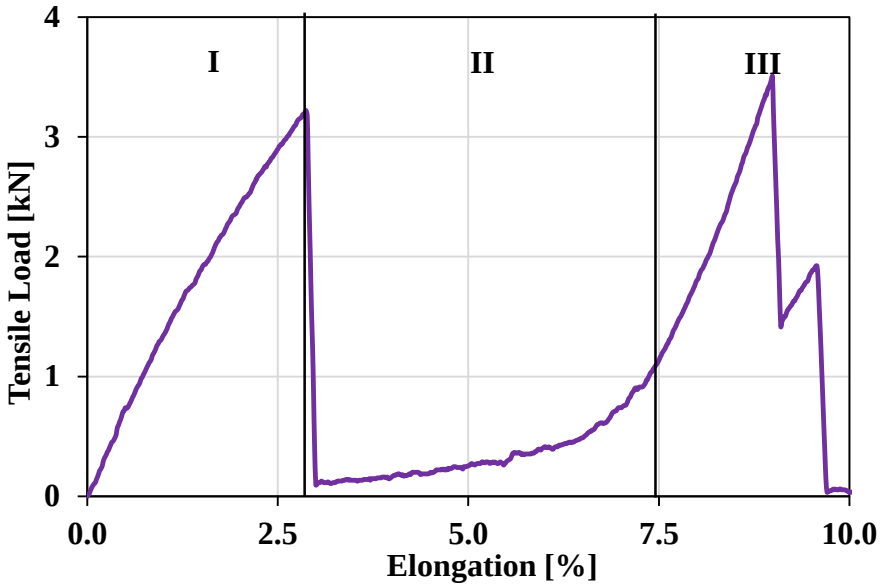

Figure 4.29. Tensile behaviour of structure-2.

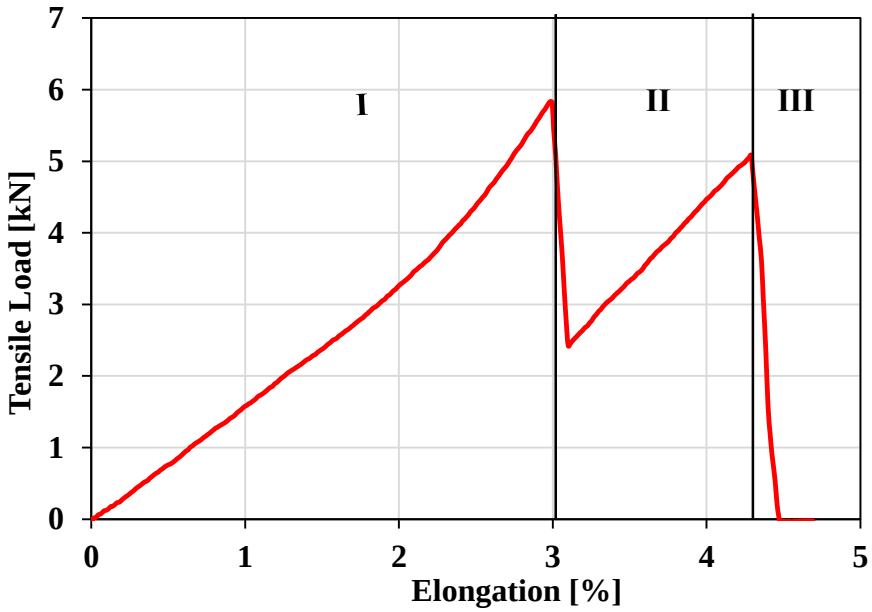

Figure 4.30. Tensile behaviour of structure-3.

Phase II

Structure-1: the vertical rods are becomes straight and started to bear more tensile load and curve is steep in this phase.

Structure-2: the straightened vertical undulation rods started to bear more loads so the curve become steep again.

Structure-3: straightened vertical rods started to take more loads, so the curves are steep again.

The Figure 4.32 shows the structures at phase II.

Phase III

Structure-1: the vertical rods were failed one by one in this stage. The failure takes place at the bending points of rods. Because the undulation causes growth of weak points in the core fibre at the bending and stress concentrates at this points, and therefore, breaking of rods happened at this weak points.

Structure-2 & 3: the straightened vertical undulation rods failed one by one. The failure takes place bending points of rods and the reason explained in the previous paragraph. The Figure 4.33 shows the structures at phase III.

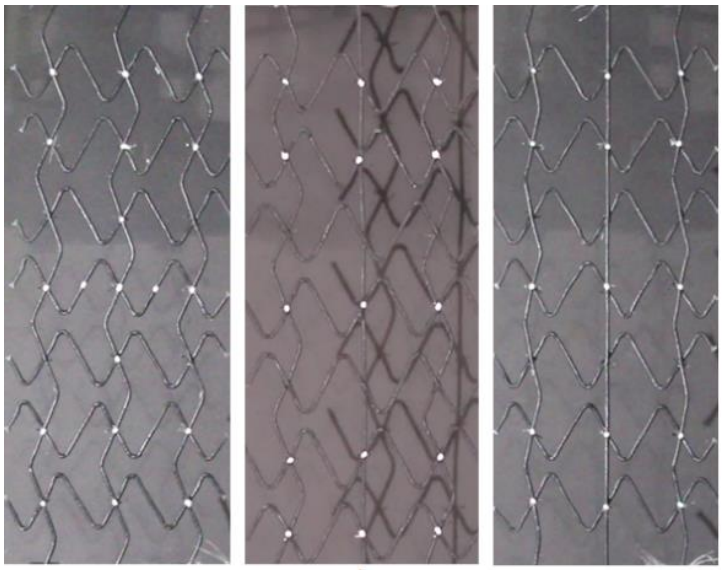

Figure 4.31. Structures at phase I: a) structure-1, b) structure-2, and c) structure-3.

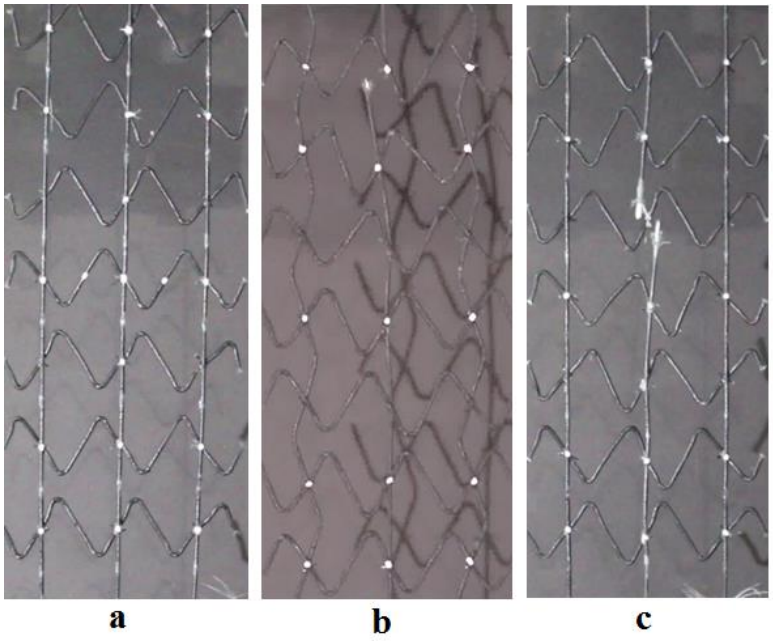

Figure 4.32. Structures at phase II: a) structure-1, b) structure-2, and c) structure-3.

Maximum tensile load for the structure-1 is more compared to structure-2 and 3. Because, in structure-1 all the three vertical rods bearing loads at once, whereas in structure- 2 and 3 the load bearing capacity was distributed in two phase. However, the energy absorption is more for structure-2 and 3 compared to structure-1.

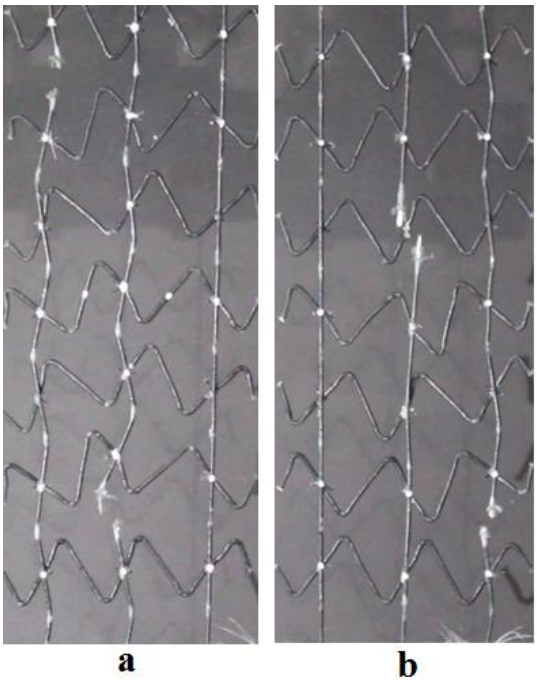

Figure 4.33. Structure at phase III: (a) structure-1 and (b) structure-2 and structure-3.

4.3.3.7. Work of rupture of the auxetic structures

Work of rupture (J) calculated for the developed auxetic structures are given in Table 4.7. As expected, the work of rupture increases with increase of linear density of glass fibre and increase of structure initial angle φ for the structure-1 and the work of rupture of the structures developed from the different core fibres as follows: glass < basalt < carbon. Work of rupture for the structures developed from glass fibre (4800 tex) is in the order: structure-1< structure-2 < structure-3. As structure-3 exhibits higher work of rupture and better tensile properties than the other two structures, it is here proposed for civil engineering applications. As structure-3 consists of both straight and undulation vertical rods, it will give strengthening as well as ductility in balanced way more than other structures. The core fibre of the BCRs can be chosen depending up on the nature and requirement of a given specific application.

4.4. Conclusion

The auxetic structures studied in the preliminary work had some drawbacks concern with civil engineering applications like no load capacity at lower tensile strain, less energy absorption and more space between longitudinal and transverse elements of the structures. So the design is modified and optimized and studied auxetic and tensile behaviour in detailed manner. Simple Image analysis software was used to measure strain components of the structures which undergone tensile tests with a balanced compromise between spatial resolution and accuracy. Poisson's ratio was calculated using strain components (both longitudinal and transverse) obtained through the image analysis.

All structures exhibited negative Poisson's ratio and Poisson's ratio was dependent on the initial value of structural angle (φ). Poisson's ratio was found to increase with the increase in the initial angle φ. Also, the Poisson's ratio of the structures varied slightly by varying the BCRs diameter and doesn't change for changing core fibre of BCRs. And, the lower diameter BCRs shows higher Poisson's ratio value compared higher diameter BCRs structures. Modified auxetic structures (structure-2 and structure-3 consists of straight vertical rod) also exhibits negative Poisson's ratio, but lesser than basic structure (structure-1). This is due to the presence of longitudinal straight rods which restricts the transverse movement compared to structure-1.

The work of rupture and tensile behaviour of the structures also depends up on the structure angle, BCRs diameter and type of fibres. The higher work of rupture and tensile behaviour was observed for the structures with higher angle, higher BCRs diameter and high stiffness fibre (e.g. carbon fibre). The structures work of rupture and tensile behaviour enhanced by modifying the structure with straight vertical rod (structure-2 and structure-3). This modification of the structures will be helpful while strengthening with civil structural elements. Structure-3 exhibits maximum energy absorption and good strengthening at lower strain, so it is proposed for the civil engineering applications.

Chapter 5

Development and Optimization of Auxetic Structures Based on Re-entrant Hexagon Design

5.1. Introduction

In the previous chapter, the development and optimization of auxetic structures based on missing rib or lozenge grid have been discussed. The successful development of auxetic structures from braided composites gave motivation to develop another novel auxetic structure from braided composites which may give different auxetic and tensile behaviour. The design chosen for this new structure is re-entrant hexagon or bow-tie design.

Re-entrant hexagon or bow-tie or butterfly design [114] was chosen due to its simple design and easy to develop structure from braided composite materials. Re-entrant is the internal geometry of the system, which can be observed in the macro, micro and nano structure [107]. Re-entrant design was adopted and produced the following auxetic materials: foams for sandwich panel core for aerospace and air filtration applications [19, 115, 116], flat and warp knitted fabric [107, 117], molecular auxetic, i.e. (n,m) – reflexyne [15, 38], cellular tubes for angioplasty or Annuloplasty rings [118], honeycomb core from Kevlar/epoxy and recycled rubber core materials for sandwich applications [119 – 122].

The mechanical properties of these materials are not sufficient to use them as strengthening materials for civil engineering applications.

Auxetic structures based on re-entrant hexagon were produced from glass, basalt and carbon fibre reinforced braided composites and the results were compared. Also, effect of varying linear density of glass fibre roving and angle on auxetic and tensile behaviour was studied. Later, the basic auxetic design have been modified with straight vertical rods to improve the strengthening characteristics of the structure considering civil engineering applications and auxetic and tensile behaviour have been studied in detailed manner in this chapter.

5.2. Development of auxetic structures

Triaxial braided structures were produced in a vertical braiding machine using polyester multi-filament yarns (with linear density of 110 tex) in the sheath and glass/basalt/carbon multifilament rovings as the core material. During the braiding process, sixteen polyester filament bobbins were used to supply the sheath yarns, which were then braided around the core fibres. Produced braided structures were next used to develop three types of auxetic structures, as shown in Figure 5.1. The first structure (structure-1) was developed using the basic re-entrant honeycomb design. In structure-2, the basic design was modified with straight longitudinal rods. Structure-2 was further modified to improve the tensile behaviour using higher angle of longitudinal rods, resulting in structure-3. For each type, three samples were produced keeping the total length and width as 40 cm and 11 cm, respectively, with additional length for clamping during tensile testing. Following steps were performed to produce the auxetic structures: (1) the auxetic structural design (Figure 5.1) was drawn on a white chart paper; (2) the chart paper was placed on a board and the braided structures were placed over the drawn design firmly with help of adhesive tape; (3) the joints were tied by polyester filaments and epoxy resin was applied over the structures using a brush; (4) after curing, the structures were removed from the board. The braided structures after resin application and curing became circular composites termed as braided composite rods (BCR). The weight percentage of core fibre in each of these rods was around 51 ± 2%.

Resin application was necessary to give sufficient mechanical stability to the braided materials in order to handle them easily and turn them in to auxetic structures.

Also, the braided structures display suitable mechanical properties necessary for the targeted use only after resin application and formation of BCR, since the epoxy matrix holds the various components (core and sheath) of braided structures together, enabling them to act as a single structure. In absence of resin, there may be slippage between the core and sheath as well as between the core fibres causing poor mechanical properties.

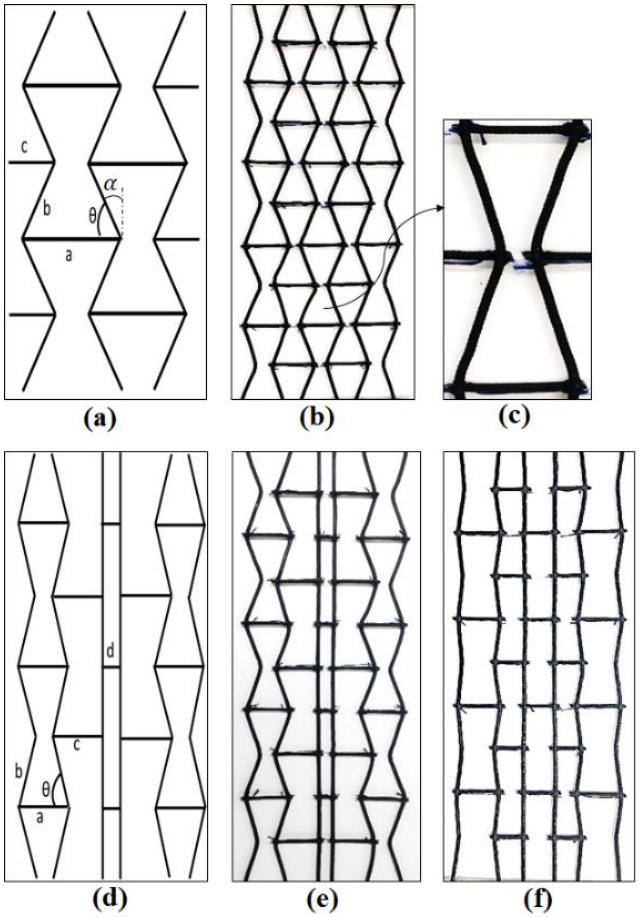

Figure 5.1 a) Basic re-entrant honeycomb design, a – horizontal rib length, b – diagonal rib length, c – half of the 'a', θ – angle formed between diagonal and horizontal rib and α – angle between diagonal rib to vertical axis, b) auxetic structure developed from BCR (structure-1), c) repeat unit cell of structure 1, d) schematic design of structure-2, e) structure-2, and f) structure-3.

5.3. Parameters of developed structures

The influence of structural and material parameters were studied by analytical and experimental methods, i.e. material parameters (linear density, type of fibres) and structural parameter (angle θ) are studied experimentally. Auxetic structures were produced from BCRs contain different linear density (2400 Tex, 4800 Tex and 6000 Tex) of glass fibre as core and also the structures produced by changing their core fibres, i.e. basalt fibre (4800 Tex) and carbon fibre (4800 Tex). The glass, basalt and carbon fibre rovings were purchased from commercially available sources from different countries. The basic design was modified with straight vertical rods to improve their tensile characteristics at low strain levels. This modified designs referred as structure-2 and it is further modified to improve of tensile behaviour with higher angle of vertical undulation rods and referred as structure-3 later in this work.

For each type, three samples were produced and the working dimensions kept same as 40 cm in length and 11 cm in width, with additional length for clamping during tensile testing. The modified auxetic structures developed are shown in Figure 5.1. The structural parameters of auxetic structures are given in the Table 5.1.

Table 5.1. Structural parameters of the re-entrant auxetic structures

Structure	**Core fibres**	**Core fibre linear density, tex**	**Angle**	**Value, °**	**Rib**	**Length, cm**
1	Glass Basalt Carbon	2400, 4800, 6000 4800 4800	θ	76	a	3.0
					b	4.1
2	Glass	4800	θ	76	a	3.0
					b	4.1
					c	3.0
					d	1.0
3	Glass	4800	θ	83	a	3.0
					b	4.0
					c	2.0
					d	2.0

5.4. Evaluation of the auxetic behaviour by image analysis method

The measurement of Poisson's ratio and tensile properties of the auxetic structures developed were carried out by using tensile testing machine. The cross-head speed of tensile testing machine was kept at 25 mm/min. The marking was provided on the structures at top, middle and bottom of the structures. During tensile testing the video was captured by using Canon EOS 650D and later the video was converted into images at required interval (for example per second). The distance between the points marked in the structures both in lateral and longitudinal direction were measured in pixels using ImageJ software. Poisson's ratios were calculated by using the lateral and longitudinal strain the.

5.5. Results and discussion

5.5.1. Auxetic behaviour of the basic structures

The developed auxetic structures based on re-entrant hexagon design exhibits negative Poisson's ratio. While applying tensile load longitudinally to the structure, the vertical inclined rods becoming straight, which results in transverse deformation of structure with help of horizontal connecting rods. The maximum transverse deformation of structure achieved when the vertical rods inclination become straight. The deformation of repeat unit cell of re-entrant hexagon in the auxetic structure at various stages during tensile testing are schematically shown in Figure 5.2.

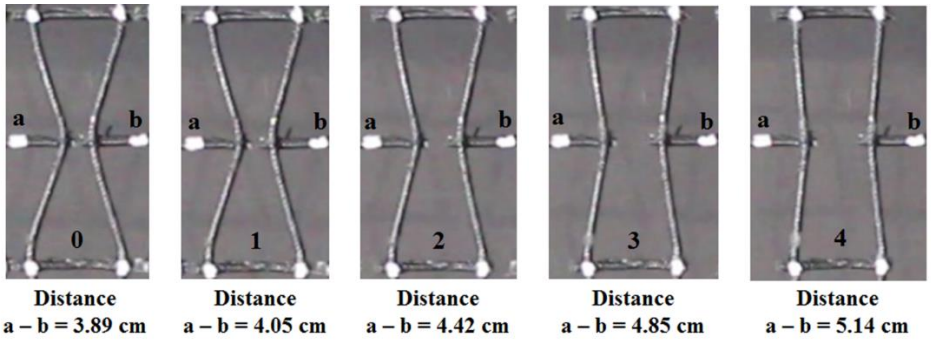

Figure 5.2. Deformation of repeat unit cell of re-entrant hexagon in auxetic structure during tensile loading.

5.5.2. Effect of core fibre on auxetic behaviour of structures

In order to investigate the influence of core fibre type, auxetic structures were produced with BCRs consisting of glass, basalt and carbon core fibres with same linear density, 4800 Tex. As shown in Figure 5.3 and listed in Table 5.2, the core fibre type exhibit significant influence on auxetic behaviour and the trend of Poisson's ratio change with longitudinal strain is the same for all the fibres. Poisson's ratio first increases with strain and then decreases with further strain increment.

The decrease in Poisson's ratio after certain strain level is attributed to the restriction in the free transverse movement of the structures by the clamping systems present at top and bottom of the structures. It results in first bending and subsequently breakage of the transverse rods prior to the longitudinal rods' failure. The highest auxetic behaviour is noticed for glass fibre structure, followed by basalt and carbon fibre structures. Maximum Poisson's ratio obtained with glass fibre was ~8% and ~13% higher as compared to basalt and carbon fibre based structures, respectively. This difference in auxetic behaviour of the structures is related to their stiffness. The stiffer structures (based carbon fibres) exhibit lower Poisson's ratio. Therefore, the developed structures show Poisson's ratio in the following order, which is reverse to the stiffness of core fibres: Poisson's ratio $_{\text{glass structure}}$ > Poisson's ratio $_{\text{basalt structure}}$ > Poisson's ratio $_{\text{carbon structure}}$.

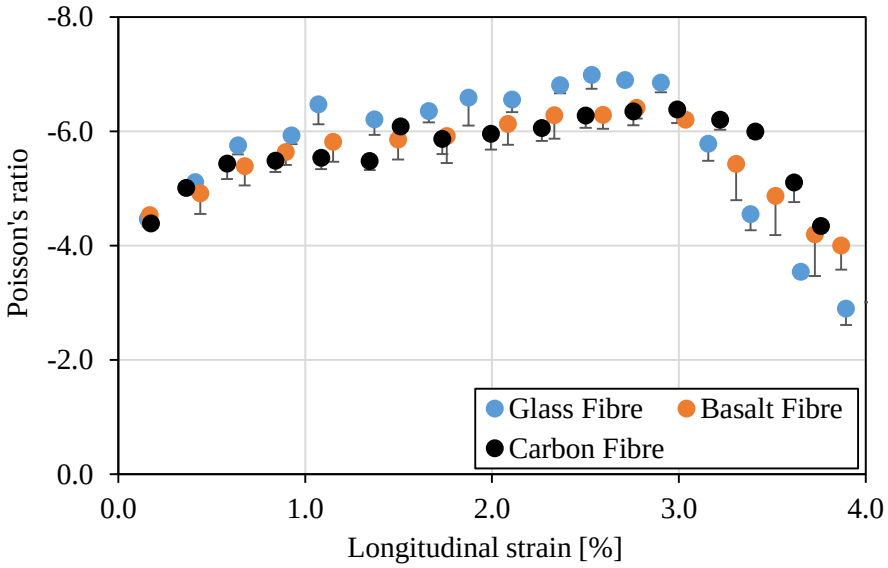

Figure 5.3. Auxetic behaviour of structure-1 containing different types of core fibres (linear density 4800 tex).

Table 5.2. Poisson's ratio of auxetic structures produced from glass, basalt and carbon fibres

Core fibre (tex)	Type of fibre	Avg. diameter of BCR (mm)	Avg. Poisson's ratio at around 1% strain	Percentage of change in Poisson's ratio w.r.t glass
4800	Glass	2.39 (2.08)	-6.77 (4.8)	--
4800	Basalt	2.39 (3.24)	-6.20 (10.3)	↓ 8.4
4800	Carbon	2.91 (4.00)	-5.90 (4.1)	↓ 12.8

Note: Values of CV% are given inside brackets.

Table 5.3. Poisson's ratio of auxetic structures produced from glass fibres with different linear densities

Glass fibre (Tex)	Avg. diameter of BCR (mm)	Avg. Poisson's ratio at around 1% strain	Percentage of change in Poisson's ratio w.r.t 2400 tex
2400	2.06 (3.90)	-7.57 (12.7)	--
4800	2.39 (2.08)	-6.77 (4.8)	↓ 10.6
6000	2.73 (2.45)	-6.41 (9.6)	↓ 15.3

Note: Values of CV% are given inside brackets.

5.5.3. Effect of linear density of braided composite rods on auxetic behaviour

The influence of linear density of core fibres on Poisson's ratio of developed structures can be noticed from Table 5.3 and Figure 5.4 It is also clear from Table 5.3 that the diameter of BCRs increases with increasing linear density of core fibre. An increase in linear density of core fibres results in decrease in the auxetic behaviour of developed structures. A decrease in negative Poisson's ratio by ~15% is noticed by increasing glass core linear density from 2400 tex to 6000 tex. This is attributed to the fact that higher diameter (i.e. high linear density core) horizontal and vertical elements present higher stiffness resulting in lower structural movement and Poisson's ratio.

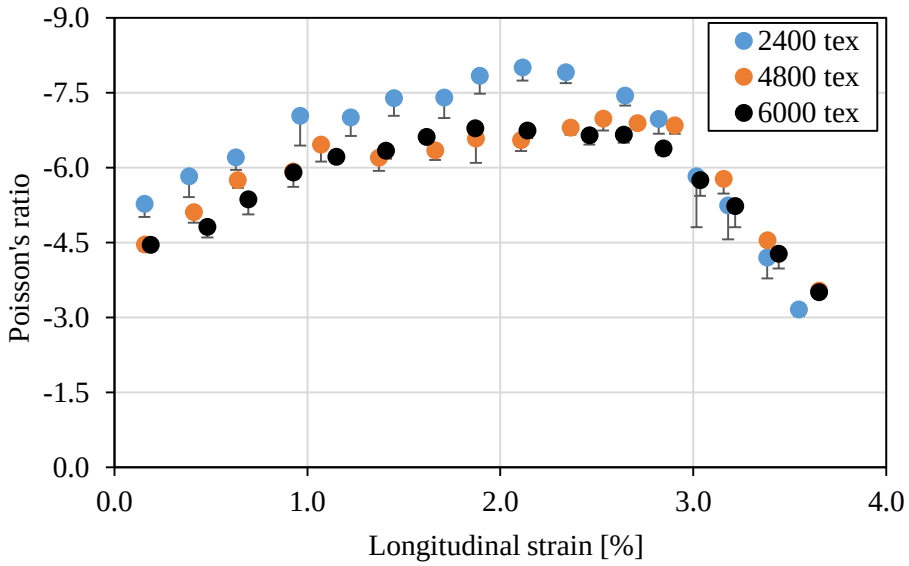

Figure 5.4. Auxetic behaviour of structure-1 having different linear density of glass fibre roving as core materials.

5.5.4. Effect of angle on auxetic behaviour of structures

Table 5.4 shows the influence of structural angle θ on Poisson's ratio of structure-1. It should be noted that θ has been measured from the same structure during tensile deformation at different strain levels. It can be seen that an increase in θ by keeping other structural parameters 'a' and 'b' constant, Poisson's ratio increases. This is due to the fact that when the angle of longitudinal rods increases, they take higher axial loads as compared to the rods with lower angles, leading to higher structural deformation and Poisson's ratio. By changing θ from 74.5 to 85.0, Poisson's ratio increases by 54%. Therefore, it is possible to obtain auxetic structures with different Poisson's ratio through easy adjustment of their structural angles.

Table 5.4. Structural angle and Poisson's ratio of structure-1 at various stages of loading

Stage	Angle θ	Experimental			
		Transverse strain, %	Longitudinal strain, %	Poisson's ratio	Percentage of increase in Poisson's ratio
1	74.5	1.03	0.22	-4.57	
2	77.0	7.41	1.58	-4.70	2.8
3	80.0	16.53	2.63	-6.28	37.4
4	81.5	19.22	2.89	-6.64	45.3
5	83.0	24.94	3.69	-6.70	46.6
6	85.0	29.66	4.21	-7.05	54.3
a – 2.89 cm and b – 3.98 cm					

5.5.5. Influence of structural modification on auxetic behaviour

The re-entrant auxetic structure, i.e. the basic structure was modified with straight longitudinal rods to improve their tensile behaviour, so that these auxetic structures could be suitable for strengthening of structural elements. The auxetic behaviour of the modified structure-2 is shown in Figure 5.5. The results show that auxetic behaviour of structure-2 decreases as compared to the basic structure and the maximum achievable Poisson's ratio is -3.60. The overall decrease in the Poisson's ratio of structure-2 is attributed to the existence of straight rods, which restricts lateral deformation of structures. The trend of Poisson's ratio change with tensile strain is, however, very similar to the basic structure, except in a strain region (indicted in the graph by arrow) in which Poisson's ratio decreases with strain. This region is due to the breakage of straight longitudinal rods, after which load is completely transferred to the diagonal longitudinal rods and the structure behaves again in the similar way to the basic structure. However, structure-3, in which the angle was further increased besides incorporating straight longitudinal rods, shows similar behaviour to the basic structure. The region in which Poisson's ratio decreases with strain, as observed in case of structure-2, is absent due to well balance of load sharing by the straight and diagonal longitudinal rods and smooth transfer of load, once the straight rods break. Poisson's ratio is also higher in this case due to higher structural angle, as shown in Figure 5.6, reaching maximum Poisson's ratio of -5.15.

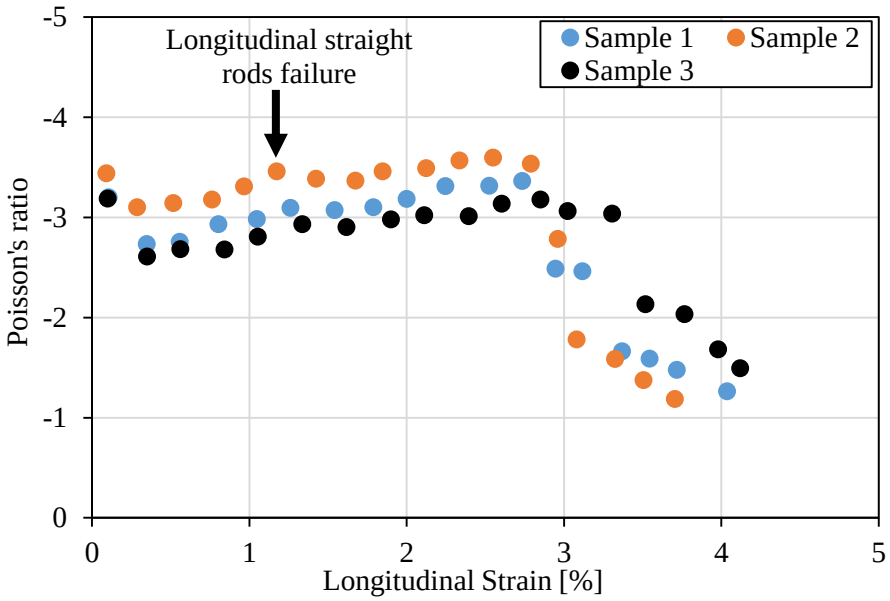

Figure 5.5. Auxetic behaviour of structure-2 made of glass fibre BCRs.

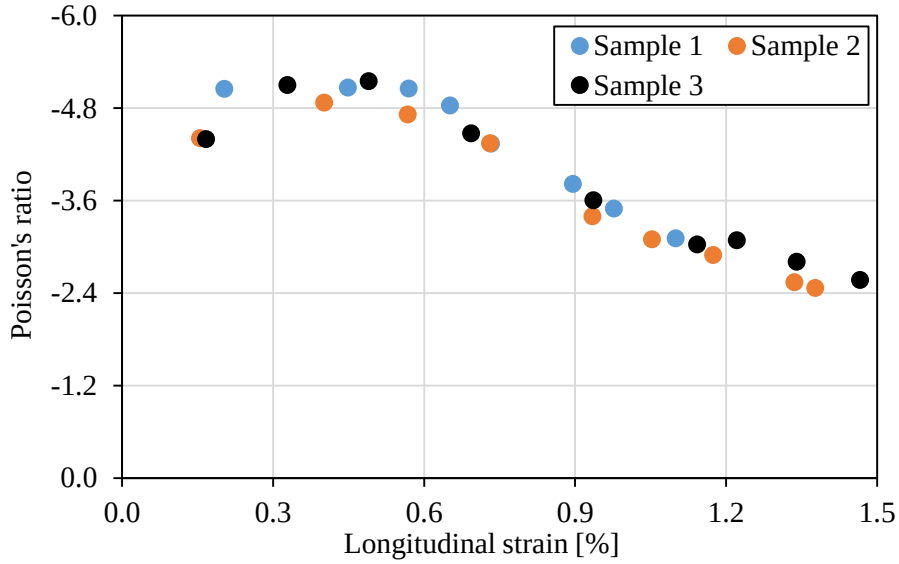

Figure 5.6. Auxetic behaviour of structure-3 made of glass fibre BCRs.

5.6. Tensile properties of auxetic structures

5.6.1 Tensile behaviour of auxetic structures

The tensile properties of auxetic structure-1 produced by varying type of fibre and linear density and structure-2 and structure-3 is provided in Table 5.5. The tensile loads was higher for carbon, which was followed by basalt and glass, in decreasing order. It is obvious that carbon fibre is stiffer than glass and basalt, so it has provided highest tensile load. Though, glass and basalt fibre almost similar in chemical composition, the basalt

exhibits high tensile load than glass fibre, which was used in this study. The typical tensile behaviour of structure-1 is shown in Figure 5.7.

Table 5.5. Tensile properties of various developed auxetic structures.

Structure	Fibre type	Tex	Avg. max. tensile load, kN	Avg. elongation at max. tensile load, %
S – 1	Glass	2400	9.21 (0.46)	5.72 (2.10)
S – 1	Glass	4800	10.40 (8.33)	5.14 (5.45)
S – 1	Glass	6000	15.43 (8.33)	4.82 (9.63)
S – 1	Basalt	4800	14.58 (9.85)	5.92 (10.88)
S – 1	Carbon	4800	22.25 (12.08)	6.20 (12.49)
S – 2	Glass	4800	8.23 (7.31)	4.90 (6.57)
S – 3	Glass	4800	15.23 (0.88)	4.04 (12.15)

Note: Values of CV% are given inside brackets.

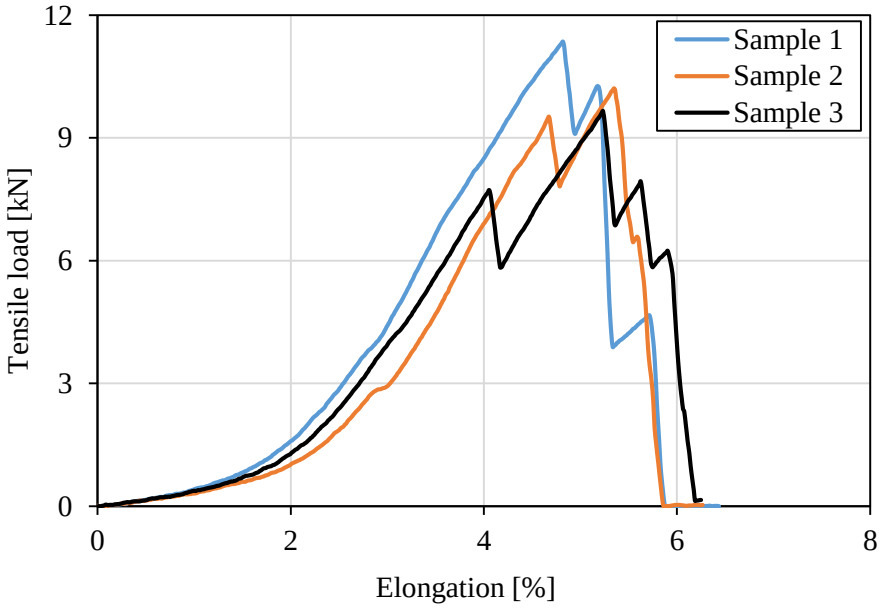

Figure 5.7. Tensile behaviour of structure-1 made of glass fibre BCRs.

The tensile behaviour of modified structures referred as structure-2 and structure-3 made by glass fibre BCRs are shown in Figure 5.8 and Figure 5.9. The results show that tensile behaviour of the structure-2 improved significantly compared to structure-1 (basic, refer Figure 5.7). The tensile characteristics of the structure enhanced further by increasing the vertical rods angle, which is in undulation form. The increase of tensile characteristic of structure-2 compared to structure-1 was due to the vertical straight rods

in the structure -2, whereas the improved tensile characteristics of structure-3 than structure-2 is due to higher angle of undulation rods in the structure than structure-2. The higher angle of vertical undulation rods leads to quick straightening while applying tensile load and started to bear high loads. However, this behaviour is opposite in the structure with less angle of vertical undulation rods, i.e. the undulation rods takes more time to become straight.

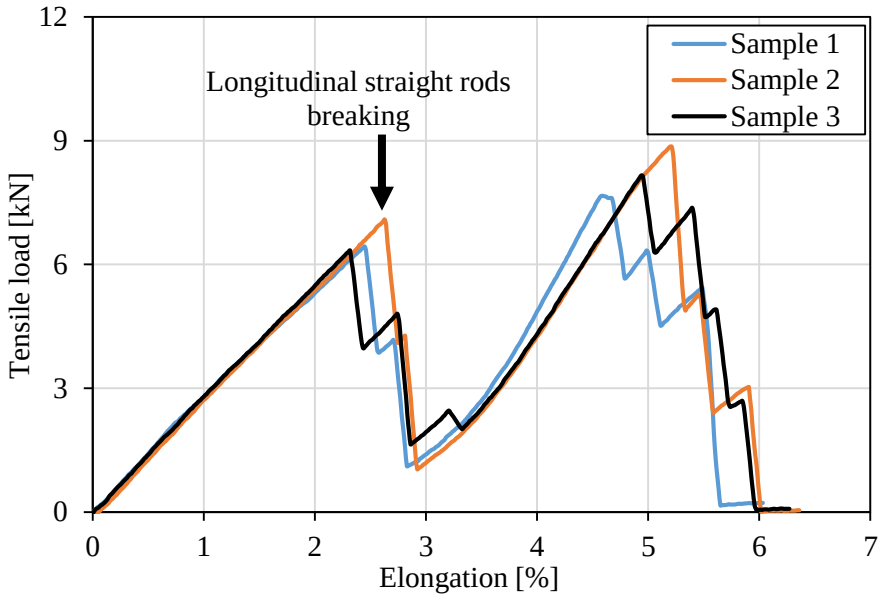

Figure 5.8. Tensile behaviour of structure-2 made of glass fibre BCRs.

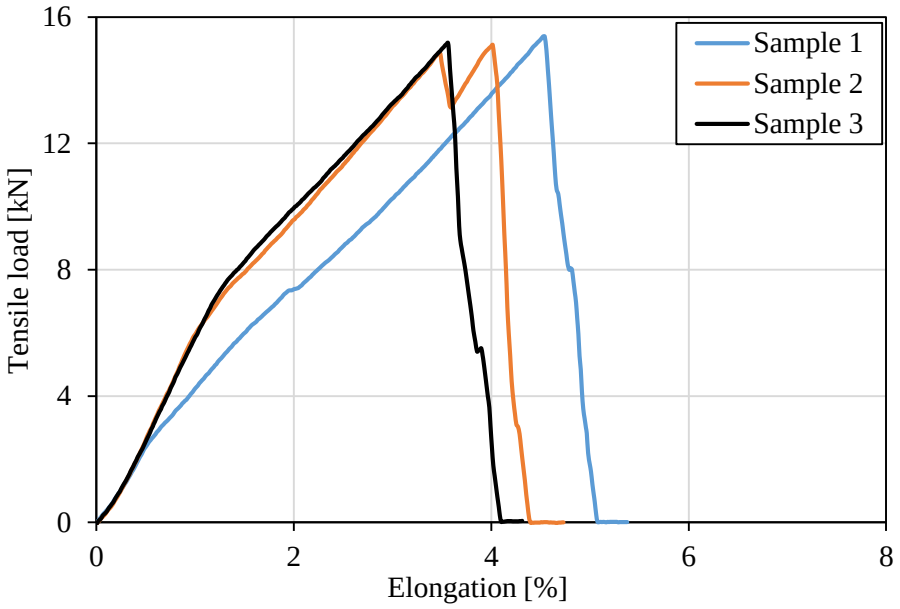

Figure 5.9. Tensile behaviour of structure-3 made of glass fibre BCRs.

Tensile behaviour of structure-1 – 3 is explained in detailed manner by dividing the tensile vs. elongation curve in three phase and it is shown in Figure 5.10, Figure 5.11, and Figure 5.12.

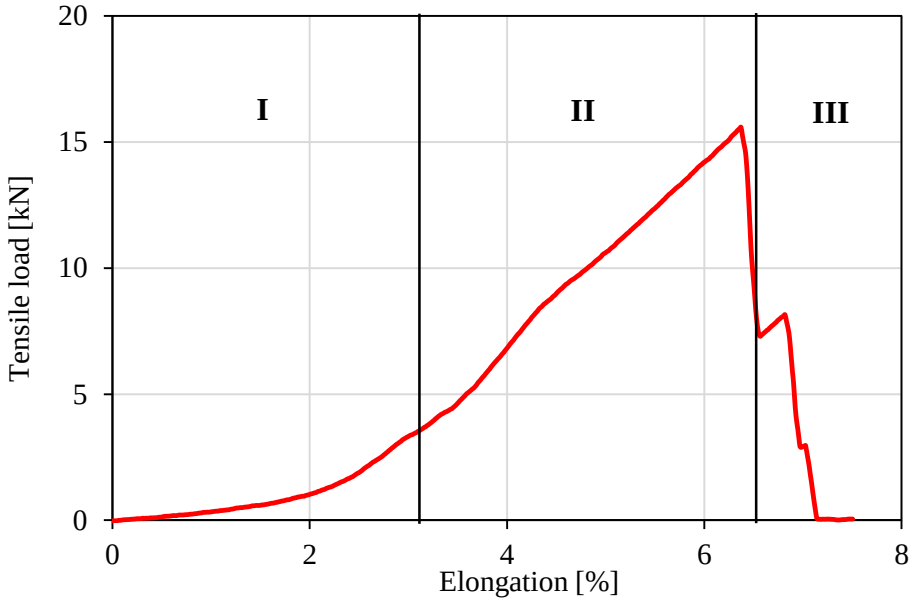

Figure 5.10. Tensile behaviour of structure-1 made of basalt fibre BCRs.

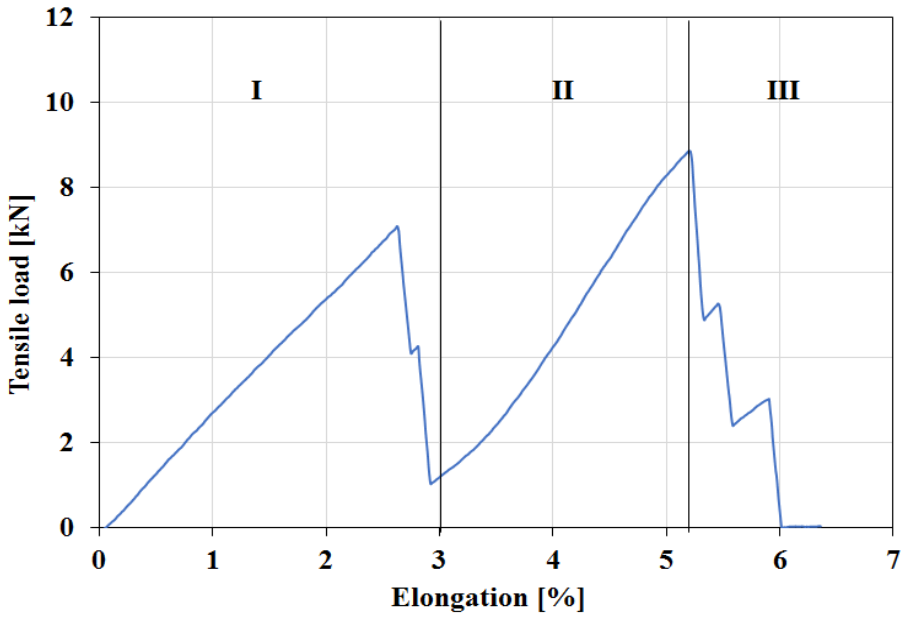

Figure 5.11. Tensile behaviour of structure-2 made of glass fibre BCRs.

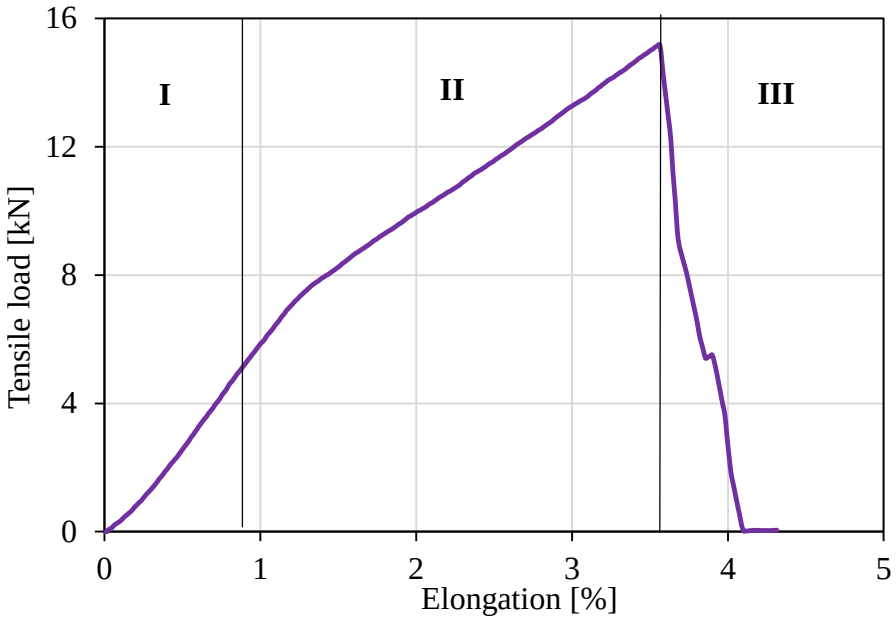

Figure 5.12. Tensile behaviour of structure-3 made of glass fibre BCRs.

Phase I

Structure-1: the tensile load applying on vertical undulation rods results straightening of undulation and becomes straight at the end of phase. The load bearing of structure is less due to undulation of vertical rods.

Structure-2: as the structure has straight vertical rods, the structure takes more load so the curve is steep. At the end of this phase the straight vertical rods were broken. Also, the structure's vertical undulation rods have become straight in this phase.

Structure-3: structure consists of straight vertical rods and less undulation vertical rods results in more bearing of tensile load compared to structure-2. This is due to undulation becomes straight quickly and start to bear more load. At 1% of longitudinal strain, structure-2 bears 3 kN load but structure-3 bears 6 kN tensile load.

The Figure 5.13 shows all the structures in Phase I.

Phase II

Structure-1: the vertical rods are becomes straight and started to bear more tensile load and curve is steep in this phase.

Structure-2: the straightened vertical undulation rods started to bear more loads so the curve become straight again.

Structure-3: all the vertical rods become straight and takes more tensile loads.

The Figure 5.14 shows the structures at phase II.

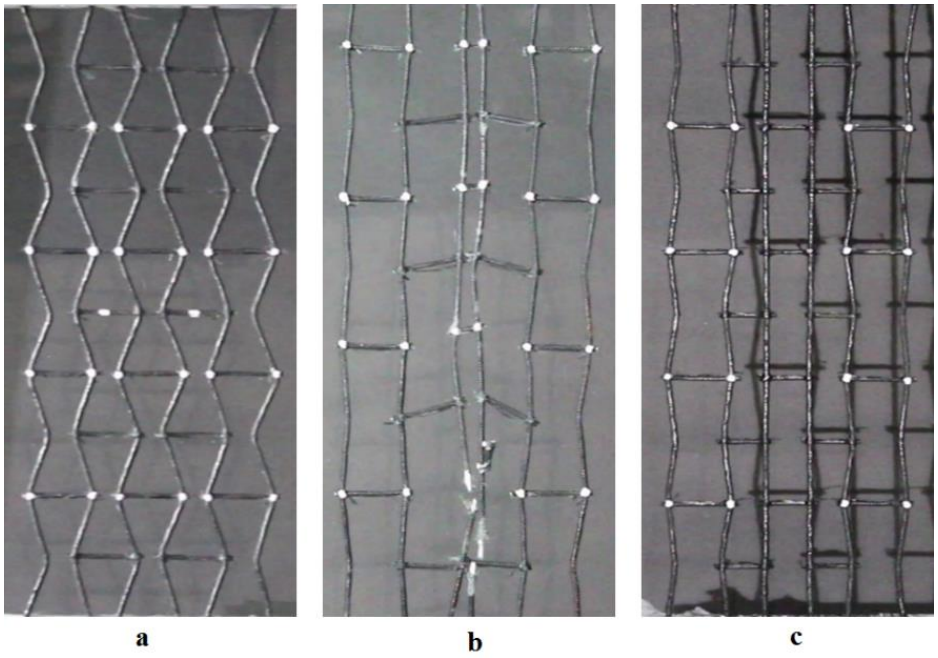

Figure 5.13. Structures at phase I: a) structure-1, b) structure-2, and c) structure-3.

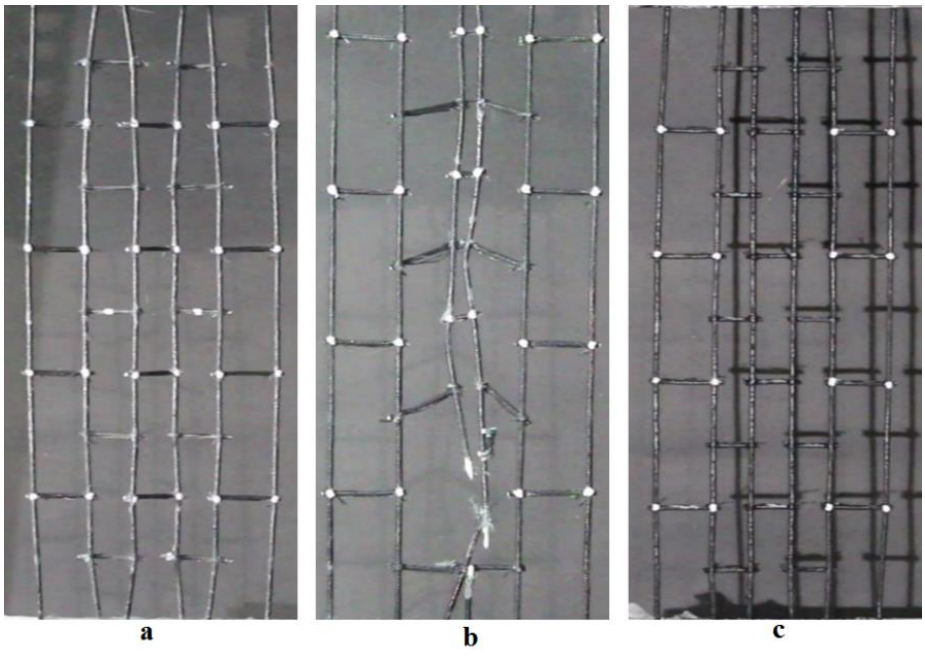

Figure 5.14. Structures at phase II: a) structure-1, b) structure-2, and c) structure-3.

Phase III

Structure-1: the vertical rods failed one by one in this stage. The failure takes place at the bending points of rods because the undulation causes growth of weak points in the core fibre at the bending and stress concentrates at these points, and therefore, breaking of rods happened at these weak points.

Structure-2 & 3: the straightened vertical undulation rods failed one by one. The failure takes place bending points of rods and the reason explained in the previous paragraph. The Figure 5.15 shows the structures at phase III.

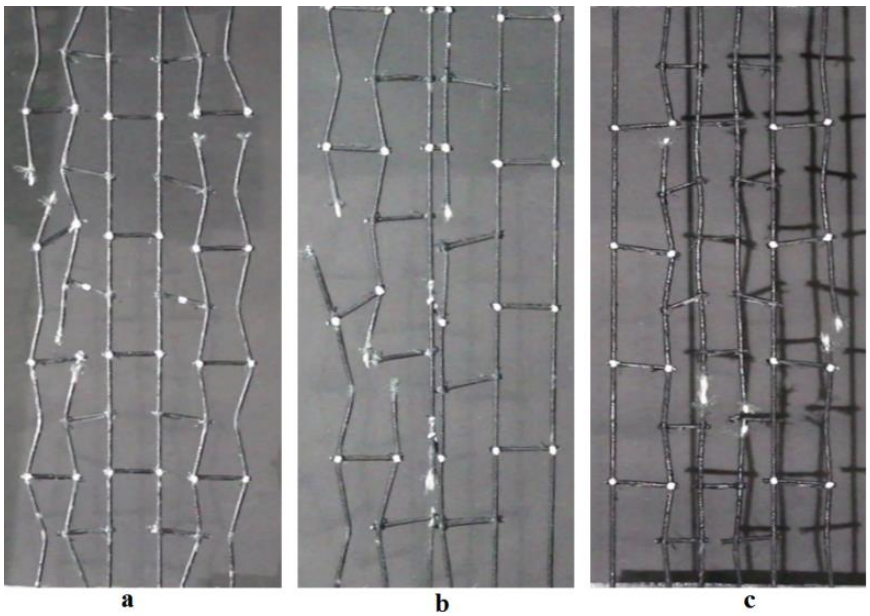

Figure 5.15. Structures at phase III: a) structure-1, b) structure-2, and c) structure-3.

5.6.2 Work of rupture of the auxetic structures

Work of rupture (J) calculated for the developed auxetic structures are given in Table 5.6. As expected, the work of rupture increases with increase of linear density of glass fibre for the structure-1 and the work of rupture of the structure developed from the different core fibres as follows: glass < basalt < carbon. Work of rupture for the structures developed glass fibre is in the order: structure-1 ≤ structure-2 < structure-3. As structure-3 exhibits higher work of rupture and better tensile property than other structures, it is proposed for the structural applications. As the structure-3 consists of both straight and undulation vertical rods, it will provide strengthening as well as ductility in a balanced way, more than the other structures.

Table 5.6. Work of rupture of the developed auxetic structures

Structure	Fibre type	Linear density, tex	Avg. work of rupture, J	CV%
S - 1	Glass	2400	93.31	4.82
S - 1	Glass	4800	98.20	9.40
S - 1	Glass	6000	139.4	11.82
S - 1	Basalt	4800	147.0	8.85
S - 1	Carbon	4800	257.2	3.68
S – 2	Glass	4800	93.7	4.96
S – 3	Glass	4800	150.9	9.00

5.7. Conclusion

In this work, novel auxetic structures at macro scale was developed using braided composite rods and the influence of various structural and material parameters on both auxetic and tensile properties was thoroughly studied and compared with analytical models. Following major conclusions can be drawn from the present research:

The developed auxetic structures exhibit negative Poisson's ratio with maximum value of -8.00. Poisson's ratio of these structures strongly depends on the structural parameters such as structural angle, and also dependent to a lesser extent on the material parameters such as core fibre type and linear density. The increase in the core fibre linear density (which in turns increases the diameter of longitudinal and transverse elements) results in decrease in Poisson's ratio and vice-versa. Similarly, change in core fibre type (which changes the strength and stiffness of longitudinal and transverse elements) changes the Poisson's ratio; stiffer and stronger fibre such as carbon results in lower Poisson's ratio as compared to glass and basalt fibres. The structural parameter angle θ has a strong influence on Poisson's ratio and an increase in θ results in considerable increase in Poisson's ratio of developed structures.

Tensile behaviour of the auxetic structures also depends significantly on the material and structural parameters. Higher tensile strength is observed in structures developed using stronger fibres (carbon > basalt > glass) and with higher linear density (6000 tex > 4800 tex > 2400 tex). It is also possible to tailor the mechanical properties of developed structures through incorporation of additional straight longitudinal elements.

The structures developed using straight longitudinal elements (structure-2), however, exhibit lower Poison's ratio and tensile properties compared to the basic structures. Further modification of structure-2 by increasing angle θ (i.e. structure-3) results in higher Poisson's ratio, tensile strength as well as work of rupture. Among the different fibres, carbon based auxetic structures exhibit the highest work of rupture, followed by basalt and glass. An increase in liner density of core fibres also increases the work of rupture of the auxetic structures. It can be concluded that the modified auxetic structures (structure-3) developed within this study can be applied for structural applications due to their good auxetic property as well as high strength and work of rupture or energy absorption capability.

Chapter 6
Analytical and Numerical Modelling of Auxetic Structures

6.1. Introduction

It is important to develop an analytical and numerical model for the purpose of predicting mechanical and auxetic behaviour of the structures from braided composites, presented in chapter 4 and 5, for the designing purpose. In this chapter, a new analytical model has been developed for structure-1, structure-2 and structure-4 (see Figure 6.1) to calculate their Poisson's ratio and an existing analytical model was used to calculate the Poisson's ratio of structure-3 (refer Figure 6.1). Also, numerical modelling of auxetic structures were carried out and explained in this chapter.

Finite element analysis will be useful to predict these structures behaviour. Previously researchers were successfully used finite element analysis (ANSYS and ABAQUS) to predict the Poisson's ratio of the auxetic closed cell foam, auxetic 3D fabric (Structure contains three yarn systems, namely warp, weft and stitch yarn), 3D auxetic cellular honeycomb structure, 2D re-entrant auxetic structures, microstructures of auxetic materials, etc. [123 – 127]. Finite Element code DIANA was used here to develop a two dimensional model to predict the tensile behaviour and Poisson's ratio of the developed auxetic structures.

6.1.1. Structures used for modelling

The auxetic structures considered for analytical and numerical modelling is shown in Figure 6.1. The structural parameters of the developed auxetic structures, which were used to calculate the Poisson's ratio are shown in Figure 6.2.

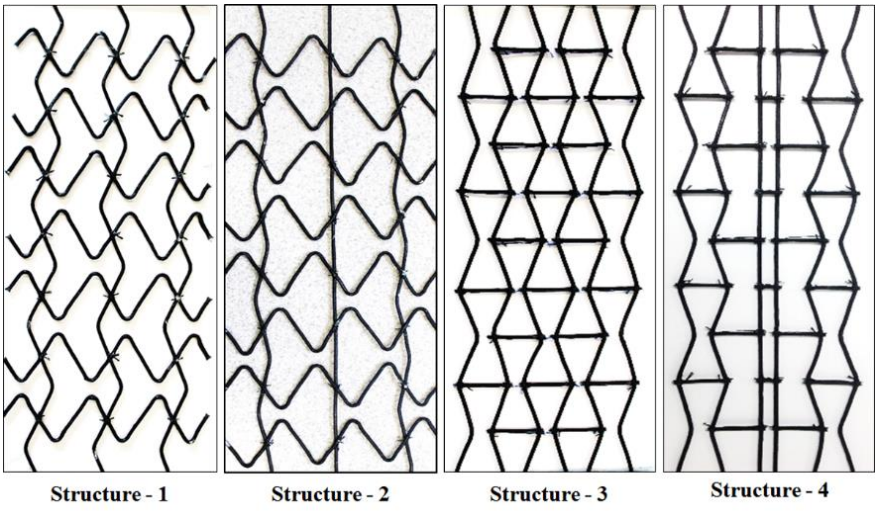

Figure 6.1. Auxetic structures. Structure 1 – Basic lozenge grid design, structure 2 – Modified lozenge grid design, structure 3 – basic re-entrant hexagon design, and structure 4 – modified re-entrant hexagon design.

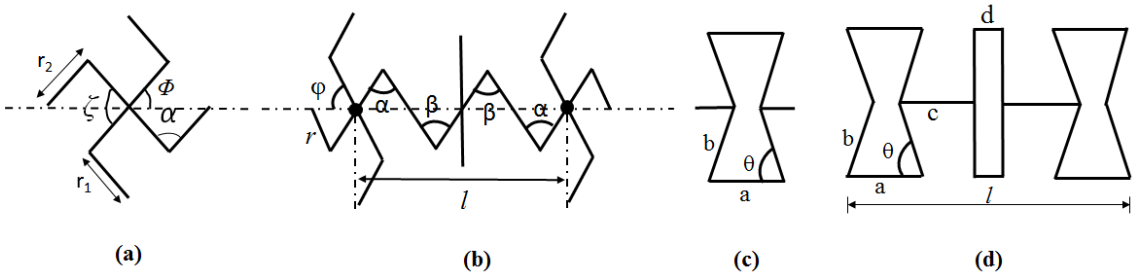

Figure 6.2. Schematic diagram. (a) Unit cell of structure 1, (b) unit cell of structure 2, (c) unit cell of structure 3, and (d) unit cell of structure 4.

6.2. Analytical modelling for auxetic structure based on Lozenge grid

6.2.1. Analytical model for basic design

6.2.1.1. Existing analytical model

Researchers developed an analytical model to calculate Poisson's ratio for 2D honeycomb structures, which is the auxetic design used in this research work. This model

has been applied to structure-1 to calculate its Poisson's ratio. The assumptions made in this analytical model are: (i) the angle between the adjacent rods deforms elastically; (ii) no change in the length of the ribs is allowed; (iii) the translational symmetry of the unit cell is maintained throughout deformation [20]. The elastic angular deformation is defined by $m_A = k_A d_A$ $(A = \varphi, \zeta)$, where m_A is the force moment about a rib, d_A is the increment of rib angle and k_A is the linear spring constant. This model also assumes that the central spring constant is much greater than the outer ones ($k_\zeta \gg k\varphi$) in order to prevent flexing of central spring and have negligible effect of concurrent deformation. In the present work, flexing of spring is included by considering the change of angle ζ as a fraction (κ) of change of angle φ. Hence,

$$\Delta\zeta = \kappa\, \Delta\varphi, \text{ where } \Delta\zeta = \zeta_n - \zeta_0. \tag{6.1}$$

All references to angle ζ can then be written in terms of angle φ by

$$\zeta_n = \zeta_0 + \kappa\, \Delta\varphi \tag{6.2}$$

6.2.1.2. Calculation of engineering strain and Poisson´s ratio

To calculate Poisson's ratio of auxetic structure using the above analytical model, structure-1 (basic lozenge grid design) have been chosen. The calculation of engineering strain is performed using the following equation [20]

$$\epsilon_x = 4r\left(\frac{Cos\left(\zeta_0 - \Phi_0 + \Delta\Phi(k-1)\right)}{\mathrm{Cos}(\zeta_0 - \Phi_0)} - 1\right), \tag{6.3}$$

$$\epsilon_y = 4r\left(\frac{\mathrm{Sin}\,\Phi_n}{Sin\Phi_0} - 1\right), \tag{6.4}$$

where $\kappa = \Delta\zeta/\Delta\varphi$ is a measure of the relative deformation between ζ and φ springs. Poisson's ratio at strain point n is given by,

$$v_{xy}^{ratio} = -\frac{\left(\mathrm{Cos}\left(\zeta_0 + \Phi_0 + \Delta\Phi(\kappa-1)\right) - \mathrm{Cos}(\zeta_0 - \Phi_0)\right) Sin\Phi_0}{(\mathrm{Sin}\,\Phi_n - Sin\Phi_0)\,\mathrm{Cos}(\zeta_0 - \Phi_0)} \tag{6.5}$$

6.2.1.3. Comparison of Poisson's ratio: Experimental vs. Analytical

The mean values of the angles (ζ, φ) (refer Figure 6.2) measured from the structure-1 (refer Figure 6.1) having glass fibre as core with initial angle φ - 66 at different strain points are given in Table 6.1.

Table 6.1. Mean values of angles (TC is the total change in the angle value between initial and final strain point and SD is the standard deviation).

Structure	Angle	Angle data at different strain point								
		0	**1**	**2**	**3**	**4**	**5**	**6**	**7**	**8**
1	φ	67.4	68.0	68.4	69.2	69.6	70.1	70.8	71.6	72.3
	ζ	128.3	129.3	129.3	129.4	129.4	129.4	129.3	129.7	129.3

Angle data at different strain point							TC	SD
9	**10**	**11**	**12**	**13**	**14**	**15**		
72.8	73.5	74.1	74.7	75.4	76.1	76.9	23	7.0
130.1	130.1	130.8	130.9	131.6	131.3	132.2	6.5	2.4

The parameter *k* is obtained from the gradients of best fitted linear function, as shown in Figure 6.3, to the curves representing the relationship between changes in angle ζ with φ at different strain points. The values of $\Delta\zeta$ and $\Delta\varphi$ are obtained from the measured values of angle ζ and φ at different strain points and therefore, parameter *k* is actually measured from the real structures and used in the model. Poisson's ratio is then calculated using values of κ, ζ and φ. So, Poisson's ratio has been calculated in this research using the above analytical model based on the parameters experimentally measured from the developed structures. In fact, these parameters were measured from the real structures so that the model will take into account the real deformations of the BCRs (i.e. true behaviour of fibre, matrix and interface) in order to correlate well with the experimental results.

Figure 6.4 shows Poisson's ratio of structure obtained from the analytical model and experiments. In this case, k = 0.32, as calculated according to Figure 6.3 has been used. The experiment Poisson's ratio values are significantly lower when compared to the analytical model Poisson's ratio. This may be due to the assumptions considered during the development of the analytical model. For example, some deformations of the structures were not considered. The change of r_1 and r_2 during tensile loading and opening of the transverse rods were not considered. The model also assumed that the unit cell deformed uniformly throughout the loading cycle, but actually it might not happen and possibly influenced the measured Poisson's ratio.

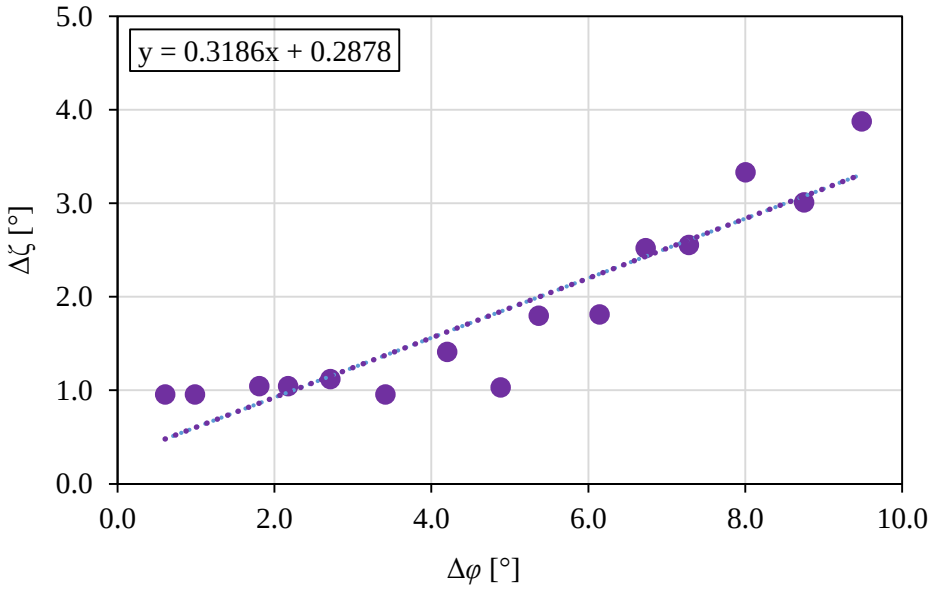

Figure 6.3. Relationship between Δζ and Δφ from different strain points and fitting of linear function for measuring k value for structure-1.

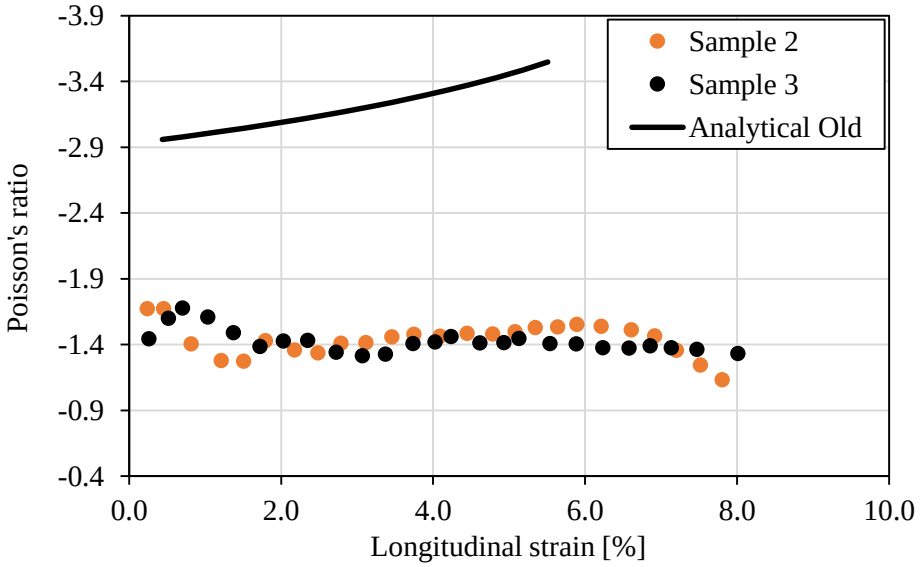

Figure 6.4. Poisson's ratio of structure-1 calculated from analytical and experimental.

6.2.2. Revised analytical model for basic design

The model discussed in the previous section has been revised to fit well with experimental results. In the present analytical model both angle ζ, and φ are related with each other and both with respect to vertical undulation rods. Actually in the structure the transverse expansion occurs due to the opening of horizontal undulation rods, which is not considered in the existing model used. So, in the revised analytical model the angle α (refer Figure 6.2) is introduced and change of angle α is measured from different strain values. Change of angle α is a function of change of angle φ.

$$\alpha = f(\varphi) \tag{6.6}$$

To calculate the angle α, the equation is derived with help of angle (α, φ) measured from different strain points and it is shown in Figure 6.5.

The function α = 0.9484φ - 6.8197 is now used to calculate the angle α. The calculated angle α is given in the Table 6. 2. Later, the transversal and longitudinal strains are calculated by using following formulae,

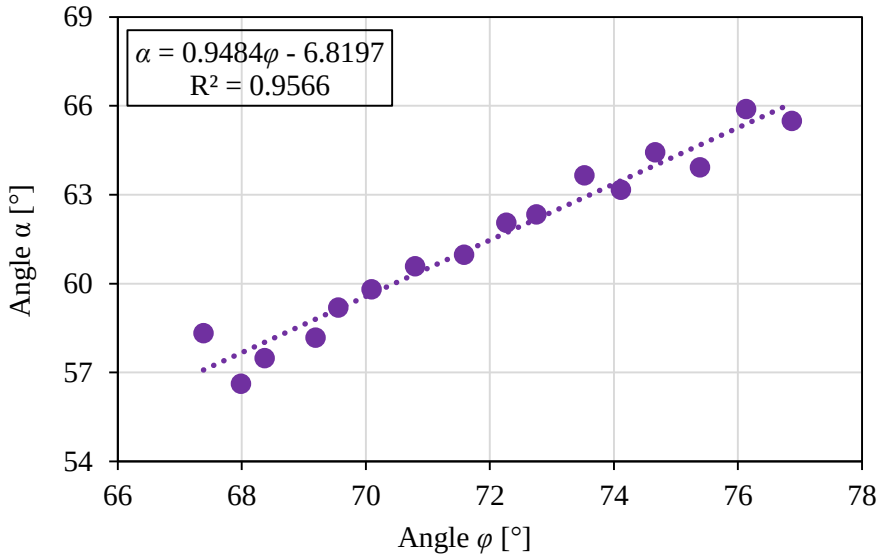

Figure 6.5. Relationship between angle φ and angle α.

$$\epsilon_x = \left(\frac{Sin\ \alpha_n}{Sin\ \alpha_0} - 1\right), \tag{6.7}$$

$$\epsilon_y = \left(\frac{\mathrm{Sin}\,\varphi_n}{Sin\varphi_0} - 1\right), \tag{6.8}$$

$$\nu_{xy} = -\frac{\epsilon_x}{\epsilon_y} \tag{6.9}$$

Table 6. 2. Angle α calculated using function of α = 0.9484φ - 6.8197 (TC is the total change in the angle value between initial and final strain point and SD is the standard deviation).

Structure	**Angle**	**Angle data at different strain point**								
		0	**1**	**2**	**3**	**4**	**5**	**6**	**7**	**8**
1	α	59.5	60.1	60.5	61.3	61.6	62.2	62.8	63.6	64.3

Angle data at different strain point								**TC**	**SD**
9	**10**	**11**	**12**	**13**	**14**	**15**			
64.8	65.5	66.1	66.7	67.4	68.1	68.8		9.3	3.0

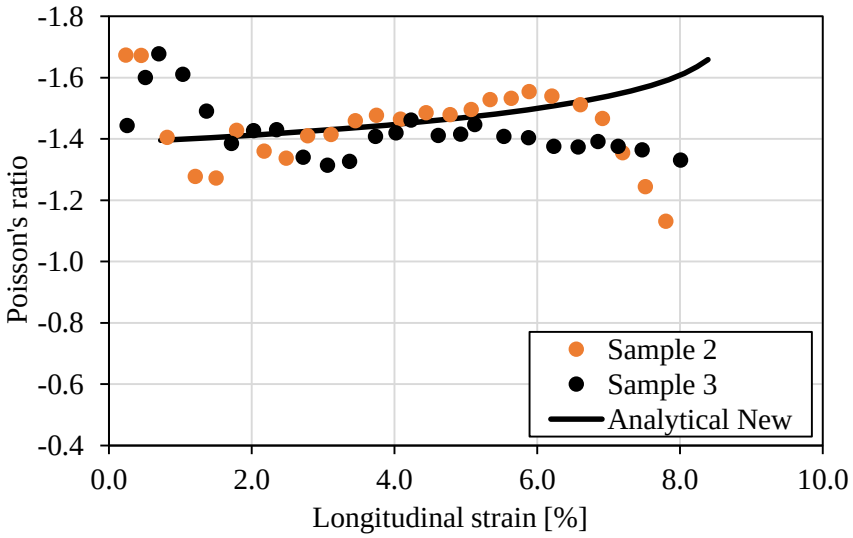

Figure 6.6. Modelled and experimental Poisson's ratio of structure-1.

Figure 6.6 shows Poisson's ratio of structure-1 calculated from revised analytical model and compared with experimental Poisson's ratio. The results show that the Poisson's ratio calculated from the revised analytical model is well fitted with experimental results. In Figure 6.6 it is observed that after 6% longitudinal strain the analytical Poisson's ratio value is getting increase, but the experimental Poisson's ratio getting decrease. This may be due to the analytical model assumed the structure expands

freely in the transverse direction, but in the case experimental due to clamping of structure it doesn't expand freely in the transverse direction. This difference causes change in value of Poisson's ratio.

6.2.3. Analytical model for modified lozenge grid design

For analytical simulation of the modified design of missing rib or lozenge grid (structures-2 and 3), development of a new analytical formula was necessary. For this purpose the auxetic structure-2 (modified missing rib or lozenge grid design) is considered. In order to study the analytical auxetic behaviour of structure-2 Eq. (6.8) can be used to calculate longitudinal strains as a function of angle, φ. However, Eq. (6.7) needs to be revised as the unit cell is different in this structure. According to the experimental observations on the deformational mode of the structure-2, Eq. (6.7) can be rewritten at the structural level, i.e. it can be assumed that the whole tested structure is a unit cell (see Figure 6. **7**). In this unit cell, the change of transverse length is mainly due to the change of angle α and not angle β because angle β is closer to the vertical straight rod and it doesn't change much during tensile loading as compared to angle α. This is justified through the relation between angle φ vs angle α and angle β (see Figure 6.8). All the angles (φ, α, and β) were measured from the images taken during tensile loading. So, the change of transverse length is equal to, $\Delta l = 4r\,[\mathrm{Sin}\left(\frac{\alpha_n}{2}\right) - Sin(\frac{\alpha_0}{2})]$ and the transversal strain is, $\Delta l/l$. Therefore, the transversal strain of the structure-2 can be obtained as follows:

$$\varepsilon_T = \frac{\Delta l}{l} = \frac{4r\,[\mathrm{Sin}\left(\frac{\alpha_n}{2}\right) - Sin(\frac{\alpha_0}{2})]}{l} \tag{6.10}$$

Figure 6.8 shows that the angle α can be presented as a function of angle φ based on the obtained experimental results:

$$\alpha = 0.9622\,\varphi - 7.5212 \tag{6.11}$$

Using the Eq. 6.11 the angle α is calculated with respect to varying angle φ periodically from the initial angle (φ-66°). By using angle α and φ the transverse strain and longitudinal strain were calculated from Eq. (6.10 and 6.7) and using both strain values analytical Poisson's ratio can be obtained (Eq. 6.9). Poisson's ratio of the structure-2 calculated by analytical and experimental methods are shown in the Figure 6.9.

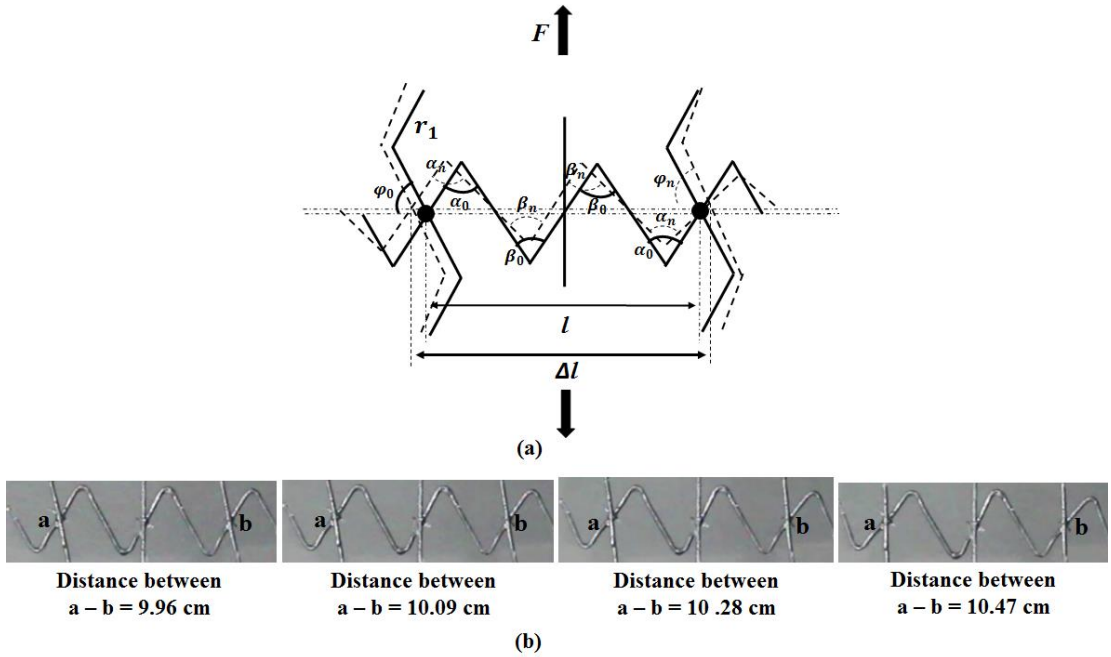

Figure 6. 7. Unit cell of structure-2. (a) Force acting and displacement of unit cell, and (b) displacement of unit cell (real structure-2) at different stages of loading. (α and β – angle formed at the bending of horizontal undulation rod nearer to the vertical undulation rods and nearer to the vertical straight rod, respectively).

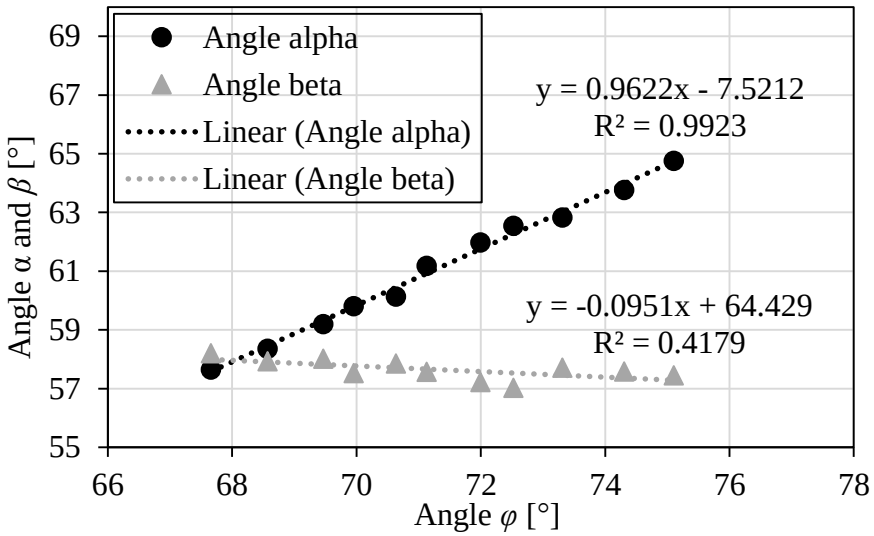

Figure 6.8. Relation between angle φ vs angle α and β.

The results show that Poisson's ratio calculated analytically is similar to experimental values. There is a difference in the Poisson's ratio between the analytical and experimental results and as the previous structure, this may be due to the assumptions considered in the analytical model, i.e. the structures deforms freely in the transversal direction which does not occur in this case as well due to the clamping system.

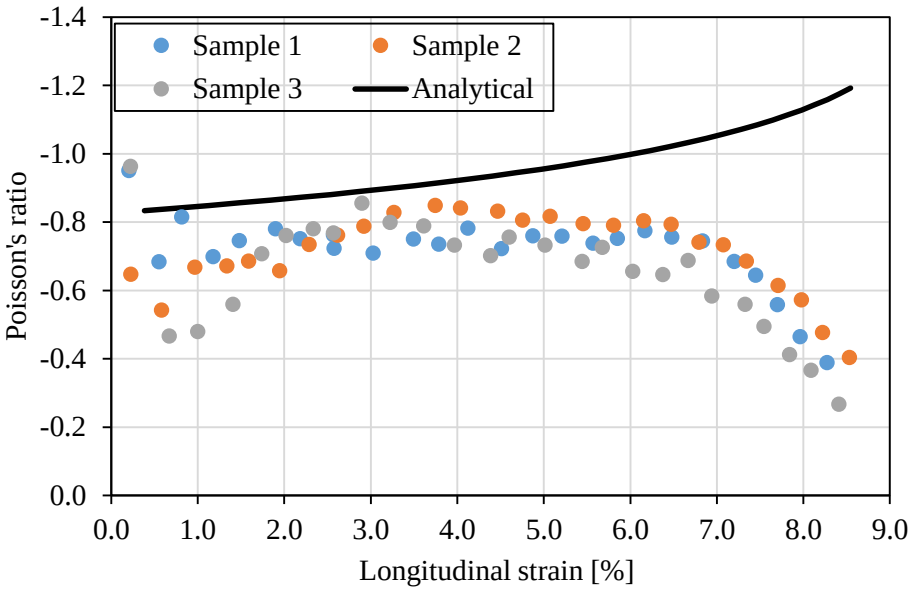

Figure 6.9. Modelled and experimental Poisson's ratio of structure-2.

6.3. Analytical model for auxetic structure based on re-entrant hexagon design

6.3.1. Basic re-entrant hexagon design

The re-entrant auxetic structure (Figure 6.1, structure-3) will expand transversely while loading is applied in the longitudinal direction. This is due to the fact that diagonal longitudinal ribs or elements will move to the longitudinal disposition, which results in an increase of the distance between the diagonal elements through the connection of horizontal elements. Consequently, the auxetic effect is achieved. Based on the geometrical analysis, Poisson's ratio (ν), axial strain (ε_a) and transversal strain of the re-entrant auxetic structure formed with rigid rods can be theoretically calculated by following formulae's [107],

$$\nu = \frac{b\,sin\theta_0(cos\theta_0 - cos\theta)}{(a - b\,cos\theta_0)(sin\theta_0 - sin\theta)} \tag{6.12}$$

$$\varepsilon_L = \frac{\sin\theta}{\sin\theta_0} - 1 \tag{6.13}$$

$$\varepsilon_T = \frac{b\,(cos\theta_0 - cos\theta)}{(a - b\,cos\theta_0)} \tag{6.14}$$

The auxetic behaviour of structure-3 has been calculated using Eq. 6.12 and compared with experimental results in Figure 6.10. The parameters *a*, *b* and angle θ which are required for analytical calculations are measured from images taken during testing at different stages. The results show that the analytical and experimental Poisson's ratio values are closer with each other. There is a difference in the Poisson's ratio between the analytical and experimental results (after 2.0% strain) and this may be due to the assumptions considered in the analytical model, i.e. the structures deforms freely in the transversal direction, which does not occur due to the clamping system.

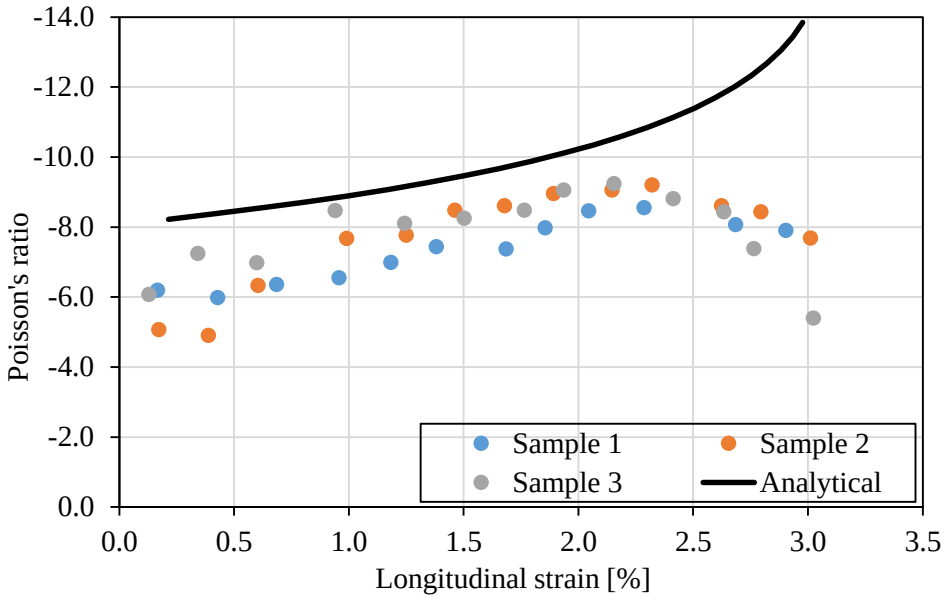

Figure 6.10. Poisson's ratio of auxetic structure-3: Analytical vs. experimental results.

6.3.2. Modified re-entrant hexagon design

To study the auxetic behaviour of structure-4 analytically Eq. (6.13) can be used to calculate the longitudinal strains as a function of angle, θ. However, Eq. (6.14) needs some revision as the unit cell is different in this structure. According to the experimental observations, the deformational mode of the structure is presented in Figure 6.11b. Assuming that the whole tested structure is a unit cell, the transverse strain can be written as presented in Eq. (6.15). The width of the structure (unit cell) is taken equal to *l*. Having the change of the unit cell width in each load level, Δl, the transverse strain can be obtained as $\varepsilon_T = \frac{\Delta l}{l}$. The deformed shape and free body diagram of half of the unit cell (due to its symmetry) is presented in Figure 6.11b. According to this diagram, the width

can be obtained as $\frac{L}{2} = \frac{d}{2} + c + (a - bCos\ \theta)$. The changes in the width with the changes of θ can be obtained as $\Delta l/2 = b(Cos\theta - Cos\ \theta_0)$ leading to the following relation for the transverse strain:

$$\varepsilon_T = \frac{\Delta l}{l} = \frac{2b\,[\mathrm{Cos}\,\theta n - Cos\theta_0]}{l} \tag{6.15}$$

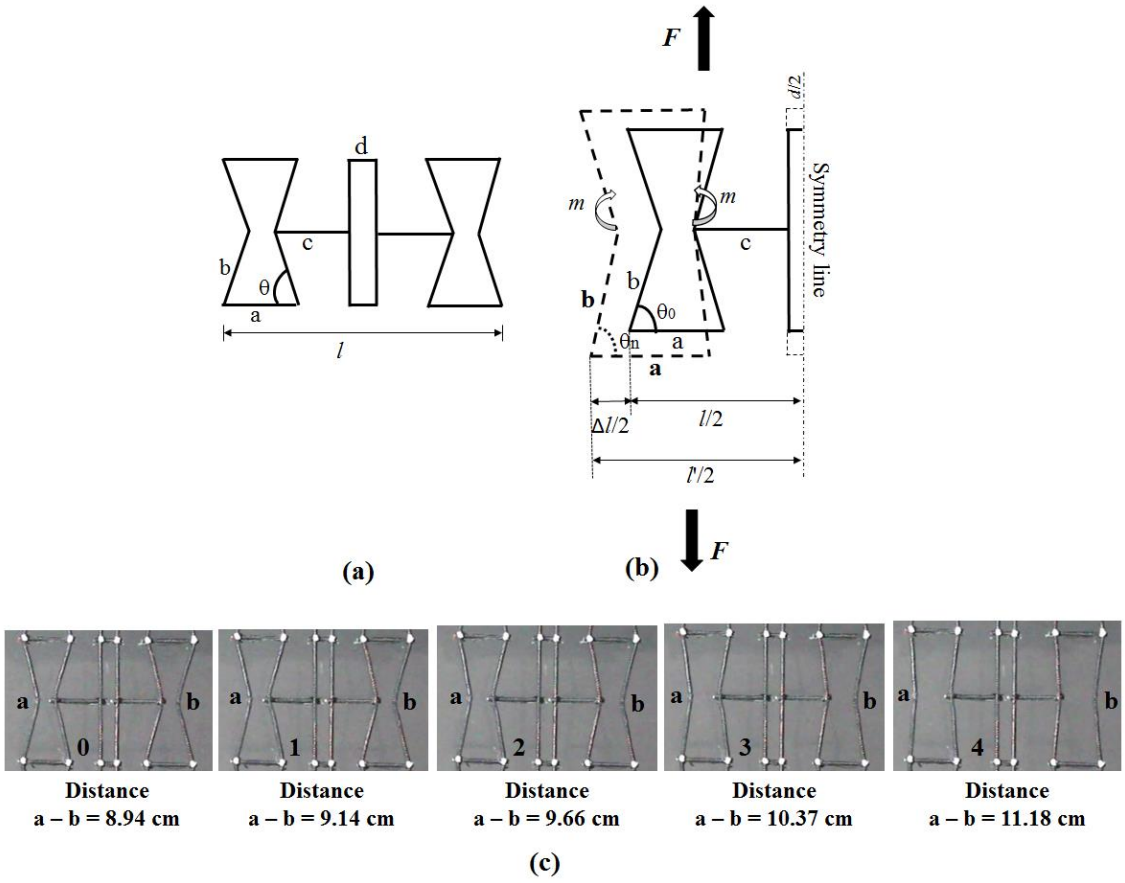

Figure 6.11. (a) Unit cell of structure-4, (b) load and momentum act on the unit cell while axial loading, and (c) unit cell displacement while testing.

Using the longitudinal and transverse strains, the structural Poisson's ratio can be obtained. Poisson's ratio of this structure calculated by analytical and experimental methods are shown in the Figure 6.12. The results show that Poisson's ratio calculated analytically is almost similar to experimental values. It is found that the Poisson's ratio of structure-2 can be predicted accurately by given analytical formulae.

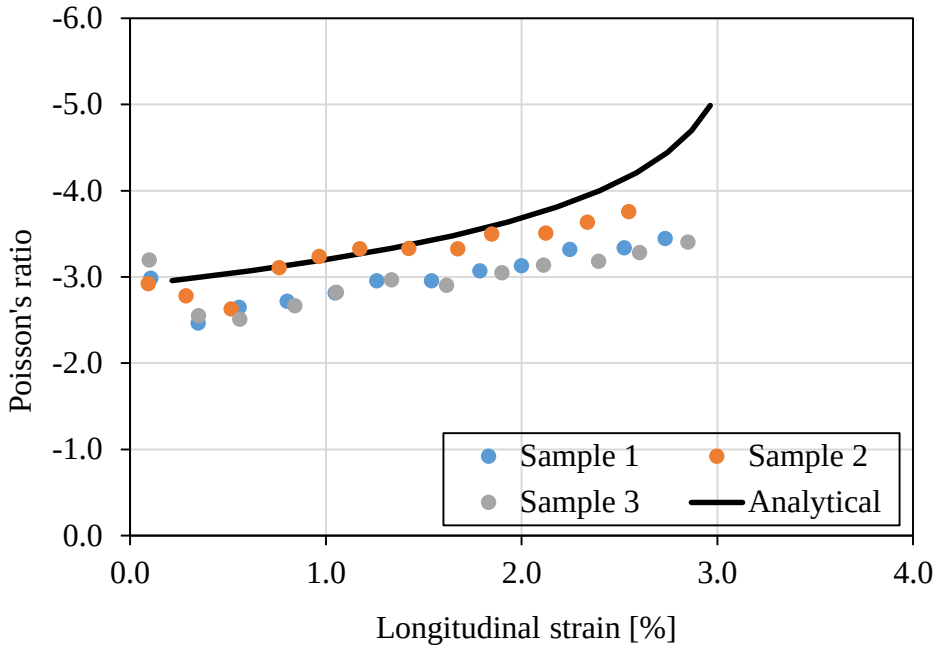

Figure 6.12. Poisson's ratio of the structure-4: analytical vs. experimental results.

6.4. Numerical modelling of auxetic structures

6.4.1. Finite element (FE) modelling

6.4.1.1. Modelling strategy

A two dimensional model is produced in FE code DIANA to simulate the response of the developed auxetic structures. According to the experimental results, the composite material used for preparation of the specimens have a linear elastic behaviour until failure. The observed nonlinear force-displacement and auxetic behaviour of the structures are thus due to the large deformation and geometric nonlinearity of the system, which should be taken into account in the numerical modelling.

The FE model is produced based on the geometry of the tested structures. A simple modelling strategy is adopted using linear three-node beam elements (labelled as L7BEN in DIANA) to represent the ribs and linear rotational spring elements (labelled as SP2RO in DIANA) for simulating the ribs rotational stiffness at the curvature points, see Figure 6.13. The beams have a circular cross-section with diameter of 2.83 mm according to the experimental measurements. The intersection of the vertical and the horizontal joints are modelled with continuous elements without introducing any extra degree of freedom. The constraints and loading conditions are applied to the model as the experimental tests were performed, i.e. the displacements of the structure at both ends are constrained in both *x*

and *y* directions. An incremental monotonic displacement load is applied to one side of the structures for simulating the tensile test conditions.

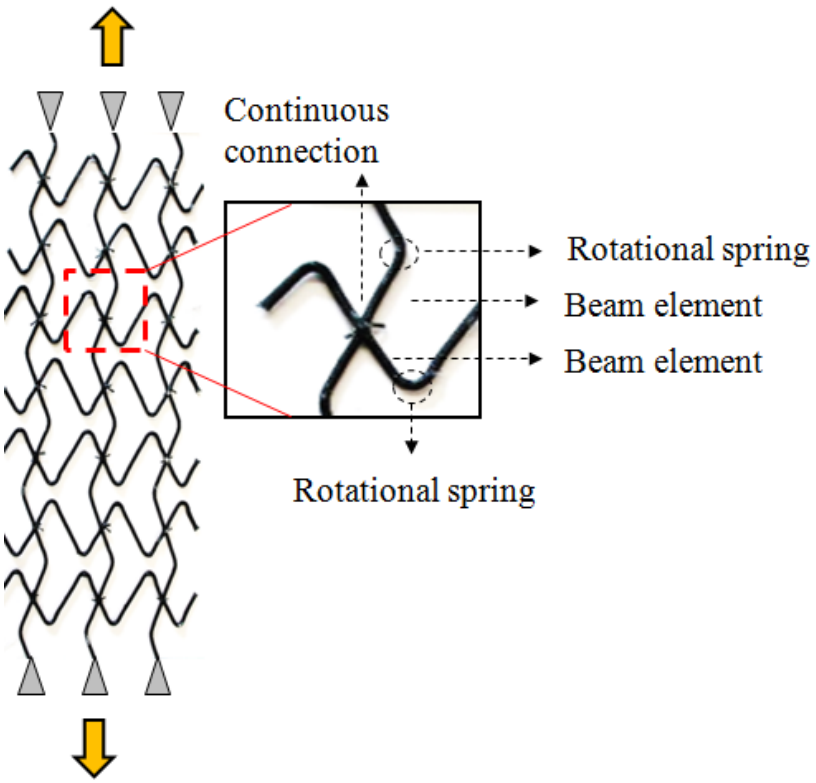

Figure 6.13. FE modelling strategy.

A linear elastic with brittle failure material model and a linear elastic rotational spring are adopted for the ribs and the springs, respectively. The elastic modulus, *E*, of rods was taken 14.2 GPa according to experimental results. The properties of rotational springs are obtained by performing a parametric analysis as explained in sec. 6.4.1.2.

A geometric nonlinear analysis with total Lagrange formulation is performed to simulate the large deformation and auxetic behaviour of the structures. The total Lagrange formulation is useful when rotations and displacements are large and strains are small as is the case of the structures under study.

As explained before, the force-displacement response of original auxetic structures (e.g. structure-1, and structure-3) consisted of two main phases. In the initial phase, the response was governed by large deformation and low load resistance. After a certain deformation level, in the second phase, the structure resisted higher loads with lower deformation capacity. Different solution strategies deemed necessary for numerically simulating the structural response in each phase. A modified Newton-Raphson iterative

together with the line search method and displacement convergence criteria are used for solving the nonlinear equations in the initial phase of structural behaviour. The analysis is then continued, in the second phase, with a quasi-Newton iterative method and force (or energy) convergence criteria. On the other hand, the behaviour of modified structures (e.g. structure-2 and structure-4) generally consisted of three phases initiating with a linear elastic behaviour until the failure of the straight rods. Then, the load dropped significantly by entering the second phase which was similar to the first phase behaviour of original structures (large deformation and low load resistance) followed by the third phase (small deformation and high load resistance). A similar solution strategy as the original structures was adopted for each phase of the analysis to ease the convergence of the numerical problem.

6.4.1.2. Springs' properties validation

A numerical back analysis was performed for estimating the rotational stiffness of the springs. For this reason, tensile tests were performed on two types of specimens each consisting of five straight rods and four curvature points, see Figure 6.14. The specimens had different connection angles of 19° and 29° (three specimens for each angle).

The numerical analysis was performed to simulate the experimental tensile behaviour of each specimen type following the same modelling strategy as explained in sec 6.4.1.1. Having the elastic modulus of the rods, a parametric study was performed on the stiffness of the rotational springs for obtaining the best simulation of experimental results. It was observed that a rotational stiffness of k =1000 N.mm/rad leads to an acceptable prediction of the experimental behaviour in both specimen types, see Figure 6.15. It can be seen that the numerical results show good agreement with experimental ones. The stiffness of the rotational springs are thus assumed as 1000 N.mm/rad hereafter.

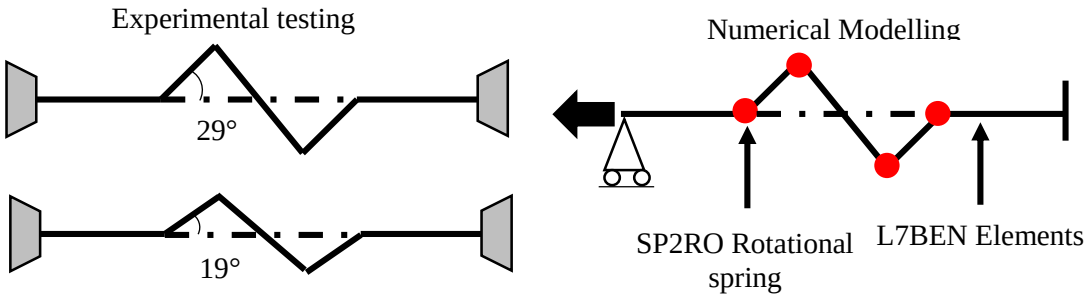

Figure 6.14. Validation of the mechanical properties for rotational springs.

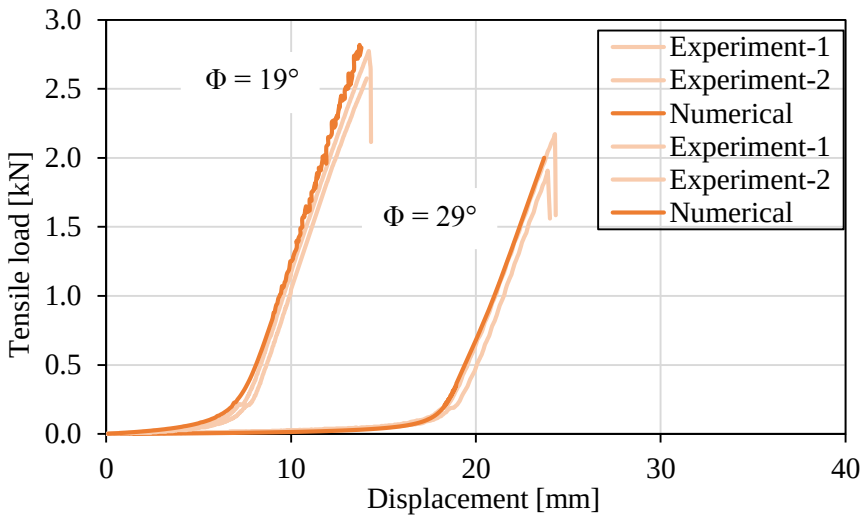

Figure 6.15. Comparison of experimental and numerical results for single rod tests.

6.4.1.3. FE simulations of Poisson's ratio and tensile behaviour of the structures

The modelling strategy and material models presented in Sec. 6.4.1.2 are used for simulating the observed experimental behaviour of four auxetic structures, see Figure 6.1. The main focus is on prediction of the force-displacement behaviour and the changes of the Poisson's ratio during the tests. The numerical results are presented in Figure 6.16 to Figure 6.19 in comparison to the experimental observations. It can be seen that the numerical predictions are in good agreement with experimental results in both predictions of the load-displacement response and Poisson's ratio. The changes of the Poisson's ratio have some differences with the experimental results in some cases, structure-2 and structure-3. These differences are in acceptable range and can be attributed to the imperfections of the handmade specimens and simplifying assumptions of the numerical model. In general, the developed numerical model, although being simple, suitably predicted the global response and local deformation of different auxetic structures, being the evidence of applicability of this modelling strategy for predictive purposes or simulating the behaviour of auxetic structures at the structural level.

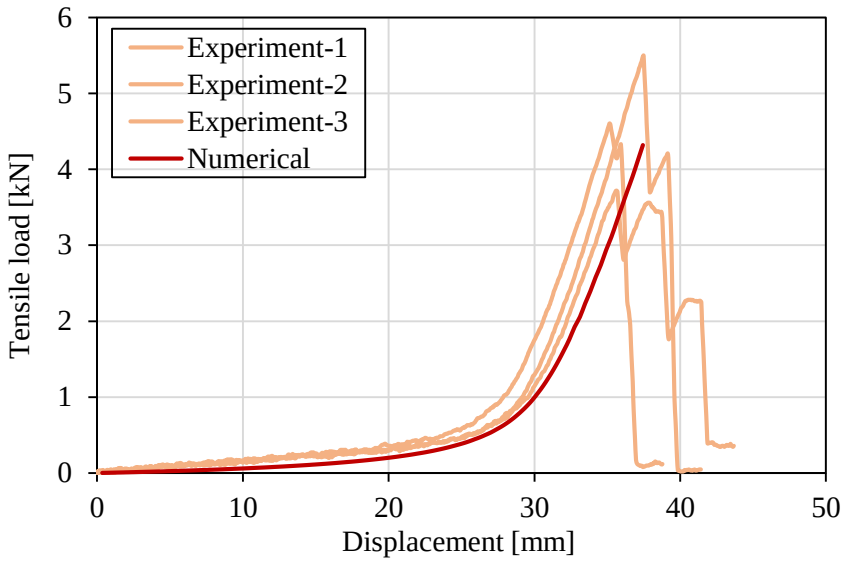

(a)

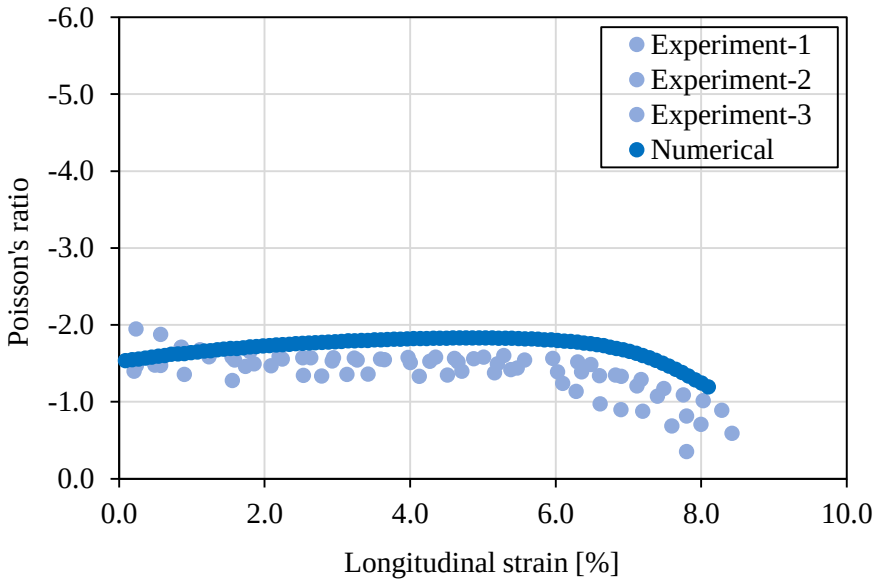

(b)

Figure 6.16. Experimental and numerical results for structure-1: (a) force-displacement behaviour; (b) Poisson's ratio.

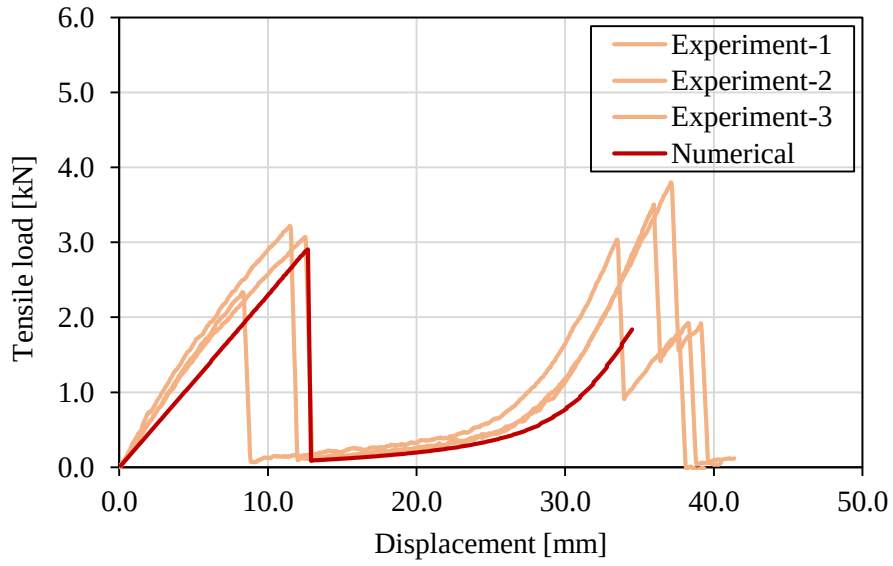

(a)

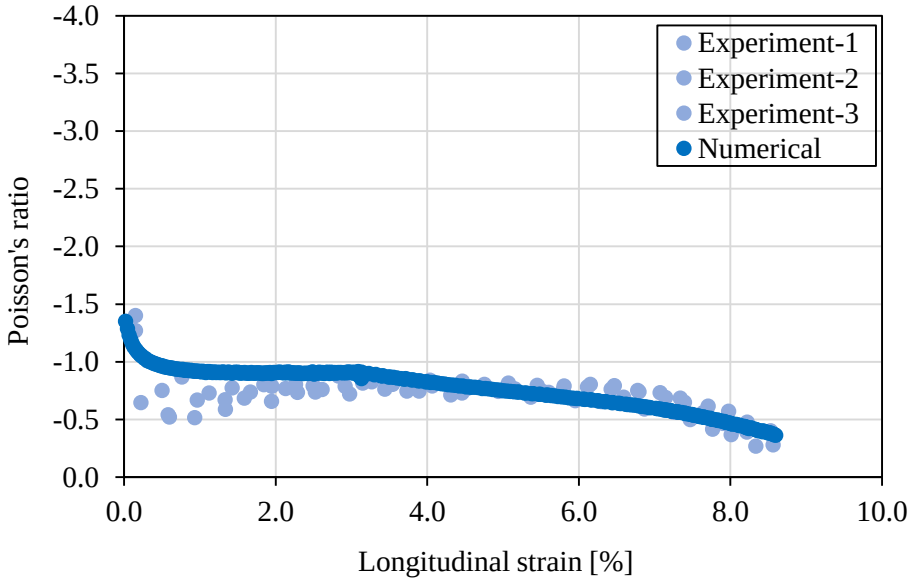

(b)

Figure 6.17. Experimental and numerical results for structure-2: (a) force-displacement behaviour; (b) Poisson's ratio.

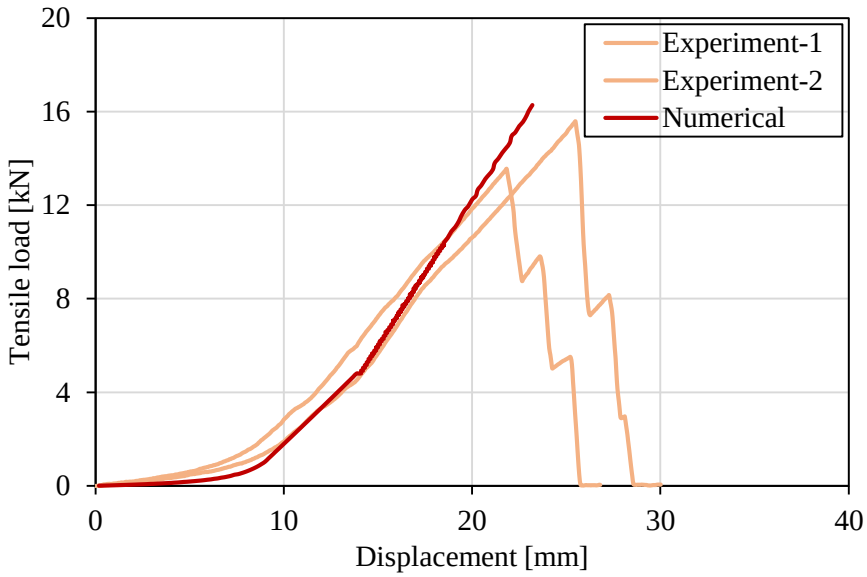

(a)

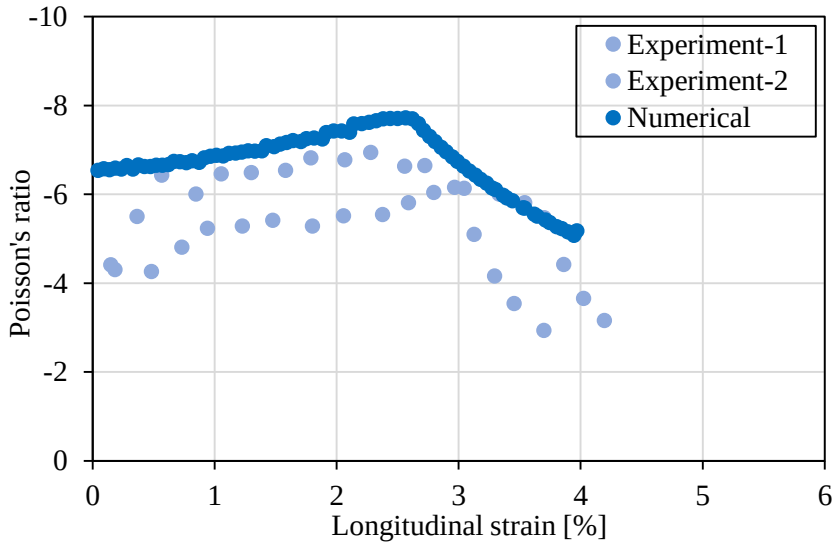

(b)

Figure 6.18. Experimental and numerical results for structure-3: (a) force-displacement behaviour; (b) Poisson's ratio.

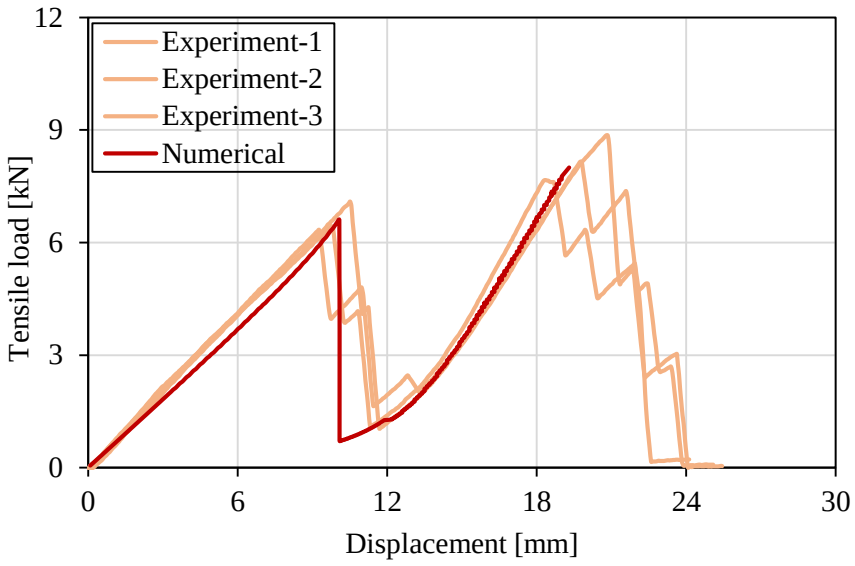

(a)

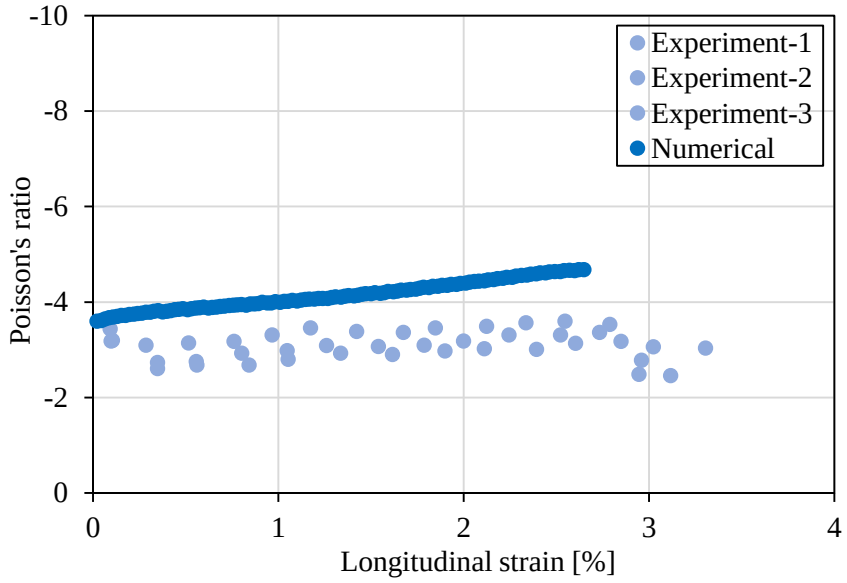

(b)

Figure 6.19. Experimental and numerical results for structure-4: (a) force-displacement behaviour; (b) Poisson's ratio.

6.5. Conclusion

In this chapter, the Poisson's ratio of the developed auxetic structures was calculated analytically and compared with the experimental results. New analytical formulas were developed for structures based on lozenge grid (both basic and modified design). Whereas, for basic re-entrant hexagon existing formulae was used to calculate the Poisson's ratio and for modified re-entrant hexagon, new analytical formulae was

derived. The results show that experimental results were closer with analytical results except for basic re-entrant hexagon design. The reasons were explained in the section 6.2 and 6.3.

Also, numerical modelling by using FE code of DIANA was used to predict the Poisson's ratio of the developed structures and their tensile behaviour. The numerical model was developed based on the elastic modulus of braided composite rod (experimental results) using concept of rotation spring element. The numerical analysis exhibits better agreement with the experimental results (both tensile and auxetic behaviours).

Chapter 7

Auxetic Structures Reinforced Structural Elements

7.1. Introduction

The auxetic structures are developed from fibre reinforced braided composite rods based on lozenge grid and re-entrant hexagon design. The auxetic structures were optimized by studying their structural parameter (angle) and material parameters (linear density and type of core fibres). Also, the auxetic structures were optimized by modifying basic design through introduction of vertical straight rods. This improves the structures tensile behaviour at lower strain levels. This is critical while reinforcing into structural elements, which has less strain (brittle materials) values compared to textile materials.

In order to study the application of auxetic structures as strengthening elements for civil structures, the optimized auxetic structures were placed as reinforcement into structural elements and their performance was studied under tensile and flexural load. To study the tensile behaviour, the auxetic structures are reinforced into the mortar (plaster mortar) and their performance was compared with plain grid (commercial design) reinforced mortar. In addition, to study the flexural behaviour, the auxetic structures were reinforced to the masonry (built with cement hollow bricks) externally with mortar

(plaster mortar) in one side. The flexural behaviour auxetic reinforced masonry was compared with non-reinforced and plain grid reinforced masonry specimens.

7.2. Sample preparation

7.2.1. Preparation of auxetic structures reinforced mortar

Regarding the structures reinforced mortar, the understanding of cracking behaviour is an important factor along with load bearing capacity and deformation to design serviceability. For the purpose of analysis of tensile behaviour of structure reinforced mortar, specimens with 120 mm x 15 mm cross-sectional area and 600 mm in length were prepared.

The reinforced mortar specimens were produced with auxetic structures (both lozenge grid and re-entrant structures), see Figure 7.1. The structures were placed in the middle of the mortar specimens. In order to get the failure in the middle of the specimens during tensile loading, in the clamp portion (top and bottom) glass grid with dimensions of 120 mm x 100 mm were placed at the both sides of the composite structures.

To prepare structures reinforced mortar specimens' acrylic mould with dimensions of 600 mm x 140 mm (see Figure 7.2), which has four parts, was used. After specimens' preparation, they were kept in curing chamber for 75 days at 20° C and 60% RH. Structures used to reinforce into the mortar are shown in the Figure 7.1 and each four samples were produced and reinforced into the mortar. The weight of the structures used in this reinforcement are 480 – 500 g/m^2 for plain grid 3VR & lozenge grid structures and 630 – 660 g/m^2 for plain grid 6VR & re-entrant structures.

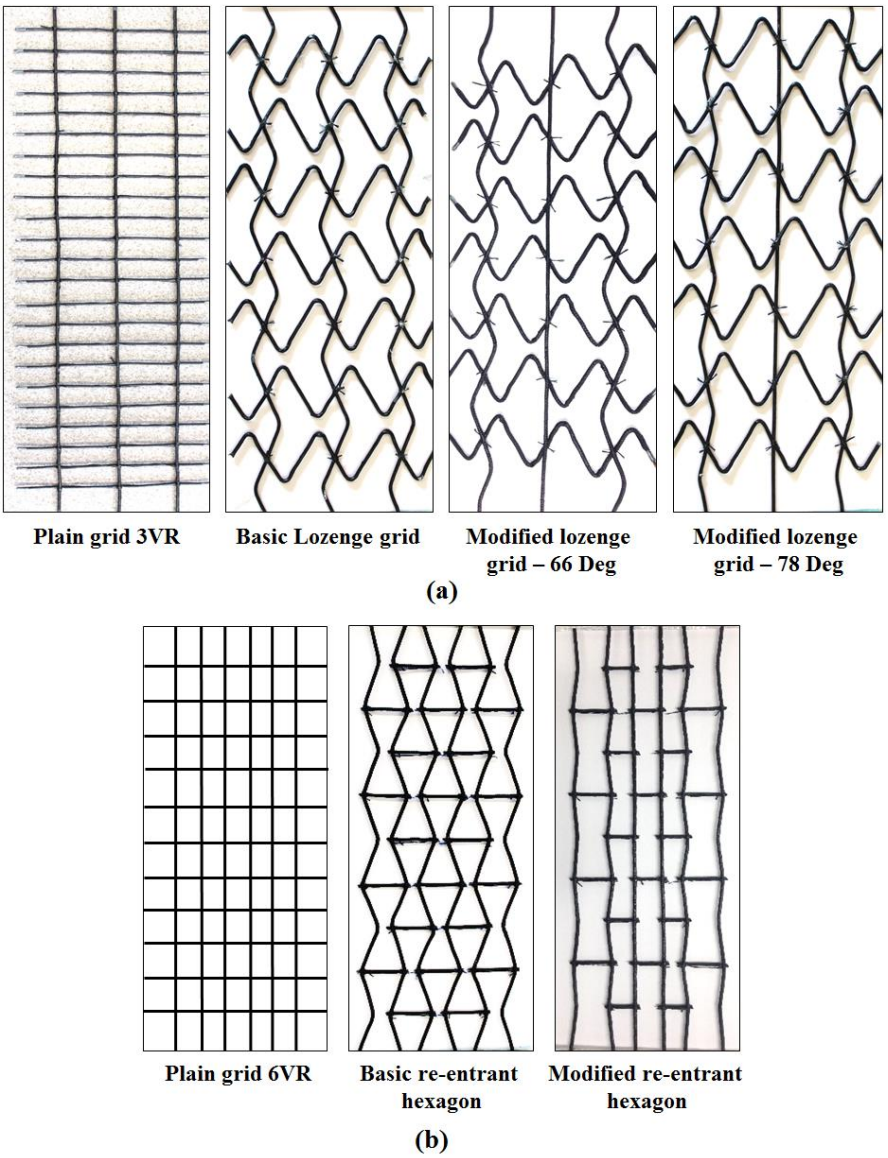

Figure 7.1. Auxetic structures used to reinforce in the mortar. (a) Structures based on lozenge grid, and (b) structures based on re-entrant hexagon.

Figure 7.2. Acrylic mould.

7.2.2. Preparation of auxetic structures reinforced masonry

For the flexural strength testing, auxetic structures reinforced masonry wall specimens were prepared according to test standard EN 1052-2:1999. The masonry walls were prepared using cement hollow bricks. The masonry wall dimensions are given in Figure 7.3.

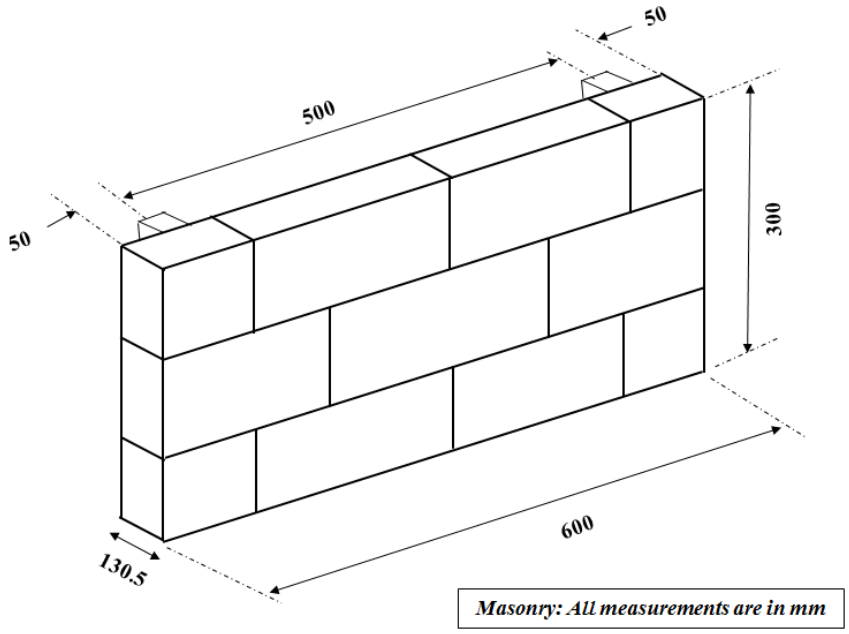

Figure 7.3. Masonry wall specimen dimensions.

The brick dimensions of 200 mm length, 100 mm width and 90 mm height and had two holes of 30 mm x 30 mm, see Figure 7.4. The masonry wall specimens were prepared by using mortar (Type G M10) and the wall specimens (Figure 7.5) are left in the room environment for the curing purpose for around 45 days.

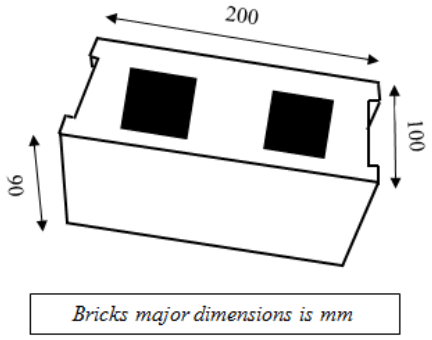

Figure 7.4. Cement hollow brick dimensions.

Figure 7.5. Masonry wall specimen without any reinforcement.

Later, the basalt fibre reinforced braided composite structures (600 mm in length and 300 mm in width) were prepared and reinforced in to masonry wall by using mortar. The mortars (joint and plaster mortar) technical specifications are provided in the Table 7.1.

Table 7.1. Properties of the mortars used provided by the manufacturer.

Joint Mortar		**Plaster Mortar**	
Properties	**Value**	**Properties**	**Value**
Chlorine content	<0.1%	Density	1500 ± 200 kg /m^3
Consistency	15.0 ± 0.5 cm	Consistency	170 ± 5 mm
Compressive strength after 28 days	> 10 MPa	Compressive strength after 28 days	> 6 MPa
Fresh density	1950 ± 200 kg /m^3	Permeability to water vapour	μ <= 15
		Thermal conductivity ($\lambda_{10,\ dry}$)	0.5 W/mK

Plaster mortar with 15 mm thickness was applied and the structure was placed at the mid of the plaster thickness. The composite structures (both plain grid and auxetic structures) used for the reinforcement are shown in Figure 7.6. Five categories of specimens were prepared as follows:

- Non-reinforcement masonry,
- plain grid (6 VR) reinforced masonry,
- plain grid (14 VR) reinforced masonry,
- lozenge grid structure reinforced masonry,

- Re-entrant structure reinforced masonry.

In each category, four samples were prepared. The weight of the structures used in this reinforcement are 489 g/m^2 for plain grid 6VR & lozenge grid and 630 g/m^2 for plain grid 14VR & re-entrant structure. Masonry wall specimen during structure reinforcement is shown in Figure 7.7. After the reinforcement of the structures, the specimens were kept in the room environment around 45 days, prior to flexural testing. The reinforced masonry wall specimen shown in the Figure 7.8.

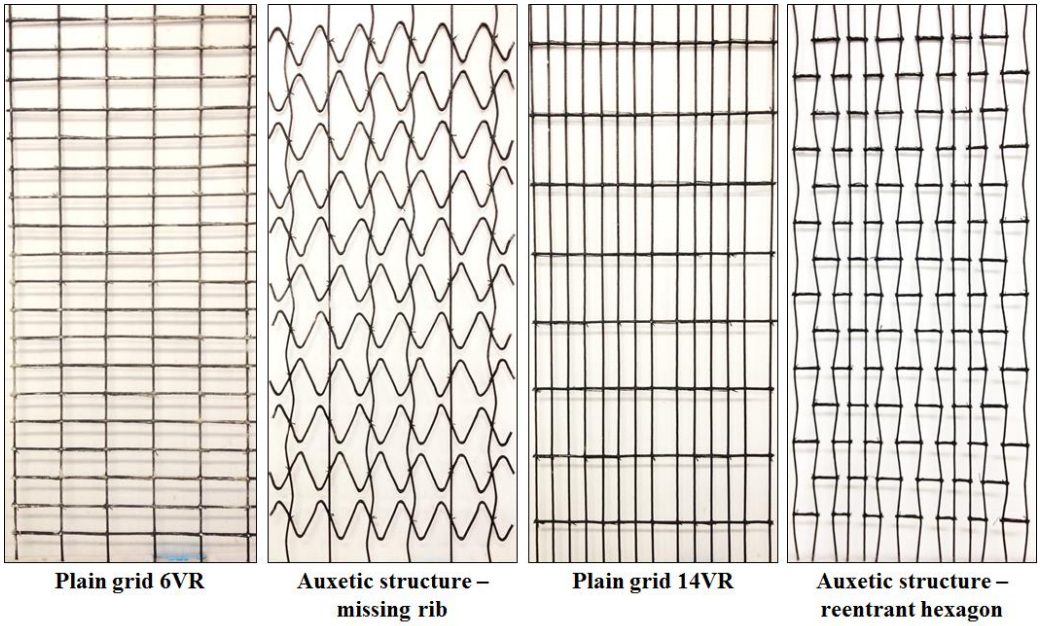

Figure 7.6. Braided composite structures used for masonry wall reinforcement. (6VR – six vertical rods and 14VR – fourteen vertical rods).

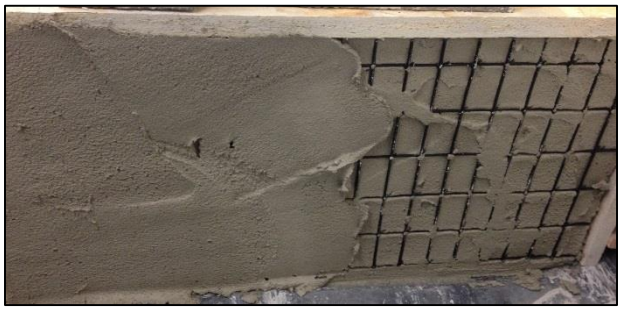

Figure 7.7. Structure reinforcement at one side of the masonry wall specimen.

Figure 7.8. Structure reinforced masonry wall specimen.

7.3. Testing of auxetic structures reinforced samples

7.3.1. Tensile testing of auxetic structures reinforced mortar

Tensile testing of reinforced mortar specimens were tested in Universal tensile testing machine. The speed of the tensile test was kept as 0.5 mm/min. To avoid crack in the sample during fixing in the machine, new bottom clamp was designed and used. The test set-up is shown in the Figure 7.9. During testing, the LVDTs are placed at front and back to measure axial displacement. Also, photos were taken during testing to observe the crack pattern.

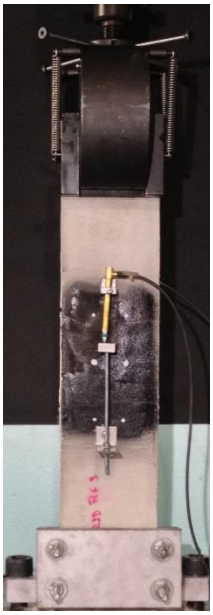

Figure 7.9. Test set-up for tensile testing.

7.3.2. Flexural testing of auxetic structures reinforced masonry

Three point flexural testing of structures strengthened masonry wall specimens were carried out in flexural testing machine. The applied flexural stress is 0.48 MPa/min (i.e. the velocity of the loading was 0.008 mm/sec). The LVDTs are placed over the sample at four places as shown in the Figure 7.10.

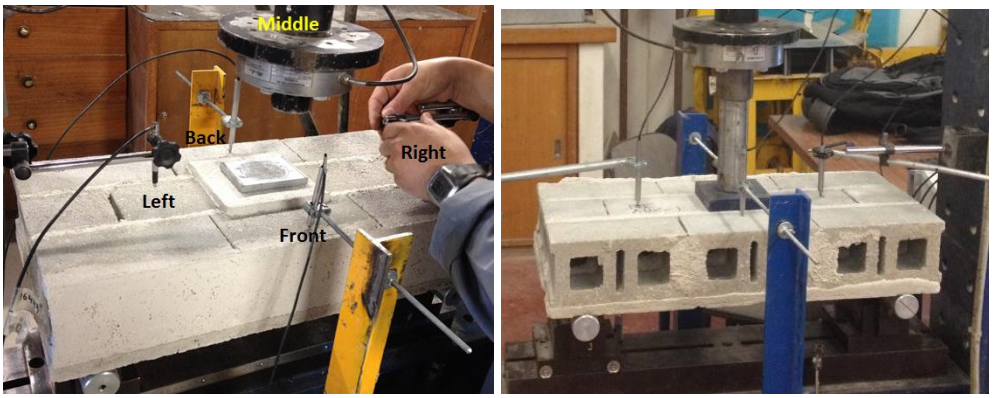

Figure 7.10.Three point loading flexural test set-up.

During testing the images were taken to observe the failure in the specimens. The flexural loads was applied opposite side of samples where there is no strengthening. The maximum flexural load and displacement of the specimen at maximum loading was noted and calculated the flexural stress (σ_f) using following formula,

$$\sigma_f = \frac{3FL}{2bd^2} \qquad [7.1]$$

Where,

F = load at a given point on the load deflection curve, (N)

L = support span, (mm)

b = width of test beam, (mm)

d = depth of tested beam, (mm)

7.4. Results and discussion

7.4.1. Tensile behaviour of auxetic structures reinforced mortar

The tensile behaviour of mortar reinforced specimens with basic auxetic structure (lozenge grid), modified auxetic structures (lozenge grid) (φ – 66° and 78°), and plain grid is shown in Figure 7.11.

The tensile strength of the reinforced mortar is as follows: plain grid > Modified design 78 > Modified design 66 > basic design. The tensile behaviour of the reinforced mortar is as expected. Basic design consists of only undulation rods in its axial direction and it exhibits less maximum tensile load and modified designs are consists of straight rods in its axial direction, so exhibited higher tensile load compared to basic design. The tensile behaviour of the modified design is based on its angle φ, i.e. higher the angle lower the undulation and vice-versa, so exhibits higher tensile load compared to lower angle φ. As plain grid doesn't consists any undulations in its axial direction, it is exhibited highest tensile load compared to other reinforced specimens. Also, the crack level of the specimens depends up on the level of undulations in the axial rods. The crack level of reinforced mortar specimens are shown in Figure 7.12.

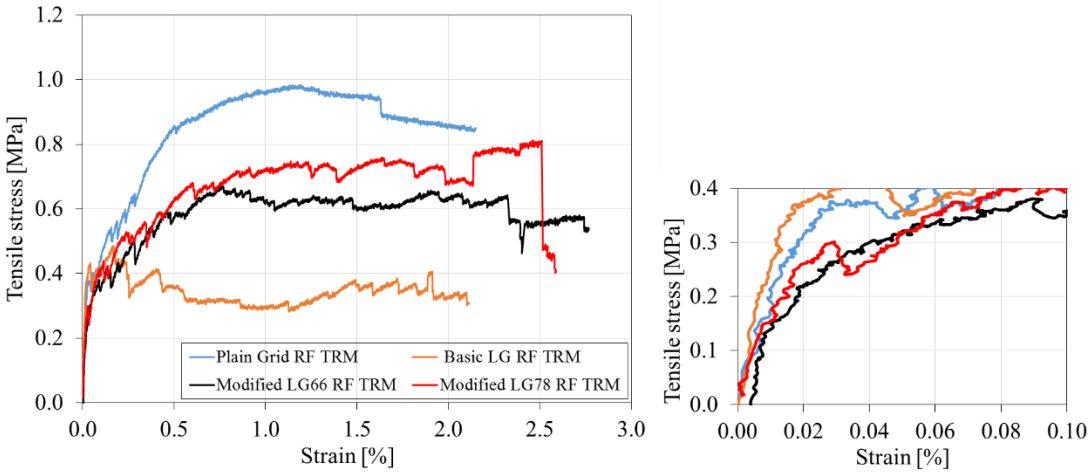

Figure 7.11. (a) Tensile behaviour of auxetic structures (lozenge grid) and plain grid reinforced mortar, and (b) Magnified part of load-elongation curve at lower strain.

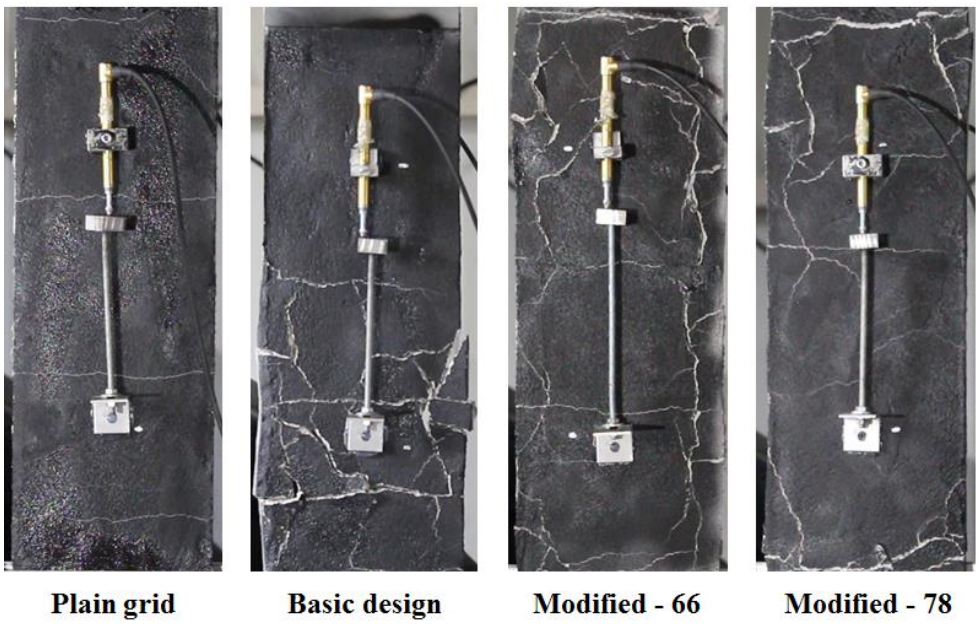

Figure 7.12. Crack level of reinforced mortar specimens at maximum tensile load.

The similar trend was observed for the auxetic structures (based on re-entrant hexagon design) reinforced mortar specimens. The tensile and crack behaviour of the structure reinforced mortar specimens are shown in the Figure 7.13 and Figure 7.14, respectively.

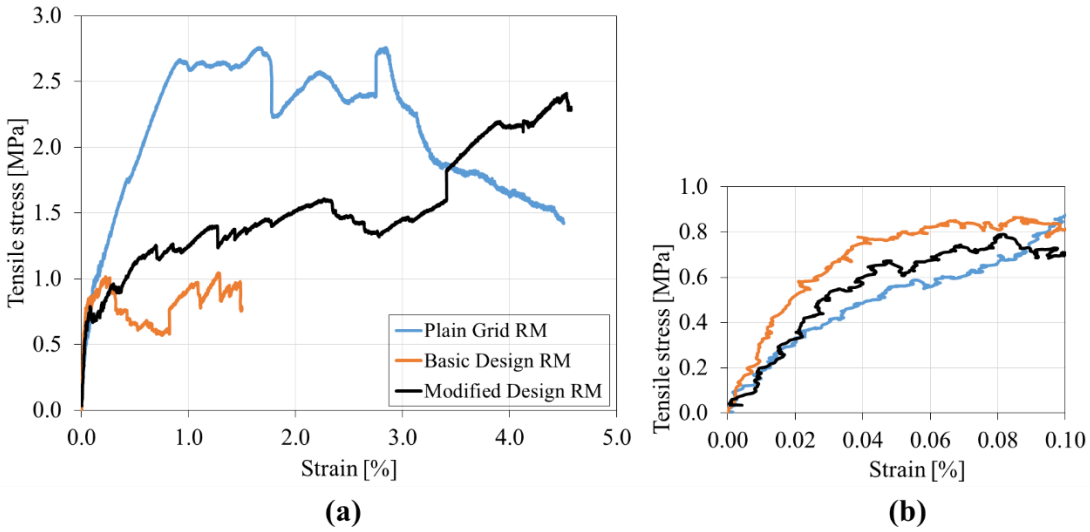

Figure 7.13. (a) Tensile behaviour of auxetic structures (re-entrant hexagon) and plain grid reinforced mortar, and (b) Magnified part of load-elongation curve at lower strain.

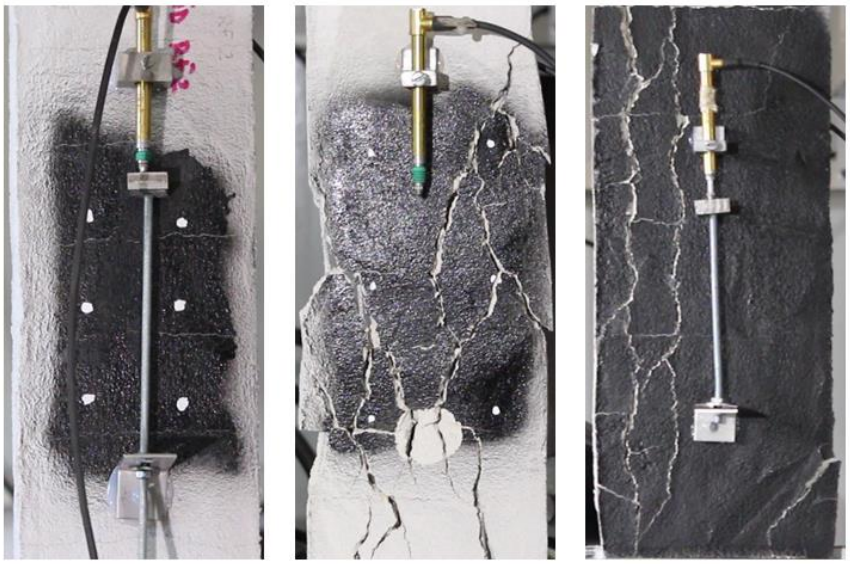

Figure 7.14. Crack level of reinforced mortar specimens at maximum tensile load.

7.4.2. Flexural behaviour of auxetic structures reinforced masonry

The flexural behaviour of the non-reinforced masonry and structures reinforced masonry are shown in the Figure 7.15 – 7.19. In these figures middle LVDT displacement is considered.

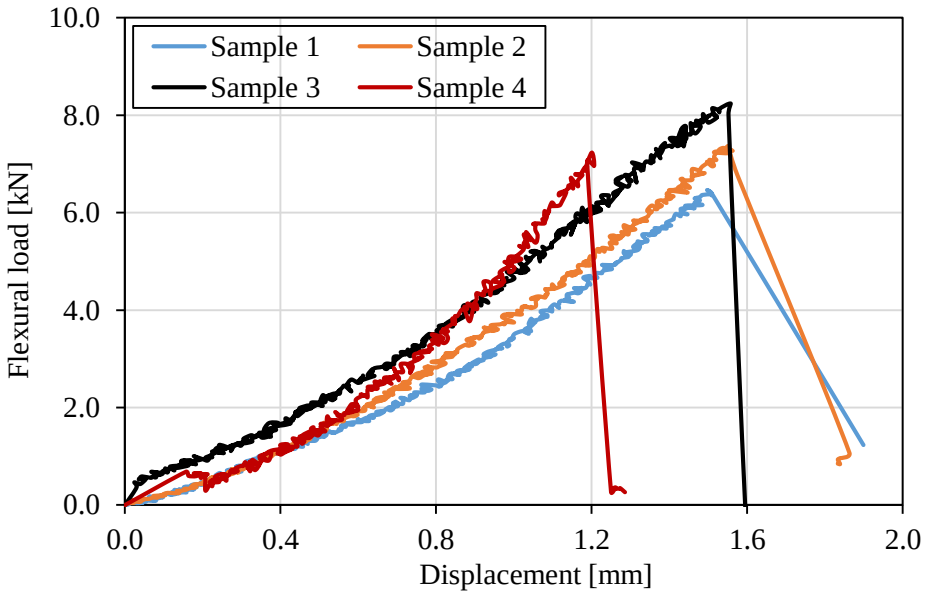

Figure 7.15. Flexural behaviour of non-reinforced masonry specimens.

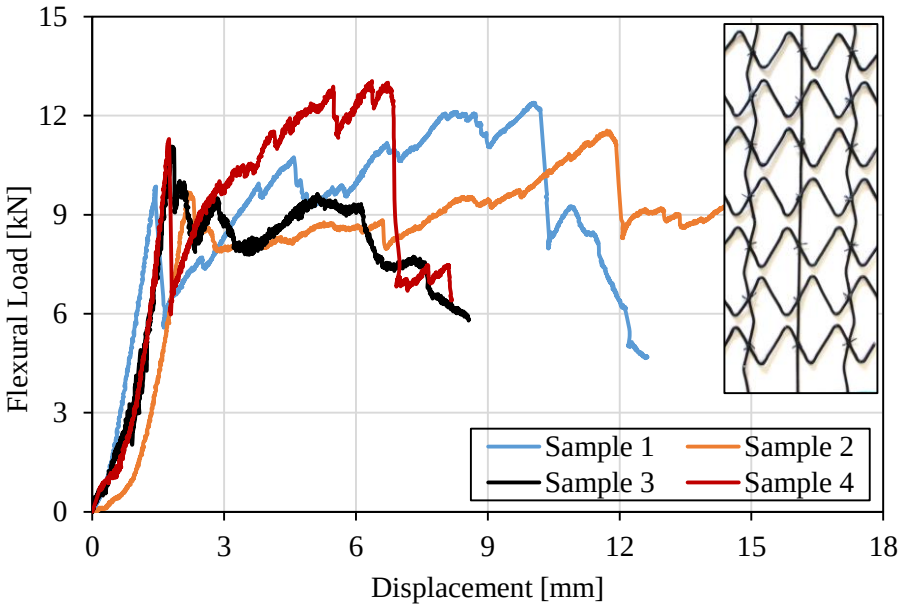

Figure 7. 16. Flexural behaviour of lozenge grid structure reinforced masonry specimens.

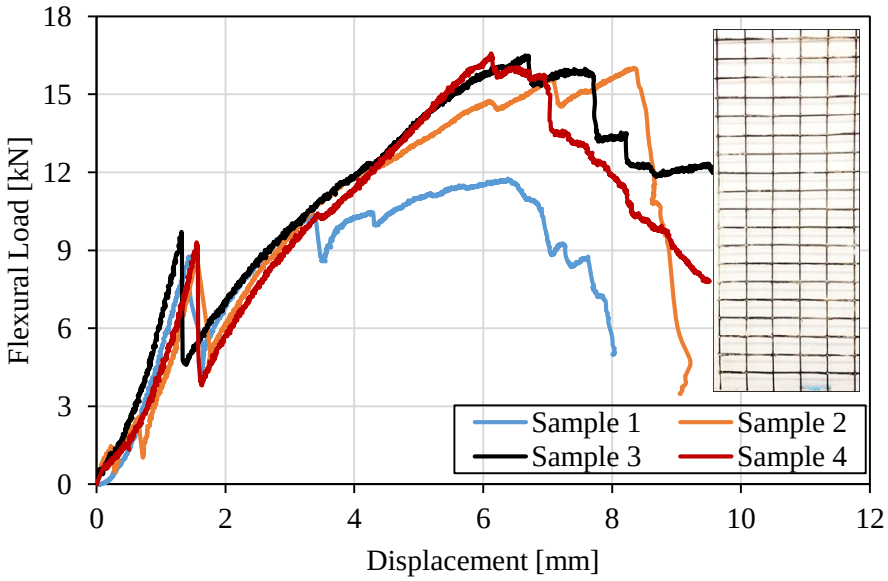

Figure 7.17. Flexural behaviour of plain grid (6VR) reinforced masonry specimens.

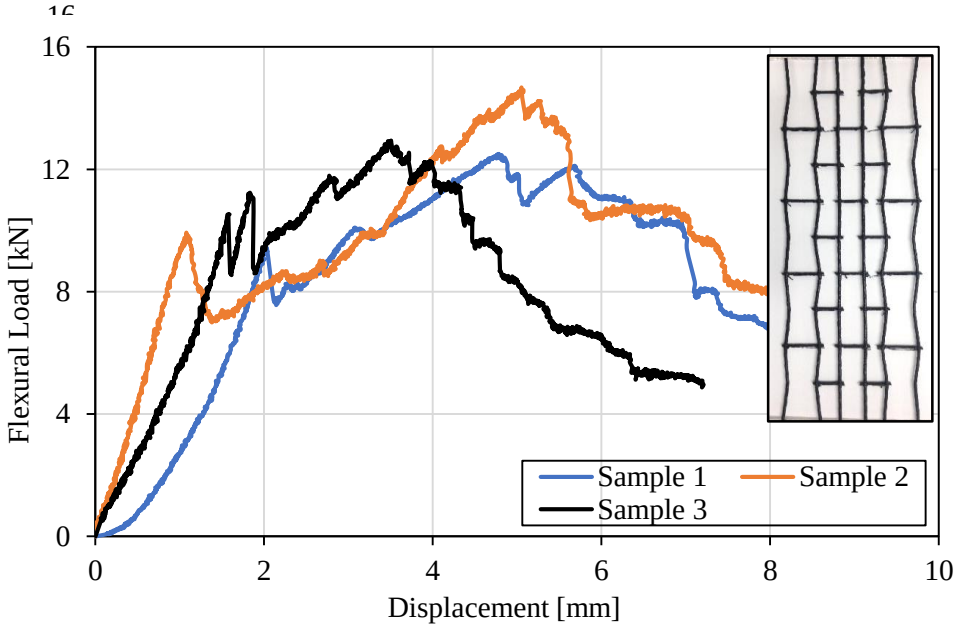

Figure 7.18. Flexural behaviour re-entrant structures reinforced masonry specimens.

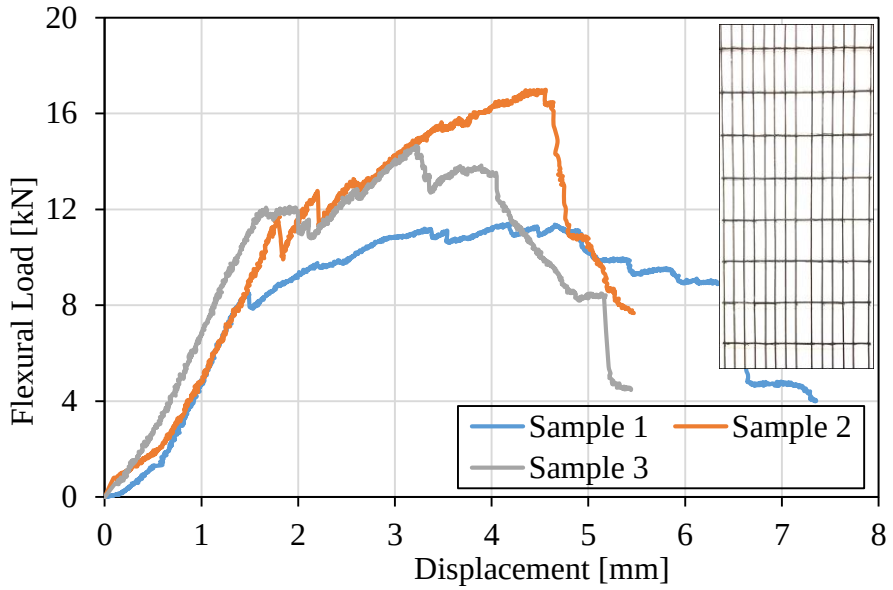

Figure 7.19. Flexural behaviour of plain grid (14VR) reinforced masonry specimens.

The results show that reinforced masonry specimens' exhibits higher flexural load compared to non-reinforced masonry. The first flexural failure occurred at around 7 kN for non-reinforcement masonry, whereas for the reinforced masonry, first flexural failure happened in the range of 9.0 – 10.5 kN.

The flexural stress σ_f is calculated by using Eq. 7.1 and the values are given in the Table 7.2. The table shows that the flexural stress value for the plain grid reinforced masonry and auxetic structures reinforced masonry are close enough. This is evident that composite auxetic structure can be good replacement for composite plain grid. Compared to plain grid, auxetic structure has more advantages like it can be cover more area under loading, more displacement, and more energy absorption.

Table 7.2. The average flexural stress value of each category of masonry specimen

S. No.	Specimen description	Flexural stress (MPa)
1	Non-reinforcement	0.68
2	Lozenge grid RF	1.15
3	Re-entrant RF	1.24
4	Plain grid (6VR) RF	1.41
5	Plain grid (14VR) RF	1.35

The maximum flexural load, displacement at maximum load and energy absorption of the non-reinforced and reinforced masonry are given in the Table 7.3. The results show that the auxetic structures exhibit higher displacement and more energy absorption than plain grid reinforced masonry specimens.

Table 7.3. Energy absorption of reinforced masonry specimens

Specimen description	Avg. peak load, kN	Avg. displacement at peak load, mm	Energy absorption, J
Non-reinforced masonry	7.3 (9.7)	1.44 (11.6)	5.6 (5.7)
Lozenge grid RF masonry	12.3 (6.1)	9.38 (29.2)	84.9 (22.6)
Plain grid (6VR) RF masonry	15.2 (8.6)	6.87 (18.6)	77.5 (22.4)
Re-entrant structure RF masonry	13.4 (15.2)	4.45 (14.5)	50.2 (20.8)
Plain grid (14VR) RF masonry	14.4 (19.5)	4.11 (18.9)	47.6 (10.7)

Note: Values of CV% are given inside brackets.

The energy absorption of reinforced masonry was calculated as shown in the Figure 7.20. Area under the curve was calculated up to 80% of peak load [128, 129]. The

failure mode of the non-reinforced and reinforced masonry is shown in Figure 7.21. The figure shows that, all the specimens undergone the flexural failure mode.

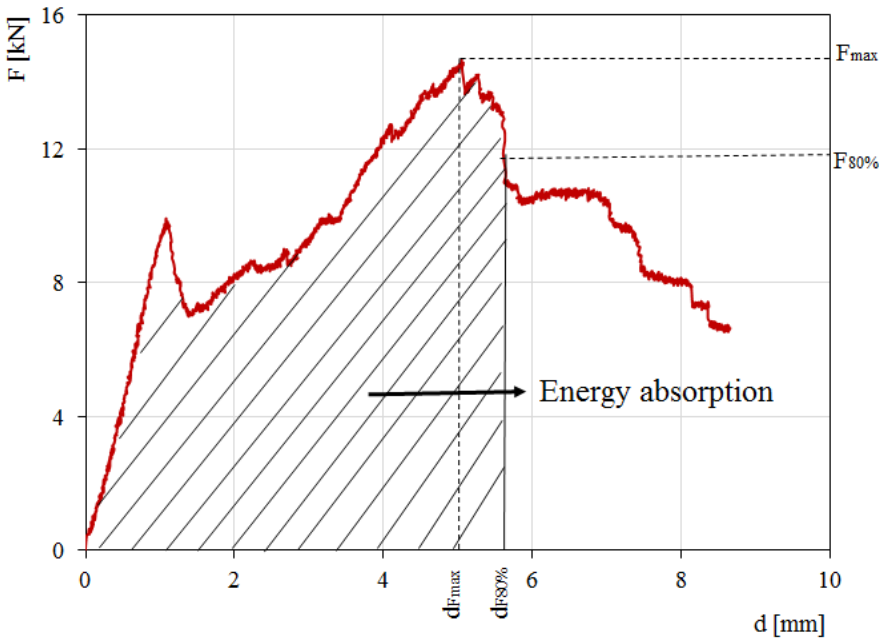

Figure 7.20. Energy absorption region of masonry reinforcements.

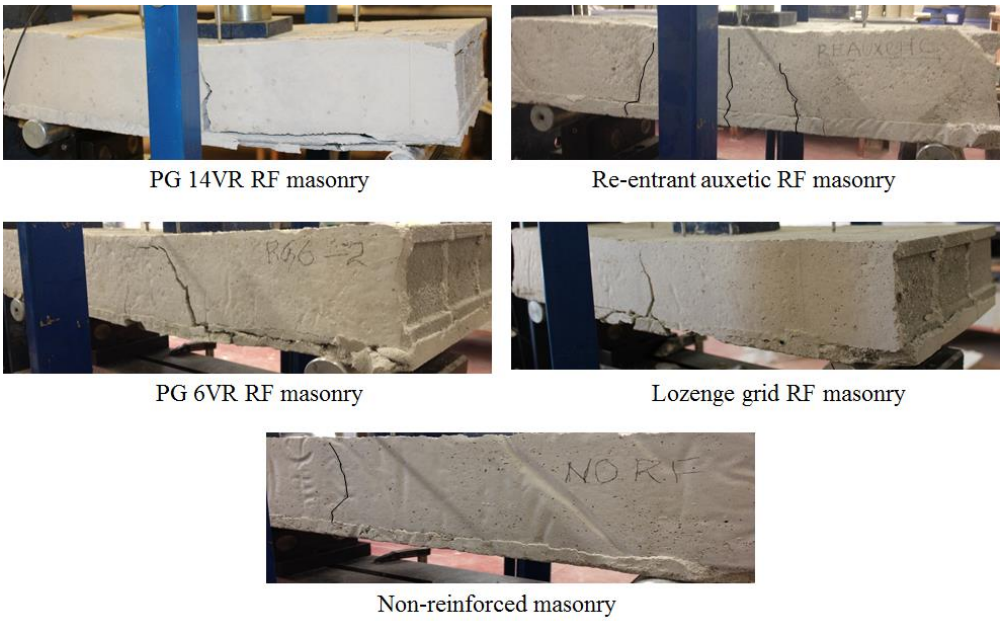

Figure 7.21. Failure mode of non-reinforced and structures reinforced masonry specimens.

The damage observations after the flexural testing of unreinforced and structure reinforced masonry samples are shown in the Figure 7.22, where it can be shown that the plain grid reinforced masonry specimens experienced less damage when compared to

auxetic structure reinforced masonry specimens. This is due to auxetic structures expansion in width wise direction.

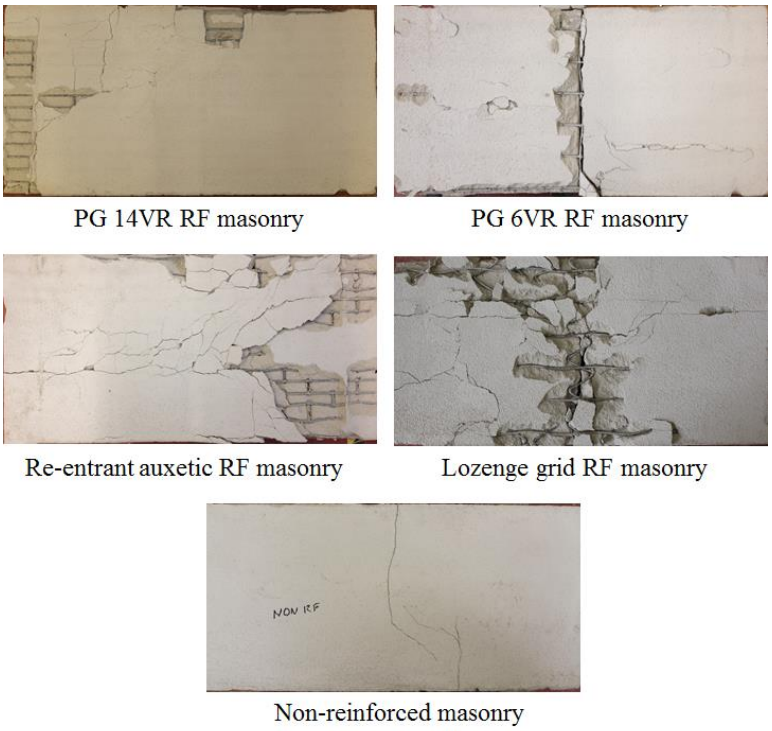

Figure 7.22. Damage observation of masonry specimens after flexural loading.

7.5. Conclusion

Auxetic structures (based on lozenge grid and re-entrant hexagon design) and plain grid structures produced from basalt fibre reinforced braided composites were reinforced into the mortar and studied their tensile behaviour. It is observed from the results that plain grid reinforced mortar specimens performed well and undergone less crack compared to auxetic structures reinforced mortar specimens. This is due to the width wise expansion of the auxetic structures during loading. In comparison between basic auxetic structure and modified auxetic structures reinforced mortar specimens experienced less cracks and this is due to modified design consist of straight rods in its loading direction. The presence of straight rods restrict transverse expansion, thus in turn decreases the level of cracks during loading.

Modified auxetic structures (based on lozenge grid and re-entrant hexagon design) and plain grid structures produced from basalt fibre reinforced braided composites were reinforced externally on masonry wall specimen and tested under flexural loads to study their performance. The results are compared with non-reinforced masonry wall specimen.

The results show that the structures both auxetic and plain grid reinforced masonry wall specimens showed higher flexural strength (σ_f) when compared to non-reinforced masonry wall specimen. But, auxetic structures reinforced masonry exhibits slightly less flexural stress compared to plain grid reinforced masonry specimens. However, auxetic structures reinforced masonry wall specimens showed higher energy absorption compared to plain grid reinforced masonry wall specimens. This is due to the presence of undulation rods presents in the auxetic structures, which cause more displacement compared to plain grid.

Chapter 8

Conclusions and Future Work

8.1. Conclusions

8.1.1. Experimental work

In this research, first time, auxetic structures were developed from fibre reinforced braided composite rods. Auxetic materials possess superior mechanical properties compared to non-auxetic material due to negative Poisson's ratio, i.e. material expands transversely during axial loading and shrinks while applying compressive loads. There are various auxetic structural designs reported in the literature (missing rib, chiral honeycomb, re-entrant honeycomb, double arrowhead, etc.). Out of many auxetic structural designs, two simple design, namely missing rib or lozenge grid and bow-tie or re-entrant hexagon have been chosen for the structure development. These two designs are simple and feasible to develop using braided composite rods.

Initially the auxetic structures were developed and studied their Poisson's ratio and tensile behaviour by image analysis technique. The objectives of developing these auxetic structures are to strengthen civil engineering structural elements and as replacement of conventional strengthening materials. Within this work, the primary auxetic structure based on auxetic structural design didn't show enough tensile behaviour,

i.e. low strength at lower strain level, which is not appropriate to use for the strengthening purpose of civil structural elements.

To over the shortcomings, the basic auxetic structural designs were modified with vertical straight rods along with undulation rods. This modification provided enough strength at lower strain and auxetic property. Also, the effect of structural parameters (angle and rib length) and material parameters (linear density of core fibre and fibre type) on auxetic and tensile behaviour of the structures studied in detailed manner. The result shows that, varying the structural parameters had significant effect of auxetic and tensile behaviours. However, the change of material parameters had little effect on auxetic behaviour, whereas the tensile behaviour is significant based on the type of fibre and linear density, i.e. higher stiffness and higher linear density exhibited higher tensile strength, vice-versa.

To study the effectiveness of the developed auxetic structures, they are used as reinforcement into mortar and masonry wall and studied their tensile and flexural behaviour, respectively. The results were compared with non-reinforced and plain grid reinforced mortar and masonry wall. The results show that plain grid reinforced mortar performed well, i.e. exhibited higher tensile results and experienced less cracks under tensile loading. However, the auxetic structures reinforced masonry showed closer flexural stress value compared with plain grid reinforced masonry specimens. Also, the auxetic structures reinforced masonry exhibited higher ductility and energy absorption compared to plain grid reinforced masonry wall specimens.

8.1.2. Analytical and numerical modelling

To study the auxetic behaviour of the developed structures, suitable analytical formula either existed or newly derived were used and compared with experimental results. The analytical results show closer agreement with experimental results. Apart from analytical model, numerical modelling using FE code of DIANA was developed to study the tensile and auxetic behaviour. The modelling results compared with experimental results and closer agreement were achieved.

8.2. Future work

Since there is very less information about composite auxetic structures and auxetic composites and their applications in civil engineering, some of the important work which can be carried out as future work is presented here,

- The surface of braided rods (i.e. contour of braided rod surface) can be altered to improve their adhesion with masonry elements. The designing process could consider to change the different parameters of surface ribs of braided rod: height, thickness, spacing and inclination of the ribs. (See Figure 8.1)

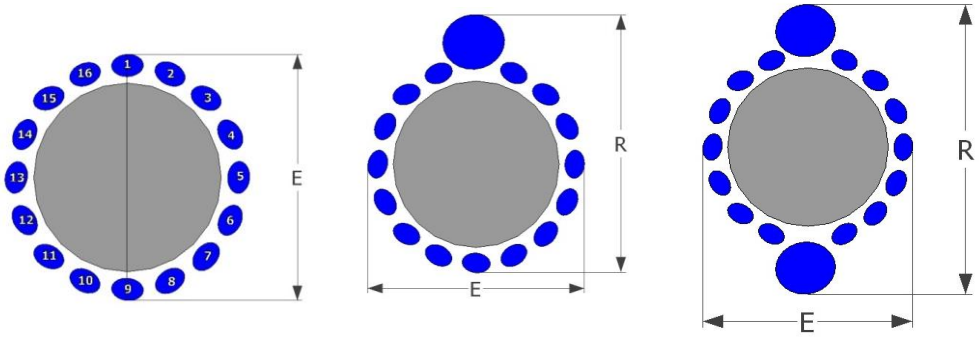

Figure 8.1. Example of yarns configuration in order to achieve different ribs configuration [130].

- Varying the rib length of re-entrant hexagon design and study auxetic behaviour and tensile properties.
- Development of analytical modelling to study tensile behaviour of developed auxetic structures based on missing rib or re-entrant hexagon design. This will be helpful to understand their tensile behaviour prior to experimental development of structures and give indirect benefits on time and cost.
- Since, the auxetic structures reinforced masonry wall specimens performed well under flexural load (flexural stress is almost close to plain grid reinforced masonry and exhibited higher energy absorption), the auxetic structures can be used as reinforcement to the masonry and study their performance under impact load. This could be a better alternative for commercial grids.
- In the literature, the route to develop an auxetic composite from technical fibres were reported and studied their mechanical behaviour (Poisson's ratio, tensile modulus, fracture toughness, etc.) in detailed manner. These type of composites are exhibited moderate tensile modulus and good energy absorption under impact

loading. So, this type of auxetic composites should be developed from technical fibres (Kevlar, Basalt, Carbon, etc.) and applied to civil structural elements to study their effectiveness under impact load, flexural load, etc. This will be an effective way to enhance the properties of existing structural elements and good replacement of conventional fibre reinforced composite panels.

- There are various routes to develop auxetic structures and auxetic materials like auxetic composite core reinforced sandwich panel, knitted auxetic fabric composite which produced from advanced technical fibres. These types of auxetic materials can be developed and used for strengthening of civil structural elements and study their performance under different loading condition (compressive load, seismic load, impact load, etc.). These novel auxetic composite materials may perform well and effective solution for many critical conditions like under blast load or seismic loading and best replacement for conventional composites.

References

[1] Campbell FC. (2010) Structural Composite Materials. *ASM International: The Materials Information Society.*

[2] Pichandi S, Rana S, Oliveira D and Fangueiro R. (2013) Fibrous and composite materials for blast protection of structural elements – a state-of-the-art review. *Journal of Reinforced Plastic and Composites*, 32(19), pp. 1477–500.

[3] Awad ZK, Aravinthan T, Zhuge Y and Gonzalez F. (2012) A review of optimization techniques used in the design of fibre composite structures for civil engineering applications. *Materials and Design,* 33, pp. 534–44.

[4] Olivito RS, Cevallos OA and Carrozzini A. (2014) Development of durable cementitious composites using sisal and flax fabrics for reinforcement of masonry structures. *Materials and Design,* 57, pp. 258–68.

[5] Gu H and Zhonge Z. (2005) Compressive behaviour of concrete cylinders reinforced by glass and polyester filaments. *Materials and Design,* 26, pp. 450–3.

[6] Pereira CG, Fangueiro R, Jalali S, Marques PP and Araujo M. (2008) Braided composite rodsto reinforce concrete subjected to aggressive environments. *International conference construction heritage in coastal and marine environments*. Lisbon, Portugal, pp. 1.

[7] Ahmadi MS, Johari MS, Sadighi M and Esfandeh M. (2009) An experimental study on mechanical properties of GFRP braid-pultruded composite rods. *EXPRESS Polymer Letters*, 3(9), pp. 560–8.

[8] Pereira CG, Fangueiro R, Jalali S, Marques PP and Araujo M. (2010) Hybrid composite rodsfor concrete reinforcement. *Struct Arch – Cruz (Ed.),* 10, pp. 1605–12.

[9] Shokrieh MM and Assadi A. (2011) Determination of maximum negative Poisson's ratio for laminate fibre composites. *Phys Status Solidi B*, 248(5), pp. 1237–41.

[10] Strek T and Jopek H. (2012) Effective mechanical properties of concentric cylindrical composites with auxetic phase. *Phys Status Solidi B,* pp. 1-7.

[11] Donoghue JP, Alderson KL and Evans KE. (2009) The fracture toughness of composite laminates with a negative Poisson's ratio. *Phys Status Solidi B,* 9, pp. 2011-17.

[12] Alderson A and Alderson KL. (2007) Auxetic materials. *Journal of Aerospace Engineering*, 221, pp. 565–75.

[13] Yang W, Li ZM, Shi W, Xie BH and Yang MB. (2004) Review on auxetic materials. *Journal of Material Science*, 39, pp. 3269–79.

[14] Prawoto Y. (2012) Seeing auxetic materials from the mechanics point of view: a structural review on the negative Poisson's ratio. *Compost Mater Sci*, 58, pp. 140–5.

[15] Yao YT, Uzun M and Patel I. (2011) Working of auxetic nanomaterials. *J Achiev Mater Manuf Eng*, 49(2), pp. 585–93.

[16] Miller W, Ren Z, Smith CW and Evans KE. (2012) A negative Poisson's ratio carbon fibre composite using a negative Poisson's ratio yarn reinforcement. *Composite Science and Technology*, 72, pp. 761–6.

[17] Jayanty S, Crowe J and Berhan L. (2011) Auxetic fibre networks and their composites. *Phys Status Solidi B,* 248(1), pp. 73–81.

[18] Grima JN, Caruana-Gauci R, Attard D and Gatt R. (2013) Three-dimensional cellular structures with negative Poisson's ratio and negative compressibility properties. *P Roy Soc A, pp.* 1–18.

[19] Smith CW, Grima JN and Evans KE. (2008) A novel mechanism for generating auxetic behavior in reticulated foams: missing rib foam model. *Acta Materials,* 48, pp. 4349–56.

[20] Gaspar N, Ren XJ, Smith CW, Grima JN and Evans KE. (2005) Novels honeycombs with auxetic behavior. *Acta Materials*, 53, pp. 2439–45.

[21] Evans KE and Anderson KL. (2000) Auxetic materials: the positive side of being negative. *Eng Sci Educ J, pp.* 148 – 154.

[22] Daniel JI et al. (1996) State-of-the-art report on fibre reinforced concrete. Reported by ACI Committee 544.1R-96. pp. 1-66.

[23] Rai A and Joshi YP. (2014) Applications and properties of fibre reinforced concrete. *Int. Journal of Engineering Research and Applications*, 4(5), pp. 123-131.

[24] Ali M, Li X and Chouw N. (2013) Experimental investigations on bond strength between coconut fibre and concrete. *Materials and Design*, 44, pp. 596 – 605.

[25] Reis JML. (2012) Sisal fibre polymer mortar composites: Introductory fracture mechanics approach. *Constructions and Building Materials*, 37, pp. 177 – 180.

[26] Boghossian E and Wegner LD. (2008) Use of flax fibres to reduce plastic shrinkage cracking in concrete. *Cement and Concrete Composites*, 30, pp. 929 – 937.

[27] Al-Salloum YA and Almusallam TH. (2002) Rehabilitation of the infrastructure using composite materials: Overview and applications. *J. King Saud University*, Eng. Sci (2): 000 – 000. (A.H. 1423/2002)

[28] Buchan PA and Chen JF. (2007) Blast resistance of FRP composites and polymer strengthened concrete and masonry structures – A state-of-the-art review. *Composites: Part B,* 38, pp. 509 – 522.

[29] Bakis CE, Bank LC, Brown VL, Cosenza E, Davalos J, Lesko J, Machida A, Rizkalla S and Triantafillou T. (2002) Fibre-reinforced polymer composites for construction – State-of-the-Art Review. *J Comp. Construct*, 6 (2), pp. 73 – 87.

[30] Gangaroa VS and Vijay PV. Feasibility review of FRP materials for structural applications. Report, West Virginia University, USA, Nov 2010.

[31] Toutanji H and Deng Y. (2002) Strength and durability performance of concrete axially loaded members confined with AFRP composite sheets. *Composites: Part B*, 33, pp. 255 – 261.

[32] Einde LVD, Zhao L and Seible F. (2003). Use of FRP composites in civil structural applications. *Construction and Building Materials,* 17, pp. 389 – 403.

[33] Mosallam AS and Banerjee S. (2007) Shear enhancement of reinforced concrete beams strengthened with FRP composite laminates. *Composites: Part B,* 37, pp. 781 – 793.

[34] Mosallam A, Taha MMR, Kim JJ and Nasr A. (2012) Strength and ductility of RC slabs strengthened with hybrid high-performance composite retrofit system. *Eng. Structures*, 36, pp. 70 – 80.

[35] Sarker P, Begum M and Nasrin S. (2011) Fibre reinforced polymers for structural retrofitting: A review. *Journal of Civil Engineering*, 39(1), pp. 49 – 57.

[36] Malvar L, Crawford J and Morril K. (2007) Use of composites to resist blast. *Journal of Composites for Construction*, 11, 6(601), pp. 601 – 610.

[37] Evans KE and Anderson A. (2000) Auxetic materials: functional materials and structures from lateral thinking. *Advanced Materials*, 12(9), pp. 161 – 167.

[38] Liu Y and Hu H. (2010) A review on auxetic structures and polymeric materials. *Sci Res Essays*, 5(10), pp. 1052 – 63.

[39] Uzum M. (2012) Mechanical properties of auxetic and conventional polypropylene random short fibre reinforced composites. *FIBRES TEXT East Europe*, 20, 5(94), pp. 70 – 74.

[40] Grima JN, Attard D, Gatt R and Cassar RN. (2009) A novel process for the manufacture of auxetic foams and their re-convention to conventional foam. *Adv Eng Mater*, 11(7), pp. 533 – 535.

[41] Miller W, Ren Z, Smith CW and Evans KE. (2012) A negative Poisson's ratio carbon fibre composite using a negative Poisson's ratio yarn reinforcement. *Composite Science and Technology*, 72, pp. 761 – 766.

[42] Grima JN, Gauci RC, Attard D and Gatt R. (2013) Three-dimensional cellular structures with negative Poisson's ratio and negative compressibility properties. *P Roy Soc A*, pp. 1 – 18.

[43] Smardzewski J, Klos R and Fabisiak B. (2013) Design of small auxetic springs for furniture. *Materials and Design*, 51, pp. 723 – 728.

[44] Cripps A. (2002) Fibre reinforced polymer composites in construction. CIRIA C564.

[45] Cabral-Fonseca, S. (2005) Composite materials matrix polymer reinforced with fibres used in Civil engineering – features and applications. *Scientific and Technical Information of LNEC*, Lisbon.

[46] Gupta VB and Kothari VK. (1997) Manufactured Fibre Technology. London: Chapman and Hall, pp. 544 – 546.

[47] Fibrous and composite materials for civil engineering applications (2011). Fangueiro R (editor). Woodhead Publisher.

[48] Fibreglass and glass technology: Energy friendly compositions and applications (2010). Wallenberger FT and Bingham PA (Editors). Springer Publications.

[49] High performance fibres. (2001) Hearle JWS (editor). The Textile Institute, CRC Press and Woodhead Publishing Ltd.

[50] Composites Materials Handbook. Vol. 3. Polymer matrix composites materials usage, design and Analysis.

[51] Shakor PN and Pimplikar SS. (2011) Glass fibre reinforced concrete use in construction. International Journal of Technology and Engineering System, 2(2), pp. 1 – 6.

[52] Kene KS, Vairagade VS and Sathawane S. (2012) Bonfring International journal of Industrial Engineering and Management Science, 2(4), pp. 125 – 131.

[53] Abdullah MM and Jallo EK. (2012) Mechanical properties of glass fibre reinforced concrete, Al-Rafidain Engineering, 20(5), pp. 128 – 135.

[54] Singha K. (2012) A short review on basalt fibre. *International Journal of Textile Science*, 1(4), pp. 19 – 28.

[55] Patil RK and Kulkarni DB. (2014) Comparative study of effect of basalt, glass and steel fibre on compressive and flexural strength of concrete. *International Journal of Research in Engineering and Technology*, 3(6), pp. 436 – 438.

[56] Irine F. (2014) Strength aspects of basalt fibre reinforced concrete. *International Journal of Innovative Research in Advanced Engineering*, 1(8), pp. 192 – 198.

[57] Shrivastav PK and Tare K. (2015) Basalt fibre reinforced concrete an alternative to the synthetic fibre reinforced concrete. *International Journal for Scientific Research and Development*, 3(1), pp. 316 – 319.

[58] Gore Ketan R. (2013) The performance of basalt fibre in high strength concrete. *Journal of Information Knowledge and Research in Civil Engineering*, 2(2).

[59] Advanced Inorganic Fibres: Processes, structures, properties, applications. Wallenberger FT (editor). Kluwer Academic Publisher, Boston/Dordretcht/London, 2000.

[60] New Millennium fibres. Hongu T, Phillips GO and Takigami M (editors). The Textile Institute, CRC Press, Woodhead Publishing Ltd, 2005.

[61] http://www.slideshare.net/fathyibrahim/carbon-fibre-reinforced-concrete-carbocrete.

[62] Fundamentals of Composites Manufacturing: Materials, Methods, and Applications. 2nd Edition, Strong AB (Editor). Society of Manufacturing Engineers, Michigan, 2008.

[63] Handbook of Fibre Chemistry. Edited by Lewin M, Third Edition, CRC press, USA, 2007. Gabara V, Hartzler JD, Lee KS, Rodini DJ and Yang HH. "Aramid Fibres". pp 975.

[64] New Fibres. Edited by Hongu T and Phillips GO, Second Edition. Woodhead publishing Ltd, England, 2001, pp 14.

[65] Synthetic Fibres: Machines and Equipment, manufacture, Properties. Fourne F (editor) Hanser Publishers, Munich, 1999.

[66] Cavdar A. (2012) A study on the effects of high temperature on mechanical properties of fibre reinforced cementitious composites. *Composites: Part B*, 43, pp. 2452 – 63.

[67] Patel PA, Desai AK and Desai JA. (2012) Evaluation of Engineering Properties for Polypropylene Fibre Reinforced Concrete. *International Journal of Advanced Engineering Technology*, 3(1), pp. 42-45.

[68] Anbuvelan K, Khadar MM. Lakshmipathy M and Sathyanarayanan KS. (2007) Studies on properties of concretes containing polypropylene, steel and reengineered plastic shred fibre. *Indian Concrete Journal*, 81(4), pp. 1724

[69] Ramadevi V and Venkatesh Babu DL. (2012) Flexural behavior of hybrid (steel and polypropylene) fibre reinforced concrete beams. *European Journal of Scientific Research*, 70(1), pp. 81-87.

[70] Tamil Selvi M and Thandavamoorthy TS. (2013) Studies on the properties of steel and polypropylene fibre reinforced concrete without any admixture. *International Journal of Engineering and Innovative Technology*, 3(1), pp. 411 – 416.

[71] Qian C and Stroeven P. (2000) Fracture properties concrete reinforced with steel-polypropylene hybrid fibres. *Cement and concrete composites*, 22, pp. 343 - 351.

[72] Hsie M, Tu C and Song PS. (2008) Mechanical properties of polypropylene hybrid fibre reinforced concrete. *Materials Science and Engineering, A* 494, pp. 153 – 157.

[73] Madhavi TC, Raju LS and Mathur D. (2014) Polypropylene fibre reinforced concrete – a review. *International Journal of Emerging Technology and Advanced Engineering*, 4(4), pp. 114 – 119.

[74] Filho RDT, Ghavami K, England GL and Scrivener K. (2003) Development of vegetable fibre-mortar composites of improved durability. *Cement and Concrete Composites*, 25 (2), pp. 185 – 196.

[75] John VM, Cincotto MA, Sjostrom C, Agopyan V and OliveiraCTA. (2005) Durability of slag mortar reinforced with coconut fibre. *Cement & Concrete Composites*, 27, pp. 565 – 574.

[76] Ramakrishna G and Sundararajan T. (2005) Impact strength of few natural reinforced cement mortar slabs: a comparative study. *Cement and Concrete Composites*, 27, pp. 547 – 553.

[77] Hasan R. Influence of fibre architecture on mechanical properties of Jute fibre reinforced composites. Master Thesis. 2012

[78] State-of-the-art Report on Fibre Reinforced Plastic Reinforcement for Concrete Structures. ACI440R-96. *American Concrete Institute*, 1996.

[79] Cowie JMG. Polymers: Chemistry & Physics of Modern Materials, Blackie Academic Professional, 1991.

[80] Hollaway LC, Head PR. Advanced Polymer Composites and Polymers in Civil Infrastructure. Elsevier, 2001.

[81] Benmokrane B, Chaallal O and Masmoudi R. (1995) Glass fibre reinforced plastic (GFRP) rebars for concrete structures. *Construction and Building Materials*, 9(6), pp. 353 – 364.

[82] Simonelli G. *Finite element analysis of RC beams retrofitted with Fibre Reinforced Polymers*. London: 2005, p. 17.

[83] Karbhari VM and Lee LS. Key issues in the use of FRP composites in the rehabilitation and retrofitting of concrete structures. *In:* Hollaway LC (eds) *Service life estimation and extension of civil engineering structures*. 1st ed. UK: Woodhead Publishing Ltd, 2011, pp. 3 – 74.

[84] Brown JP and Maji AK. Blast proofing of unreinforced masonry (URM) walls with GFRP. *15th ASCE Engineering Mechanics Conference* (ed Smyth A), New York, USA, 2 June – 5 june 2002, pp. 1 – 8. New York: 15th ASCE.

[85] Maji AK, Brown JP and Urgessa GS. (2008) Full-scale testing and analysis for blast resistant design. *Journal of Aerospace Engineering,* ASCE: pp. 217 – 225.

[86] Myers JJ, Belarbi A and El-Domiaty KA. (2004) Blast resistance of FRP retrofitted Un-reinforced masonry walls with and without arching action. *TMS Journal, pp.* 9 – 26.

[87] Myers JJ and Carney P. Out-of-plane static and blast resistance of unreinforced masonry wall connections strengthened with FRP. Report, University of Missouri-Rolla, USA, 2003.

[88] Baylot J, Bullock B, Slawson T and Woodson S. (2005) Blast response of lightly attached concrete masonry unit walls. *Journal of structural engineering,* ASCE, pp. 1186 – 1193.

[89] Fourne F. Synthetic fibres – Machines and equipment, manufacture, properties. Munich: Carl Hanser Verlag, 1999, p. 578.

[90] Wu Z, Wang X and Iwashita K. State-of-art of advanced FRP applications in civil infrastructure in Japan. *COMPOSITES & POLYCON* 2007. *American Composite Manufacture Association*, Tempa, USA, 17 Oct – 19 Oct 2007, p.1 – 13. Tempa: ACMA.

[91] Rai G and Indolia Y. (2011) Fibre reinforced polymer composites, a novel way for strengthening structures. *National Conference on Repair and Rehabilitation of Concrete Structures*, Noida, UP, India, May 6 – 7.

[92] Malvar JL, Crawford JE and Morrill KB. (2007) Use of composites to resist blast. *Journal of Composites for Construction*, ASCE, pp. 601 – 610.

[93] Das SC and Nizam EH. (2014) Applications of fibre reinforced polymer composites in civil engineering. *International Journal of Advanced Structures and Geotechnical Engineering*, 3(3), pp. 299 – 309.

[94] Laser Applications in material science and Industry. Kesabamoorthy R, Arora AK, Rao CB and Kalyanasundaram P. (editors). Allied Publishers, India. 1997.

[95] Ayranci C and Carey J. (2008) 2D braided composites: A review for stiffness critical applications. *Composite Structures*, 85, pp. 43 – 58.

[96] Ahmadi MS, Johari MS, Sadighi M and Esfandeh M. (2009) An experimental study on mechanical properties of GFRP braid pultruded composite rods. *eXPRESS Polymer Letters*, 3(9), pp. 560 – 568.

[97] Pereira CG, Fangueiro R, Jalali S, Marques P and Araujo MD. (2008) Braided composite rods to reinforce concrete subjected to aggressive environments. *International Conference Construction Heritage in Coastal and Marine Environments*. Lisbon, Portugal.

[98] Pendhari SS, Kant T and Desai YM. (2008) Applications of polymer composites in civil construction: A general review. *Composite Structures*, 84(2), pp. 114 – 124.

[99] Subramani P, Rana S, Oliveira DV, Fangueiro R and Xavier J. (2014) Development of novel auxetic structures based on braided composites. *Materials and Design*, 61, pp. 286 – 295.

[100] Ravirala N, Alderson A, Alderson KL and Davies PJ. (2005) Expanding the range of auxetic polymeric products using a novel melt-spinning route. *Phys. Stat. Sol. (b)*, 242 (3), pp. 653 – 664.

[101] Ravirala N, Alderson KL, Davies PJ, Simkins VR and Alderson A. (2006) Negative Poisson's ratio polyester fibres. *Textile Research Journal*, 76(7), pp. 540 – 546.

[102] Alderson KL, Alderson A, Davies PJ, Smart G, Ravirala N and Simkins G. (2007) The effect of processing parameters on the mechanical properties of auxetic polymeric fibres. *Journal of Material Science*, 42, pp. 7991 – 8000.

[103] Sloan MR, Wright JR and Evans KE. (2011) The helical auxetic yarn – a novel structure for composites and textiles; geometry, manufacture and mechanical properties. *Mechanics of Materials*, 43, pp. 476 – 486.

[104] Wright JR, Sloan MR and Evans KE. (2010) Tensile properties of helical auxetic structures: A numerical study. *Journal of Applied Physics*, 108, 044905, pp. 1 – 8.

[105] Miller W, Hook PB, Smith CW, Wang X and Evans KE. (2009) The manufacture and characterization of a novel, low modulus, negative Poisson's ratio composite. *Composite Science and Technology*, 69, pp. 651 – 655.

[106] Liu Y, Hu H, Lam JKC and Liu S. (2010) Negative Poisson's ratio weft-knitted fabrics. *Textile Research Journal*, 80(9), pp. 856 – 863.

[107] Hu H, Wang Z and Liu S. (2011) Development of auxetic fabrics using flat knitting technology. *Textile Research Journal*, 81(14), pp. 1493 – 1502.

[108] Alderson K, Alderson A, Anand S, Simkins V, Nazare S and Ravirala N. (2012) Auxetic warp knitted textile structures. *Phys. Status Solidi B*, pp. 1 – 8.

[109] Wang Z and Hu H. (2014) 3D auxetic warp-knitted spacer fabrics. *Phys. Status Solidi B*, 2, pp. 281 – 288.

[110] Xavier J, Pereira JCR and de Jesus AMP. (2014) Characterisation of steel components under monotonic loading by means of image-based methods. *Opt Laser Engineering*, 53, pp. 142-51.

[111] Ghiassi B, Xavier J, Oliveira D and Lourenco P. (2013) Application of digital image correlation in investigating the bond between FRP and masonry. Composites structures, 106, pp. 340-49.

[112] Xavier J, de Jesus AMP, Morais JJL and Pinto JMT. (2012) Stereovision measurements on evaluating the modulus of elasticity of wood by compression tests parallel to the grain. *Construction Building Materials*, 26(1), pp.207-15.

[113] Sousa AMR, Xavier J,Vaz M, Morais JJL and Filipe VMJ. (2011) Cross-correlation and differential technique combination to determine displacement fields. *Strain*, 47 (SUPPL. 2), pp. 87-98.

[114] Scarpa F. (2008) Auxetic materials for bio prostheses. *IEEE signal Process magazine*.

[115] White L. (2009) Auxetic foam set for use in smart filters and wound dressings. Urethanes Technol Int, 26(4), pp. 34–36.

[116] Alderson A, Rasburn J, Evans KE and Grima JN. (2001) Auxetic polymeric filters display enhanced de-fouling and pressure- compensation properties. Membrane Technology, 137, pp.6–8.

[117] Ugbolue SC, Kim YK, Warner SB, Fan Q, Yang CL, Kyzymchuk O, Feng Y and Lord J. (2012) Engineered warp knit auxetic fabrics. *Journal of Textile Science and Engineering*, 2(1), pp.1-8.

[118] Karnessis N and Burriesci G. (2013) Uniaxial and buckling mechanical response of auxetic cellular tubes. *Smart Materials Structures*, 22, pp. 1-9.

[119] Scarpa F, Panayiotou P and Tomlinson G. (2000) Numerical and experimental uniaxial loading on in-plane auxetic honeycombs. *J Strain Anal Eng*, 35(5), pp. 383-88.

[120] Hou Y, Neville R, Scarpa F, Remillat C, Gu B and Ruzzene M. (2014) Graded conventional-auxetic Kirigami sandwich structures: Flatwise compression and edgewise loading. *Composites Part B*, 59, pp. 33-42.

[121] Silva TAA, Panzera TH, Brandão LC, Lauro CH, Boba K and Scarpa F. (2012) Preliminary investigations on auxetic structures based on recycled rubber. *Phys Status Solidi B,* 249(7), pp. 1353–58.

[122] Saito K, Scarpa F and Neville R. Origami composite auxetic honeycomb. 16th ICCS FEUP Porto 2011.

[123] Shilko S and Konyok D. (2004) Numerical and experimental study of auxetic closed cell foams. *Computational Methods in Science and Technology*, 10(2), pp. 197 – 202.

[124] Ge Z, Hu H and Liu Y. (2013) A finite element analysis of a 3D auxetic textile structure for composite reinforcement. Smart Materials and Structures, 22, pp. 1 – 8.

[125] Roa MS, Ahmad Z and Alias A. (2015) Computational approach in formulating mechanical characteristics of 3D star honeycomb auxetic structure. *Advances in Mater Science and Engineering*, pp. 1 – 11.

[126] Javadi AA, Faramarzi A and Farmani R. (2012) Design and optimization of microstructure of auxetic materials. *International Journal for Computer Aided Engineering and Software,* 29(3), pp. 260 – 76.

[127] Rad MS and Ahmad Z. Finite Element Modelling of different 2D re-entrant structure for auxetic materials. *Proceedings of the 2nd International Conference on Advances in Mechanical and Automation Engineering* – MAE 2015.

[128] Park R. (1989) Evaluation of ductility of structures and structural assemblages from laboratory testing. *Bulletin of the New Zealand Society for Earthquake Engineering*, *22*(2), pp. 155–166.

[129] Frumento S, Magenes G, Morandi P and Calvi GM. (2009) Interpretation of experimental shear tests on clay brick masonry walls and evaluation of q-factors for seismic design. Pavia: IUSS Press.

[130] Cunha F. (2012) Development of braided fibrous materials for retrofitting non-loadbearing masonry walls. *12th World Textile Conference AUTEX*, Zadar, Croatia.